UNIVERSITY OF HAWAII
LIBRARY
APR 2 '51

The
HILOSOPHICAL
MAGAZINE

FIRST PUBLISHED IN 1798

SEVENTH SERIES No. 324 January, 1951

A Journal of Theoretical Experimental and Applied Physics

EDITOR
PROFESSOR N. F. MOTT, M.A., D.Sc., F.R.S.

EDITORIAL BOARD
SIR LAWRENCE BRAGG, O.B.E., M.C., M.A., D.Sc., F.R.S.
ALLAN FERGUSON, M.A., D.Sc.
SIR GEORGE THOMSON, M.A., D.Sc., F.R.S.
PROFESSOR A. M. TYNDALL, C.B.E., D.Sc., F.R.S.

PRICE 12s. 0d.
Annual Subscription £6 0s. 0d. payable in advance.

D PUBLISHED BY TAYLOR & FRANCIS LTD., RED LION COURT, FLEET ST., LONDON, E.C.4.

Early Scientific Publications

DIARY OF ROBERT HOOKE, M.A., M.D., F.R.S.

1672-1680

25/-
net

Edited by **H. W. ROBINSON** and **W. ADAMS**
Recommended for publication by the Royal Society, London

"This vivid record of the scientific, artistic and social activities of a remarkable man during remarkable years has too long remained in obscurity."—Extract from foreword by Sir Frederick Gowland Hopkins, O.M., President of the Royal Society.

MATHEMATICAL WORK OF JOHN WALLIS, D.D., F.R.S.

12/6
net

By **J. F. SCOTT, Ph.D., B.A.**

"His work will be indispensable to those interested in the early history of The Royal Society. I commend to all students of the Seventeenth Century, whether scientific or humane, this learned and lucid book."—Extract from foreword by Prof. E. N. da C. Andrade, D.Sc., Ph.D., F.R.S.
Recommended for publication by University of London

CORRESPONDENCE AND PAPERS OF EDMOND HALLEY

21/-
net

Arranged and Edited by **EUGENE FAIRFIELD MACPIKE**

First published on behalf of The History of Science Society by Oxford University Press. Now re-issued by Taylor & Francis, Ltd.

MEMOIRS OF SIR ISAAC NEWTON'S LIFE

5/-
net

By **WILLIAM STUKELEY, M.D., F.R.S., 1752**
From an Original Manuscript
Now in the possession of the Royal Society, London

HEVELIUS, FLAMSTEED AND HALLEY

12/6
net

Three Contemporary Astronomers and their Mutual Relations
By **EUGENE FAIRFIELD MACPIKE**
Published by arrangement with The History of Science Society

Established
over 150 years

TAYLOR & FRANCIS, LTD.
RED LION COURT, FLEET ST., LONDON E.C.
PRINTERS & PUBLISHERS OF SCIENTIFIC BOOKS

THE

PHILOSOPHICAL MAGAZINE

A JOURNAL OF THEORETICAL EXPERIMENTAL
AND APPLIED PHYSICS

First published in 1798

[SEVENTH SERIES—VOL. 42]

I. *The Propagation of a Radio-Atmospheric.*

By K. G. Budden,
Cavendish Laboratory, Cambridge *.

[Received October 5, 1950.]

Summary.

Previous authors have discussed the propagation of radio-atmospherics by assuming that the space between the earth's surface and the ionosphere behaves like a wave-guide. If the surfaces of such a guide are treated as perfect conductors, then there is one mode of propagation, the "zero-order" mode, which is unattenuated at all frequencies. In such a guide the wave-form of the received e.m.f. due to one mode at a great distance from a lightning flash can be calculated, and for modes of non-zero order it would be of an oscillatory type similar to that observed in many atmospherics from distant sources. But it would also include a large undistorted impulse due to the energy propagated in the zero-order mode, and this is not observed in practice. Moreover, recent measurements of the amplitudes of the component frequencies of atmospherics have shown that frequencies below about 7·5 kc./s. are heavily attenuated during propagation from the source to the receiver, and this is inconsistent with the presence of a zero-order mode which is unattenuated at all frequencies.

This paper shows that if one surface of the wave-guide is an imperfect conductor, then all the modes, including the zero-order mode, are heavily attenuated below a certain critical frequency. There are two modes whose amplitudes are much greater than those of all other modes, and these both give an oscillatory response to a lightning flash at a great distance. There is no longer any mode of propagation which would give an undistorted impulse at a great distance from the source.

---

* Communicated by J. A. Ratcliffe.

The critical frequency depends most markedly on the height of the ionosphere, and to a smaller extent on the characteristics of the ionized medium. The changes in the measured curves of attenuation versus frequency from day to night, and during sudden ionospheric disturbances are consistent with the changes in the height of reflection of very long waves which are known to occur at these times.

The relation between the treatment of propagation in terms of wave-guide modes, and in terms of successively reflected "rays" is discussed.

---

§ 1. INTRODUCTION.

The nature of the radio-atmospherics observed with a receiver at a given point depends on : (*a*) the nature of the sources ; (*b*) the length and characteristics of the propagation paths. Some recent experiments (Gardner 1951, Bowe 1951) have been concerned with the characteristics of the propagation path for different frequency components in the spectrum of the atmospherics. They have shown that frequencies below about 7·5 kc./s. are heavily attenuated. The amount of attenuation, and the exact frequency below which it occurs, depends upon whether it is day or night, and changes also during a sudden ionospheric disturbance. The object of this paper is to suggest a possible mechanism to explain these results. The mechanism suggested will also account for the oscillatory nature of the wave-form of atmospherics coming from great distances.

In § 3, § 4 and § 5, it is assumed that the atmospheric travels in a "wave-guide" formed between a perfectly conducting earth and an imperfectly conducting, sharply bounded ionosphere. Previous authors have discussed the propagation of waves in this type of wave-guide, but their discussions have been inadequate for our present purpose for various reasons. Thus Hales (1948) has discussed the propagation of an atmospheric in a wave-guide with perfectly conducting walls. We shall show that, although this model at first seems attractive, the "zero-order" mode is unattenuated at all frequencies, and hence the experimental results cannot be satisfactorily explained. Eckersley (1932), in a mathematical paper designed primarily to illustrate the nature of his "phase-integral" method of calculation, arrived at expressions like those which we derive here, but he did not apply them to our problem.

Most observers are agreed that the wave-forms of atmospherics can be divided roughly into two main types (Schonland *et al.* 1940, Laby *et al.* 1940, Rivault 1945). In one type the wave-form is short and irregular in shape, but the irregularities are repeated roughly at intervals which correspond to the repeated reflection of a pulse from the ionosphere. This type of atmospheric appears to be fairly well explained by the mechanism of successive reflection. The other type is oscillatory and the wave-form is much smoother than for the first type. It has been vaguely suggested (*e. g.* Schonland *et al.* 1940, p. 184) that it could be produced by the smooth merging together of the separate reflections of the first type, but no detailed explanation has been given of how this could occur, and, indeed, the two types of wave-form are so different that it is difficult to see how one could be converted into the other.

Hales (1948) came near to explaining the wave-form of an atmospheric from a distant source. He first discussed the explanation of the oscillatory type of atmospheric in terms of a wave-guide with perfectly conducting walls, and concluded that its wave-form could be explained with this model. We show in § 6 that we do not agree with this explanation which again neglected the zero-order mode. Hales next considered the case where one boundary had a finite conductivity, and showed that, with this model, he could explain the existence of the "slow tail" of the atmospheric, but he did not reconsider the production of the oscillatory type of atmospheric by this model.

In § 6 it is shown how the oscillatory type of atmospheric would be produced by transmission in a wave-guide system of the type discussed in this paper, and in § 7 it is indicated how the transition from the first to the second type of wave-form can come about.

§ 2. THE NATURE OF THE SOURCES.

The results of Gardner and Bowe were analysed in such a way that the characteristics of the source were eliminated. In discussing the frequency dependence of the characteristics of the propagation path, therefore, it is unnecessary to consider the exact nature of the source of an atmospheric. The wave-form of a single atmospheric, however, does depend upon the disturbance producing it, and some assumption about the source must therefore be made. It will be assumed in what follows that the atmospheric is the result of the instantaneous destruction of a short vertical electric dipole situated at the surface of the earth, so that the dipole moment of the source varies with time as shown in fig. 1 (*a*). The signal that would be received at a distance in free space from such a source would be a double impulse, as shown in fig. 1 (*b*). In the continuous spectrum of this source the amplitude is proportional to the frequency.

§ 3. RAYS AND WAVE-GUIDE MODES.

The propagation of an atmospheric from the initial lightning flash to the receiver may be discussed by either of two methods ; these will be called (*a*) the method of successive reflections, (*b*) the method of wave-guide modes. In (*a*) the received e.m.f. is regarded as a succession of impulses arriving at the receiver, the first after propagation direct from the source, and the succeeding ones after one, two, etc. reflections at the ionosphere.

In method (*b*) the space between the surface of the earth and the ionosphere is treated as a wave-guide. In this guide the propagation of certain modes is possible. The characteristics of each of these modes must be found, and also the amplitude excited in each mode by a given source. The received e.m.f. is then found by adding the contributions from all the modes.

If the ionosphere is an imperfect reflector, method (*a*) is the simplest when the receiver is close to the source, say within a few hundred kilometres, since then the amplitude of the direct wave and the first and possibly second reflected waves are large compared with the reflected waves of higher order, and these can therefore be neglected. At larger distances the incidence of the waves on the ionosphere is more oblique, so that the reflection coefficient is higher, and consequently the received e.m.f. is composed of a large number of reflections of comparable amplitude. In this case method (*b*) is simpler, since it is normally found that there is a marked difference between the attenuation coefficients of the various wave-guide modes, and at large distances the least attenuated mode is much greater than all the others. At short distances, the amplitudes in a large number of modes are comparable, and calculation of the received e.m.f. by the " mode " method is therefore complicated.

Fig. 1 (*a*).

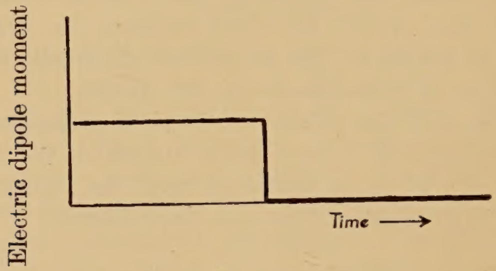

Idealized lightning flash. Variation of dipole moment of source with time.

Fig. 1 (*b*).

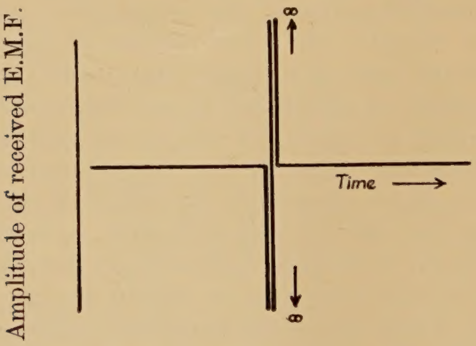

Signal received in free space from idealized lightning flash.

§ 4. Earth and Ionosphere considered as a Wave-guide.

Let us first consider the over simplified case where the earth and the ionosphere are both perfect conductors. A wave-guide of rectangular cross-section has four surfaces. We consider the limiting case where two of these surfaces are separated to an infinite distance, and we shall say that the guide has infinite horizontal width, but a finite vertical width, h. We consider only signals in which the electric vector is in the plane of propagation.

The elementary theory of wave-guides shows that waves can be propagated in a series of different modes. When both surfaces of the guide are perfect conductors, there is one mode in which the electric field is constant across the guide and perpendicular to its surfaces. This mode suffers no attenuation at any frequency. It will be called the mode of order zero. Higher-order modes are propagated without attenuation if the frequency is greater than the " cut-off " frequency, which is different for each mode, but for frequencies below the " cut-off " there is heavy attenuation. The " cut-off " frequency depends on the width of the guide, and the order of the mode.

It is tempting to suggest that this " cut-off " accounts for the great attenuation observed on the lowest frequencies, but it can readily be seen that this simplified model is not in accord with observation. Thus, if we assume a distance of 50 km. between the two boundaries, the first-order mode would cut-off at a wavelength of 100 km., *i. e.* 3 kc./s., the second-order would cut-off at 6 kc./s., and so on. The e.m.f. received at a great distance from a lightning flash, on a receiver tuned to 10 kc./s. would be comprised predominantly of four modes of orders 0, 1, 2, 3, while the e.m.f. from the same atmospheric at 5 kc./s. would include two modes of orders 0 and 1. The resulting e.m.f. at either frequency would depend on the relative phases of the e.m.f.s in the various modes, but the ratio of the resultant amplitudes received at these two frequencies would clearly be of the order of 2 : 1. The zero-order mode is propagated without attenuation, so that it is present at all frequencies, and this model therefore predicts that the signal should have appreciable amplitude, however low the frequency to which the receiver is tuned. But the observed amplitude at 10 kc./s. is very much greater than twice the amplitude at 5 kc./s., and at still lower frequencies the e.m.f.s from distant atmospherics are almost imperceptible, showing that there can be no unattenuated zero-order mode. Moreover, on this model a curve showing the variation of amplitude with frequency should have a series of approximately equal steps at, say, 3 kc./s., 6 kc./s., 9 kc./s., corresponding to the cut-off frequencies of the various modes. The curve plotted from the observations (Gardner 1950, fig. 4) shows a single steep increase at about 6 kc./s. There are no similar increases at 12 kc./s., 18 kc./s., etc.

We can therefore reject the model using a wave-guide with perfectly reflecting surfaces for two reasons :—

(*a*) Observations show that at very low frequencies the signal amplitudes from distant atmospherics are much smaller than they would be if an unattenuated zero-order mode were present.

(*b*) The observed variation of signal amplitude with frequency is of the wrong form.

As the next approximation we therefore assume that the ionosphere is a homogeneous medium, whose plane lower boundary forms the upper surface of the wave-guide which has a plane, perfectly conducting earth as its lower surface. The effect of the earth's magnetic field is neglected. The medium is assumed to contain N electrons per c.c., and these are assumed to make an average of ν collisions per second. Let p be the angular frequency of a component of the signal. At the level where very long waves are reflected ν is of the order 10^7 sec.$^{-1}$ We shall, therefore, assume that $\nu \gg p$. Then, if μ is the refractive index of the medium, we have

$$\mu^2 = 1 - jp_r/p, \qquad \dots\dots\dots\dots \quad (1)$$

where $p_r = 4\pi \mathrm{N}e^2/m\nu$,

e=charge of electron,

m=mass of electron.

We shall now investigate the modes which can be propagated in this guide. We consider only waves in which the magnetic vector is horizontal. Any one mode can be considered as composed of two component plane waves* equally inclined to the boundaries of the guide. Either of these may be considered as being continuously produced by the reflection of the other at a bounding surface. After a part of a wave-front has undergone two reflections, it is parallel to its original direction, and the phases and amplitudes of the original and of the twice reflected wave must agree. This means that only certain discrete values of the angle of inclination of the wave normal are possible. The excess path travelled by the wave-front of the twice reflected wave is $2h \cos i$. The difference of phase of the original and of the twice reflected wave is therefore $2(\cos i)h \,.\, p/c$ (this is, in general, complex), and the (complex) ratio of the amplitudes resulting from this excess path is $\exp\{-j(2 \cos i \,.\, h \,.\, p/c)\}$. There is also a change of phase and of amplitude due to the reflection of the component plane wave at the upper boundary, and if the (complex) reflection coefficient is R, then for a self-consistent mode, we shall have

$$\mathrm{R} \,.\, \exp\{-j(2 \cos i \,.\, h\, p/c)\} = 1 = e^{2\pi jn},$$

where n is an integer and is the phase difference, measured in cycles, between the original and the twice reflected wave.

---

[*] The two component plane waves which form a single mode are not, of course, to be confused with the direct and reflected rays of different order which are considered in the ray picture.

Now R is the Fresnel reflection coefficient of the upper surface for angle of incidence i. It is given by

$$\mathrm{R}=\{\mu^2 \cos i-\sqrt{(\mu^2-\sin^2 i)}\}/\{\mu^2 \cos i+\sqrt{(\mu^2-\sin^2 i)}\}, \quad . \quad . \quad . \quad (2)$$

so that we obtain

$$\{\mu^2 \cos i-\sqrt{(\mu^2-\sin^2 i)}\}/\{\mu^2 \cos i+\sqrt{(\mu^2-\sin^2 i)}\}$$
$$=\exp\{j(2 \cos i\, h\, p/c+2\pi n)\}, \quad . \quad . \quad . \quad (3)$$

where h is the width of the wave-guide (height of the ionosphere), c is the velocity of electromagnetic waves in free space, and n is a positive or negative integer which is the "order" of the mode.

This formula, in slightly different form, was given by Eckersley (1932, equation 3.21). From it the angle of incidence i can be found for each value of n, and in general i is complex. The attenuation coefficient of the mode is then easily found, and is equal to

$$|\mathscr{I}\,(\sin i)|\,.\,p/c. \quad . \quad . \quad . \quad . \quad . \quad . \quad . \quad . \quad (4)$$

("$\mathscr{I}$" means "imaginary part of").

It is still necessary to find the amplitude which is excited by a given source in each of the modes. For a vertical electric dipole, the amplitude radiated along a ray at an angle i to the vertical is proportional to sin i. This means that in a mode in which one component wave has its wave normal at an angle i to the vertical, the amplitude excited by a vertical electric dipole is proportional to sin i.

The amplitude also depends upon the frequency spectrum of the source. For a source of the type described in fig. 1, the amplitude is proportional to the frequency. On general physical grounds, therefore, we should expect the amplitude excited by a vertical electric dipole in any one mode to be proportional to

$$p\,.\sin i, \quad . \quad . \quad . \quad . \quad . \quad . \quad . \quad . \quad . \quad (5)$$

where i is given by equation (3). A more mathematical proof of this is given in Appendix A.

If R=1 (perfect reflector), sin i has the same value for modes of order n and $-n$. The nth mode is then really a degenerate case, where the two modes of orders n and $-n$ are superimposed. The degeneracy is removed when $\mathrm{R}\neq 1$. The use of a negative order to describe a mode is merely a matter of convenience. All modes, whether of positive, negative, or zero order, have the same general form. It is, however, important to stress that, by inserting values of n of equal magnitude but opposite sign in equation (3), we derive the properties of different modes.

§ 5. ATTENUATION CURVES.

Our main reason for considering the finite conductivity of the upper boundary was to see whether it alters the attenuation of the zero-order mode. The formulæ (3) and (4) have therefore been used to calculate the attenuation coefficient as a function of frequency. Equation (3) does not give a convenient explicit expression for cos i, and a method of successive approximation was therefore used. The results for the zero-order mode are shown in fig. 2 for $h=50$ km. The curves show the fractional reduction of signal amplitude for a path of 1000 km. in the wave-guide. (A similar curve has been given by Hales (1948), *loc. cit.*, fig. 4, curve, 5, but it refers to a mode of non-zero order, and no curves are given for the zero-order mode.)

The parameter p_r determines the nature of the upper boundary. When $p_r \rightarrow \infty$, the upper boundary becomes a perfect conductor, and the zero-order mode should be unattenuated at all frequencies. It will be seen that, for large values of p_r, there is very little attenuation at any frequency. For smaller values of p_r, the medium is an imperfect conductor, and there is then some attenuation which is most marked at frequencies between 2 and 8 kc./s. The increase in the attenuation as the frequency decreases from about 10 to about 5 kc./s. is very similar to that observed in the experiments mentioned in § 1. The frequency near which this decrease of amplitude occurs is seen to be fairly independent of the characteristics of the upper surface. It does, however, depend markedly on the width of the guide (height of the ionosphere), as is illustrated in fig. 3 in which the various curves all relate to the same value of p_r but different values of the height h.

Fig. 2.

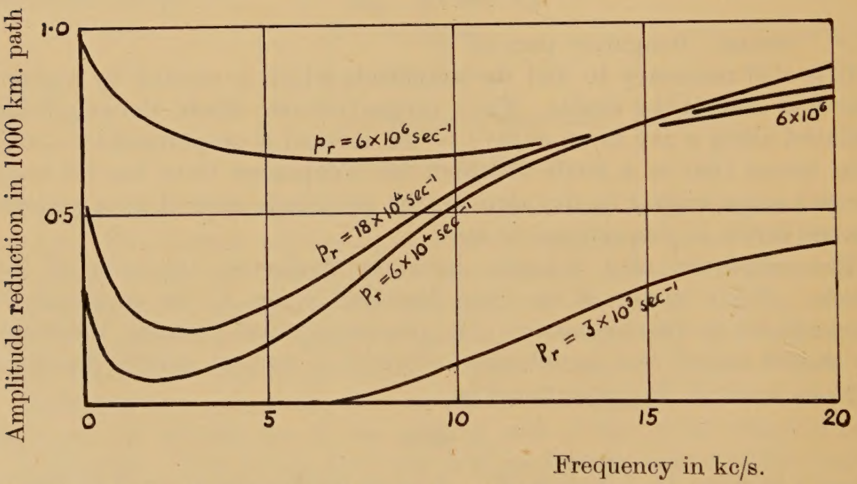

Fractional reduction in received e.m.f. for 1000 km. path in the zero-order mode, as a function of frequency. $h=50$ km.

When p_r is zero, the upper medium is a " dielectric " with dielectric constant unity. The reflection coefficient is zero, so that all the energy incident on the upper boundary is propagated into the medium. If p_r is very small, a large proportion of the energy is propagated into the medium and all the modes are heavily attenuated, and are "leaky". (For a full discussion of "leaky" modes, see Booker and Walkinshaw (1946)). It would be necessary to add the effects of a very large number of modes to calculate the received signal in this case. However, the order of magnitude of N and ν for the ionosphere are known, and these show that it is unlikely that we shall be concerned with very small values of p_r.

The form of the curves of figs. 2 and 3 depend only on the two parameters p_r and h. A small change of p_r would not result in any marked change in the frequency where the attenuation curve has greatest slope. A change of 10 km. in h would have an appreciable effect on this frequency. It has been shown (Gardner 1950, Bowe 1951) that the curve relating attenuation to frequency changes from night to day and during a Sudden Ionospheric Disturbance, in such a way that the cut-off frequency becomes greater. It is also known (Best, Ratcliffe and Wilkes 1936; Budden, Ratcliffe and Wilkes 1939; Bracewell and Straker 1949) that the height of reflection of very long waves falls in the passage from night to day, and during a Sudden Ionospheric Disturbance. It therefore seems probable that the changes in the attenuation curves are produced mainly by the changes in height of reflection.

Fig. 3.

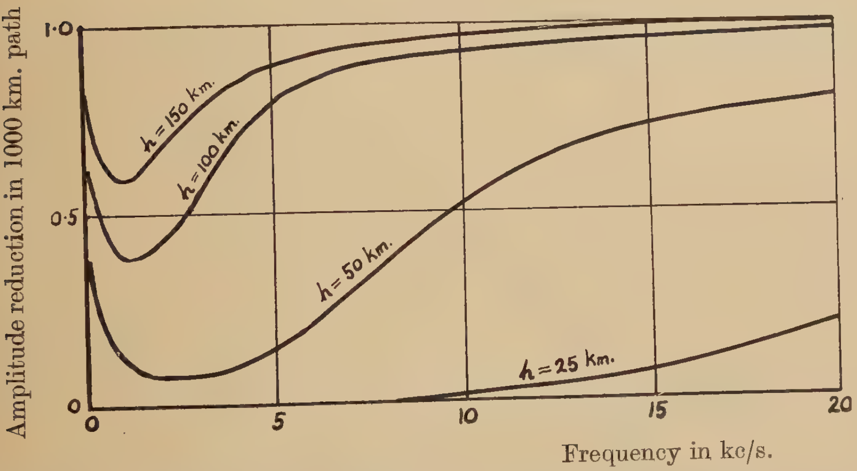

Fractional reduction in received e.m.f. for 1000 km. path in the zero-order mode, as a function of frequency. $p_r=6\times10^4$ sec.$^{-1}$

For a given value of p_r, it is necessary to find how many modes must be used to calculate the received e.m.f. at a given distance from the source. The results of calculations for the modes of order -2, -1, 0, +1, and for a distance of 1000 km., are shown in fig. 4 for the case of $p_r=6\times10^4$ sec.$^{-1}$ and $h=50$ km. These modes would have "cut-off" frequencies of 6 kc./s., 3 kc./s., 0 kc./s., 3 kc./s. respectively, if both guide-surfaces were perfectly conducting. Fig. 4 shows that for frequencies up to about 16 kc./s. the signal amplitudes at 1000 km. from the source, in the modes of orders -2 and $+1$, are much smaller than in the modes of order 0 and -1. It is readily verified that the amplitudes in modes of still higher orders are much smaller still. Hence, for an explanation of the experimental results, it is sufficient, as a first approximation, to consider modes of orders 0 and -1 only.

§ 6. The Wave-form of an Atmospheric.

In the introduction we mentioned two methods of studying the characteristics of the propagation path of an atmospheric. These were (*a*) a determination of the frequency response characteristic of the path (Gardner 1950, Bowe 1951); (*b*) the study of the wave-form of

Fig. 4.

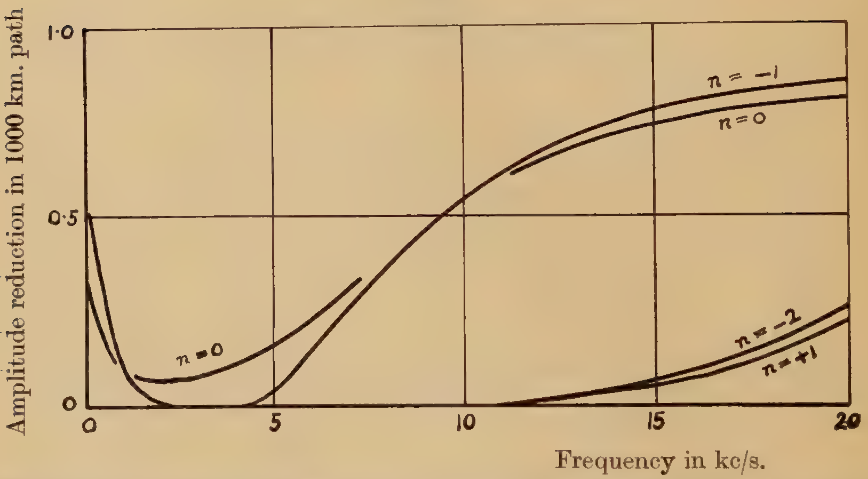

Fractional reduction in received e.m.f. for 1000 km. path in modes of various order (n). $h=50$ km. $p_r=6\times10^4$ sec.$^{-1}$

an atmospheric from a distant source. These two methods may at first appear to be unrelated, but in fact they depend on the same properties of the path. For, if the curve showing variation of amplitude with frequency is given for the path, the response of the system to an impulse can be calculated*. Hence, any model which is inadequate to explain the variation of amplitude with frequency is also inadequate to explain the oscillatory wave-form of an atmospheric from a distant source.

---

* It would seem that we should also need to know how the phase varies with frequency, but in fact the amplitude and phase characteristics of any system are interrelated, and if the amplitude curve is given, it is possible, subject to certain restrictions which do not apply here, to find both the phase characteristic and the impulse response. See, for example, Murakami and Corrington (1948).

Hales (1948) has attempted to explain the oscillatory type of atmospheric wave-form by considering the distortion of an impulse as it travelled through a wave-guide with perfectly conducting walls, but he took no account of the zero-order mode. The zero-order mode must be present, and since it would be unattenuated at all frequencies, it would not produce any distortion, and so there should be a large undistorted impulse at the beginning of an atmospheric of the oscillatory type. This is not observed, and so we cannot accept Hales' explanation without modification. We have now also shown that the observed variation of amplitude with frequency cannot be explained if the guide has perfectly conducting walls, since the zero-order mode is not attenuated. It is therefore necessary to assume that one surface of the wave-guide has finite conductivity.

We shall now examine the wave-form which we should expect to receive after an atmospheric has travelled for a considerable distance (1000 km.) through such a guide. The calculation has been made for the modes of order 0 and -1, and for a source of the type described by fig. 1. For this purpose, we have to evaluate the integral

$$\mathrm{I}(t)=\int_{-\infty}^{\infty} p \sin i \,.\, e^{jpt}\mathrm{Hi}_1(k\rho \sin i) \,.\, j \,.\, dp$$

(see Appendix B), where i is given by equation (3), ρ is the distance travelled, and $k=p/c$. It is sufficiently accurate to use the first term of the asymptotic expression for the Bessel function Hi, and with this approximation the integral reduces (omitting a constant factor) to

$$\int_{-\infty}^{\infty} (p \sin i)^{\frac{1}{2}} e^{j\pi/4} \exp\{j(pt-k\rho \sin i)\} \,.\, dp.$$

The integrals were evaluated numerically with the help of Beevers-Lipson strips (Beevers and Lipson 1936). The results for the modes of order 0 and -1 were found to be identical within about 10 per cent. This was not unexpected in view of the similarity of the two curves for these modes in fig. 4. Modes of higher orders have much smaller amplitudes (see fig. 4) and therefore are not included. Fig. 5 shows the result for either mode, and this is also the form of the e.m.f. which results when the two modes are added together. It is seen that the wave-form is oscillatory, and that the instantaneous frequency and amplitude both decrease with time. This behaviour is typical of many atmospheric wave-forms observed in practice. This calculation extends and completes that of Hales (1948), in which both walls of the wave-guide were assumed to be perfect conductors.

Hales has suggested that the characteristics of the zero-order mode at very low frequencies in a wave-guide with imperfectly conducting walls may explain the " slow tail " which is often observed to follow the main part of an atmospheric wave-form. He has shown that the observed delay between the beginning of an atmospheric and the peak of the

" slow tail " is consistent with a reasonable value of the width of the guide. (Hales' discussion of the main part of the atmospheric appears to refer only to modes of non-zero order, and his discussion of the " slow tail " only to the zero-order mode.)

Fig. 5.

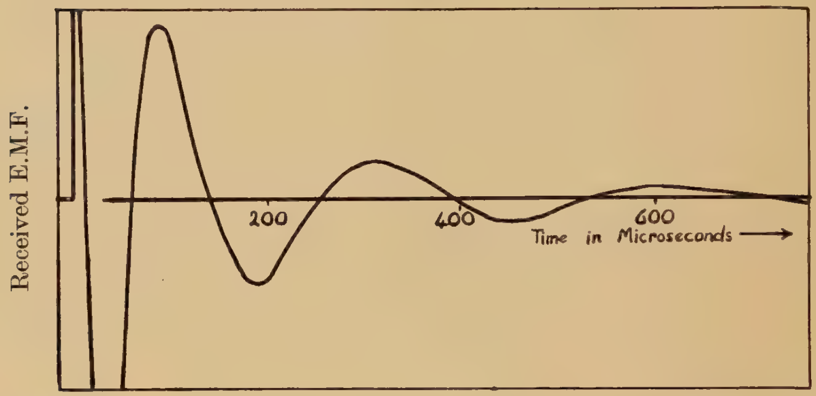

Received e.m.f. in mode of order 0 or -1 at 1000 km. from idealized lightning flash. $h=50$ km. $p_r=6\times10^4$ sec.$^{-1}$

Fig. 6.

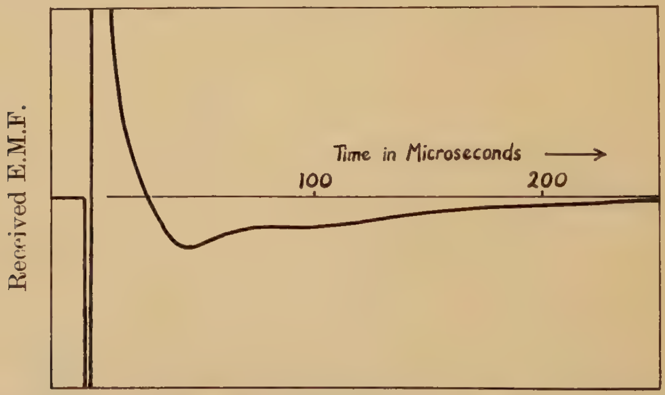

Received e.m.f. in plane wave resulting from the reflection of impulsive plane wave at the surface of an ionized medium. Angle of incidence 60°.

§ 7. Equivalence of " Ray " Picture and " Mode " Picture.

The calculations of the received signal, treated either by the ray method or by the mode method, can both be made exact, and must therefore give the same result. It is, however, interesting to discuss the interrelation of the two methods. It would seem at first sight that the ray method would result in the arrival at the receiver of a series of sharp impulses resulting from varying numbers of reflections of the origina impulse at the earth's surface and at the ionosphere, and it is difficult to see how a series of sharp impulses can combine to give a smooth curve like that of fig. 5. It must be remembered, however, that the Fresnel reflection coefficient (equation 2) is a function of frequency, and a single reflection therefore results in distortion of the incident signal. Fig. 6 shows the form of this distortion for reflection at an angle of incidence of 60° from the plane surface of an ionized medium of the type already discussed, with $p_r = 6 \times 10^4$ sec.$^{-1}$ Hence it is clear that the successive reflected waves are no longer sharp impulses, but have comparatively smooth wave-forms, which, when added together, would give a smooth curve, such as that of fig. 5.

Fig. 7 (*a*).

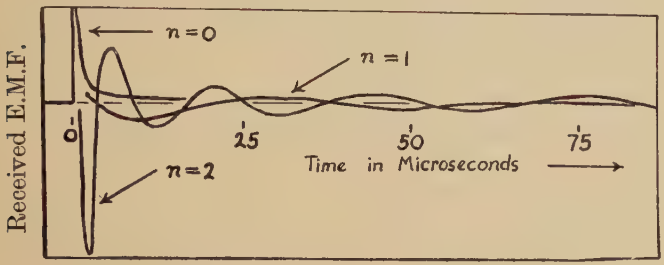

Received e.m.f. in first three modes at 1000 km. from "lightning flash". Wave-guide with perfectly conducting walls. $h = 50$ km.

Fig. 7 (*b*).

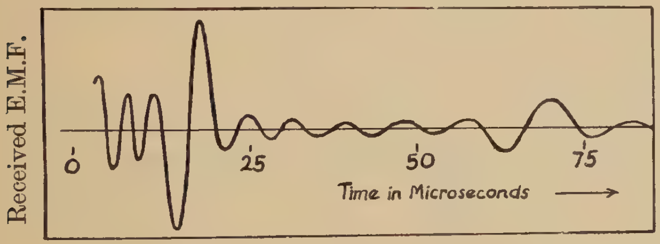

Sum of received e.m.f.s in first seven modes ($n = 0$ to 6, inclusive).

Fig. 7 (*c*).

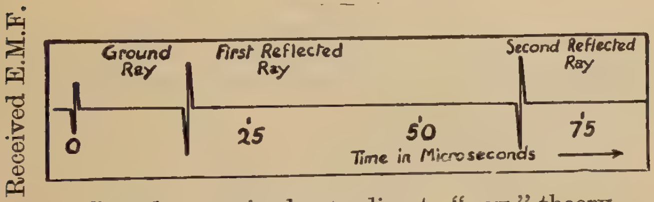

Impulses received according to "ray" theory.

If both surfaces of the wave-guide are perfect conductors, there is no distortion of the signal at reflection, and the received e.m.f. must then be a succession of sharp impulses. But this succession of impulses must also result from the addition of a large number of modes. The way in which this occurs is illustrated in fig. 7. Here the curves are plotted assuming that both guide surfaces are perfect conductors, that the source and receiver are both at the earth's surface, and that $h=50$ km. The source is assumed to be an impulse of the type described by fig. 1. There is an analytic expression for the impulse response for one mode of order n for this case, at a distance from the source. If $\rho \gg h$ and $ct-\rho \ll \rho$, this can be shown (see Appendix B) to be approximately proportional to *

$$\{\cos (\pi \mathrm{X}n/h)+(\pi \mathrm{X}n/h) \sin (\pi \mathrm{X}n/h)\}/\mathrm{X}^3, \quad . \quad . \quad . \quad . \quad . \quad (6)$$

where $\mathrm{X}^2=c^2t^2-\rho^2$.

In fig. 7 (*a*) the values of this function for the first three modes are plotted; fig. 7 (*b*) shows the result of adding together the first seven modes ($n=0$ to 6 inclusive). Fig. 7 (*c*) shows the succession of double impulses that would be received on a ray picture. With only seven modes, the first and second reflected impulses are already becoming accentuated, and it is clear that, by including a sufficient number of modes, the mode picture and the ray picture would give the same result. In this case the high-order modes are not attenuated, and therefore the mode method is not the best for calculating the received e.m.f.

We have thus shown that, when the number of modes contributing to the received e.m.f. is large, the resulting signal is a succession of impulses, so that the wave-forms are of the first type mentioned in the introduction. If the number of contributing modes is small, the received e.m.f. is oscillatory and therefore of the second type. The transition from the first to the second type could occur as the number of contributing modes decreased. Thus we might expect that atmospherics from nearby sources would be of the first type, while those from more distant sources would be of the second type.

§ 8. Possible Extensions of the Theory.

Since we are concerned with very long waves, it is probable that the ion density and collision frequency in the ionosphere vary greatly in a distance small compared with one wavelength, and therefore, in the theory of propagation of very long waves, many authors have treated the ionosphere as a sharply bounded, homogeneous medium, as a first approximation. In discussing the propagation of very long radio waves to great distances, Rydbeck (1944) has used the method of Watson (1919), which is essentially a treatment in terms of wave-guide modes. Both these authors allow for the curvature of the earth's surface. Rydbeck has discussed the cases where the ionosphere is assumed to be (*a*) a sharply bounded, homogeneous medium, (*b*) a medium in which the ion density has a maximum and varies parabolically with height, (*c*) a medium in which the ion density varies as the square of the height above its lower edge. He concludes that, for the modes of lowest order, there is not much difference in the behaviour for the three cases. Rydbeck gives numerical results for only a few single frequencies. His formulæ could be used for calculating curves showing attenuation as a function of frequency, but the calculation would be laborious because of the complexity of the formulæ.

---

* A series of terms like (6) is not uniformly convergent but can be shown to be "summable (C 2)" (see Whittaker and Watson 1935, *Modern Analysis*, para. 8.43). If the electric dipole at the source were destroyed in a small but finite time, the resulting series would be uniformly convergent.

No allowance has been made for the effect of the earth's magnetic field. If this effect is included, the ionized medium becomes doubly refracting. It is still possible to consider propagation in terms of wave-guide modes. When a plane wave is incident from below on the boundary of the medium, the state of polarization of the reflected wave is in general different from that of the incident wave. For a given mode, it is necessary to ensure that a component wave, after two reflections at the wave-guide surfaces, has not only the same amplitude and phase as the original component wave, but also the same polarization. The result is that the number of possible modes of a given order is doubled, and the electric field of the wave is no longer wholly in the plane of propagation.

Acknowledgments.

This work was carried out at the Cavendish Laboratory as part of a programme of Radio Research supported by the Department of Scientific and Industrial Research. I am indebted to Mr. J. A. Ratcliffe for helpful discussions throughout the course of the work.

References.

Beevers C. A., and Lipson, H., 1936, *Proc. Phys. Soc.*, **48**, 772.

Best, J. E., Ratcliffe, J. A., and Wilkes, M. V., 1936, *Proc. Roy. Soc.* A, **156**, 614.

Booker, H. G., and Walkinshaw, W., 1946, *Phys. Soc. Report on Meteorological Factors in Radio-wave Propagation*, p. 80.

Bowe, P. W. A., 1951 (*to be communicated to the Philosophical Magazine*).

Bracewell, R. N., and Straker, T. W., 1949, *Mon. Not. Roy. Ast. Soc.*, **109**, 28.

Budden, K. G., Ratcliffe, J. A., and Wilkes, M. V., 1939, *Proc. Roy. Soc.* A, **171**, 188.

Eckersley, T. L., 1932, *Proc. Roy. Soc.* A, **136**, 499.

Gardner, F. F., 1950, *Phil. Mag.*, **41**, 1259.

Hales, A. L., 1948, *Proc. Roy. Soc.* A, **193**, 60.

Laby, T. H., McNeill, J. J., Nicholls, F. G., and Nickson, A. F. B., 1940, *Proc. Roy. Soc.* A, **174**, 145.

Murakami, T., and Corrington, M. S., 1948, *R.C.A. Review*, **9**, 602.

Rivault, R., 1945, *Comptes Rendus, Acad. Sci. Paris*, **221**, 540, or *Notes Préliminaires du Laboratoire National de Radioélectricité*, No. 65.

Rydbeck, O., 1944, *On the Propagation of Radio Waves*; *Trans. Chalmers Univ., Gothenberg, Sweden*, Nr. 34.

Schonland, B. F. J., Elder, J. S., Hodges, D. B., Phillips, W. E., and van Wyk, J. W., 1940, *Proc. Roy. Soc.* A, **176**, 180.

Watson, G. N., 1949, *Proc. Roy. Soc.* A, **95**, 546.

APPENDIX A.

WAVE-GUIDE MODES EXCITED BY A VERTICAL DIPOLE.

In this appendix, we deduce an expression for the horizontal magnetic field produced in a wave-guide of the type discussed in the paper, by a vertical electric dipole of constant angular frequency p at the surface of the earth. In Appendix B, we shall use the result to deduce the field when the source is a lightning flash of the type shown in fig. 1, and when both surfaces of the wave-guide are perfect conductors.

Suppose the source is a vertical electric dipole of moment $P = \exp(jpt)$. Then we shall show that the horizontal magnetic field $\mathscr{H}$, at a horizontal distance ρ from the source and at height z, is proportional to

$$\sum_{n=-\infty}^{+\infty} p^2 \,.\, \sigma_n \mathrm{Hi}_1(k \,.\, \sigma_n \rho) \,.\, \cos\{(jq_n - 2\pi n)z/2h\} \exp(jpt). \quad . \quad . \quad (7)$$

Each term of this series is the field in one mode. σ_n is the value of $\sin i$, for the nth mode when n is zero or positive, and the complex conjugate of $\sin i$ when n is negative. We have written $R = e^{-q}$ and q_n is the value of q when i has the value appropriate to the nth mode. The angle i is given by equation (3). Hi is Jeffreys' notation for a Bessel function of the third kind (Jeffreys and Jeffreys 1946, *Mathematical Physics* (Cambridge), p. 544).

The expression (7) can be predicted on general physical grounds. Thus the factor $p^2\sigma_n$ when multiplied by $1/p$ (which is proportional to the amplitude of the frequency p in the dipole moment of the ideal lightning flash) gives $p \sin i$ which is simply the expression (5) of § 4. The cosine term is a "standing wave" term which arises through the combination of the upgoing and downgoing component waves of each mode. The Bessel function represents a wave propagated outwards from the source with cylindrical symmetry. For large values of ρ, it is proportional to $\{\exp(-jk\sigma_n\rho)\}/\sqrt{(k\sigma_n\rho)}$.

The mathematical derivation of (7) is given below in outline. The method used is similar to that developed by Watson (1919).

We use spherical polar coordinates r, θ, ϕ, with the dipole source at the origin. We also use z for distance measured vertically upwards, and $\rho = \sqrt{(x^2+y^2)}$ for the horizontal distance measured radially from the origin. Then the field of the dipole in free space is given by the Hertz vector $\Pi_0 = \exp(jpt) \,.\, \{\exp(-jkr)\}/r$. This may be written

$$\Pi_0 = (jk/2\pi) \,.\, \exp(jpt) \int_{\pi/2-j\infty}^{\pi/2+j\infty} d\phi \,.\, \int_{-\infty}^{\infty} (S/C)\, dS \,.\, \exp\{-jk(x\cos\phi\sin\theta + y\sin\phi\sin\theta + z\cos\theta)\},$$

where $S = \sin\theta$, $C = \cos\theta$.

The integrand represents a plane wave whose wave normal has the direction (θ, ϕ). The radiated field is thus expressed as the sum of an infinite number of such waves. Note that it is necessary to include complex values of ϕ and θ.

Each plane wave undergoes successive reflections at the earth and the ionosphere. To get the complete resultant Hertz vector, Π, we must add to the original Hertz vector the expressions for the various reflected waves. It is permissible first to perform the integration with respect to ϕ, since the reflection coefficient, R, of the ionosphere is independent of ϕ. Then we have

$$\Pi_0=\tfrac{1}{2}jk\exp(jpt)\,.\int_{-\infty}^{\infty}\mathrm{Hi}_0(k\mathrm{S}\rho)\,.\exp(-jk\mathrm{C}z)\,.(\mathrm{S}/\mathrm{C})\,.\,d\mathrm{S}.$$

The phases of the successive reflected waves are easily seen to contain factors $\exp(\pm j\,.\,2hk\mathrm{C})$, $\exp(\pm j\,.\,4hk\mathrm{C})$, etc., since they originate at image sources at heights $\pm 2h$, $\pm 4h$, etc. Hence the complete field is given by

$$\Pi=\tfrac{1}{2}jk\exp(jpt)\int_{-\infty}^{\infty}\mathrm{S}/\mathrm{C}\,.\,d\mathrm{S}\,\mathrm{Hi}_0(k\mathrm{S}\rho)$$
$$\times\left[\sum_{\nu=0}^{\infty}\mathrm{R}^{\nu}\,.\exp(-j\,.\,2\nu hk\mathrm{C})+\sum_{\nu=1}^{\infty}\mathrm{R}^{\nu}\exp(+j2\nu hk\mathrm{C})\right].$$

By suitable manipulation of the contours, this series may be transformed into another series, corresponding to the "residue" series of Watson. The result is

$$\Pi=(j\pi/2h)\exp(jpt)\left[\sum_{n=-\infty}^{-1}\mathrm{Hi}_0(k\mathrm{S}^{*}_{-n}\rho)\cos\{(jq_n-2\pi n)z/2h\}\right.$$
$$\left.+\sum_{n=0}^{+\infty}\mathrm{Hi}_0(k\mathrm{S}_n\rho)\,.\cos\{(jq_n-2\pi n)z/2h\}\right]. \quad . \quad . \quad . \quad (8)$$

Here we have written $\mathrm{R}=e^{-q}$. An asterisk * denotes a complex conjugate. The terms of the last series are the various wave-guide modes. The values S_n are the poles of the integrand, and are given by

$$2hk\mathrm{C}_n=jq_n+2\pi n, \quad . \quad . \quad . \quad . \quad . \quad . \quad . \quad . \quad (9)$$

where $\mathrm{C}_n^2=1-\mathrm{S}_n^2$.

Equation (8) is derived by an application of the "residue theorem" of complex variable theory. We note at this stage how the full mathematical treatment gives two results :—

(*a*) the characteristics of each mode; these arise from equation (9), which leads directly to equation (3) and gives the *positions* of the poles of the integrand in the complex S-plane ;

(*b*) the amplitudes excited in each mode by the source ; these are the terms of equation (8) and are the residues of the integrand at the poles.

If the ionosphere is a perfect reflector, $q=0$, and the S_n's are all real or purely imaginary. Then (8) becomes

$$\Pi=(j\pi/2h)\,.\,\exp(jpt)\left[\mathrm{Hi}_0(k\rho)+\sum_{n=1,2\,..}2\cos(\pi nz/h)\,.\,\mathrm{Hi}_0(kS_n\rho)\right]. \qquad (10)$$

The summation includes all values of n for which S_n is real. Terms for which S_n is imaginary refer to heavily attenuated (evanescent) modes, and may be neglected when ρ is large.

The horizontal magnetic field $\mathscr{H}$ of the signal is derived from the Hertz vector thus

$$\mathscr{H}=\partial^2\Pi/\partial t\,.\,\partial\rho.$$

Then for the mode of order n, we have, from (8) (imperfectly reflecting ionosphere),

$$\mathscr{H}_n=\left.\begin{matrix}S_n\\S^*_{-n}\end{matrix}\right\}(\pi p^2/2hc)\mathrm{Hi}_1\left\{k\rho\begin{matrix}S_n\\S^*_{-n}\end{matrix}\right\}\cos\{iq_n-2\pi n)z/2h\}\exp(jpt)\;\ldots\;\begin{matrix}n\geqslant0\\n<0\end{matrix}.$$

This leads to equation (7).

For a perfectly reflecting ionosphere, we have, from (10),

$$\mathscr{H}_n=(\pi p^2S_n/hc)\,.\,\mathrm{Hi}_1(kS_n\rho)\,.\,\cos(\pi nz/h)\exp(jpt).$$

APPENDIX B.

Impulse Response of one Mode.

Equations (8) and (10) give the Hertz vector of the signal when the source is a vertical electric dipole at the earth's surface, oscillating with constant angular frequency, p, and constant amplitude.

If the source is a lightning flash as illustrated in fig. 1, the dipole moment of the source (fig. 1 (*a*)) can be expressed as the Fourier integral

$$\mathrm{P}(t)=\int_{-\infty}^{\infty}\{\exp(jpt)\}/jp.\,dp.$$

Each component frequency in the Fourier spectrum initiates a series of modes such as that of equation (8) or (10).

We consider only one mode, the nth, for the case where both earth and ionosphere are perfect conductors (equation 10). We assume that the receiver is at the earth's surface, so that $z=0$. We use the value of S_n given by (9) when $q=0$. The Fourier component of angular frequency p then gives, for the nth mode only,

$$\Pi=(j\pi/2h)\exp(jpt)\,.\,2\mathrm{Hi}_0\{k\rho\sqrt{(1-\pi^2n^2/h^2k^2)}\}.$$

The complete impulse response for the nth mode is therefore

$$\Pi_{in}=(\pi/h)\int_{-\infty}^{\infty}\{\exp(jpt)\}/jp\,.\,dp\,.\,\mathrm{Hi}_0\{k\rho\sqrt{(1-\pi^2n^2/h^2k^2)}\}.$$

Hence

$$\partial\Pi_{in}/\partial t=(\pi/h)\int_{-\infty}^{\infty}\exp(jpt)\,.\,jdp\,.\,\mathrm{Hi}_0\{\sqrt{(p^2-\pi^2n^2c^2/h^2)}\,.\,\rho/c\}.$$

This integral can be reduced to a standard form (see, for example, McLachlan and Humbert 1941, *Mémorial des Sciences Mathématiques*, Fascicule 100, p. 34). Its value is

$$\partial\Pi_{in}/\partial t=(\pi c/h\mathrm{X})[\cos(\pi n\mathrm{X}/h)-(2/\pi)\sin(\pi n\mathrm{X}/h)\log_e\{(ct+\mathrm{X})/\rho\}],$$

where $\mathrm{X}^2=c^2t^2-\rho^2$.

To find the horizontal magnetic field which the nth mode contributes to the received signal, this expression must be differentiated again with respect to ρ. We are interested in values of X which are small compared with ct and ρ. We also assume $\rho\gg h$. Then it is readily shown that the log. term is negligible, and we have

$$\mathscr{H}_{in}=\partial^2\Pi_{in}/\partial t\partial\rho=(\pi c\rho/h\mathrm{X}^3)\{\cos(\pi n\mathrm{X}/h)+(\pi n\mathrm{X}/h)\sin(\pi n\mathrm{X}/h)\}.$$

This leads to equation (6).

II. *Total Cross-Sections of Hydrogen and Carbon for High Energy Neutrons.*

By A. E. TAYLOR, T. G. PICKAVANCE, J. M. CASSELS and T. C. RANDLE,
Atomic Energy Research Establishment, Harwell*.

[Received October 6, 1950.]

ABSTRACT.

Measurements of the attenuation of a beam of high energy neutrons in carbon and polythene have been made in good geometry. The total cross-sections of hydrogen and carbon have been found to be $0{\cdot}0464 \pm 0{\cdot}0012 \times 10^{-24}$ cm.^{2} and $0{\cdot}330 \pm 0{\cdot}003 \times 10^{-24}$ cm.^{2} respectively, at an effective neutron energy of 156 ± 3 MeV.

INTRODUCTION.

THE present work has been the first of a series of experiments on high energy neutrons produced by the 110-inch frequency-modulated cyclotron (Pickavance, Adams and Snowden (1950)) at the Atomic Energy Research Establishment, Harwell. In the course of the measurement of the neutron–proton cross-section, the total cross-section of carbon was also measured and this result is included. The experiments have already been reported briefly (Taylor, Pickavance, Cassels and Randle (1950)), and the purpose of the present paper is to describe the work in more detail.

The total neutron cross-section of hydrogen has been measured at 40 MeV. and 90 MeV. by Hadley, Kelly, Leith, Segrè, Wiegand and York (1949), at 95 MeV. by De Juren and Knable (1950), and at 260 MeV. by Kelly, Leith, Segrè and Wiegand (1950); recent measurements by Moyer and de Juren (1950) at energies between 90 MeV. and 270 MeV. were published almost simultaneously with our preliminary report. The experimental results so far obtained are in mutual agreement within experimental error.

The method of observation in the work described here was similar to that used at Berkeley by Hadley *et al.* (1949) and by Kelly *et al.* (1950). Measurements of the attenuation of a neutron beam in carbon and polythene were made in good geometry. The neutron detector was a triple coincidence counter telescope, into which protons were scattered from a polythene disc placed in the neutron beam.

---

* Communicated by the Authors.

APPARATUS.

Collimation of the Neutron Beam.

A beryllium target, 8·9 mm. thick, was mounted in the cyclotron vacuum chamber near the edge of the dee at a radius of $48\frac{1}{2}$ inches, where it intercepted a beam of about 1 microampere mean current of 171 MeV. protons. Neutrons emerging near the forward direction (fig. 1) passed through a thin aluminium window in the vacuum chamber wall, and were then collimated by a series of 5 cm. diameter holes in concrete blocks and shielding walls. The shielding, which was divided into three parts, had a total thickness of 4·3 metres. The neutron attenuators were placed between the second and third walls and the neutron detector was in a long tunnel beyond the third wall. The collimating holes, the polythene radiator and the neutron attenuator holder were aligned with the target with the help of a theodolite.

Fig. 1.

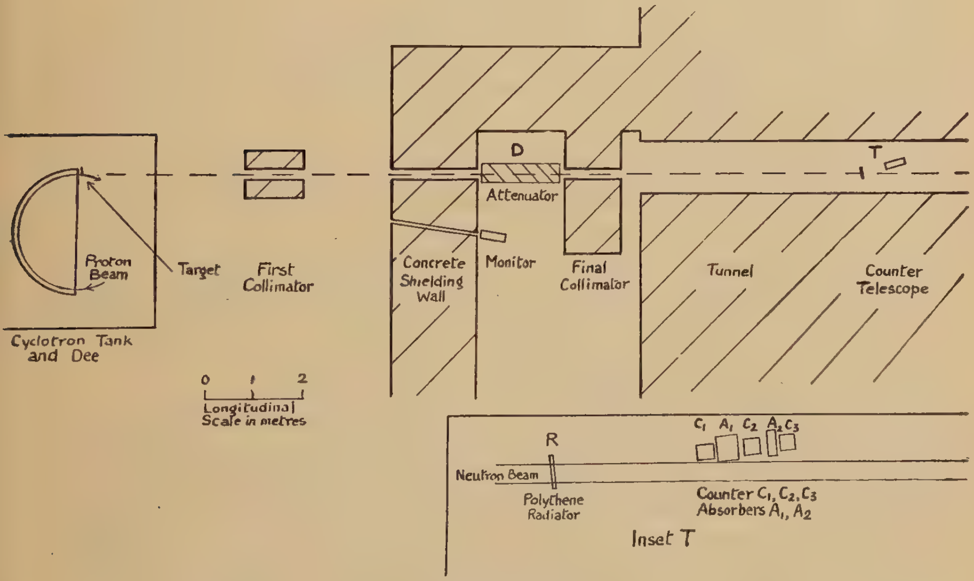

Geometrical layout.

Neutron Detector.

The proton radiator (R, fig. 1) was a polythene disk 19 mm. thick and 6·3 cm. in diameter, placed at a distance of 16 metres from the target. Protons ejected from the disc at an angle of 10° to the forward direction were detected by a telescope consisting of three proportional counters C_1, C_2, C_3 separated by carbon absorbers A_1, A_2. All the counters were clear of the main neutron beam. Each counter was cylindrical in shape, 5 cm. in diameter and 5 cm. long, with a 46 mg./cm.^{2} copper window at each end and a 0·02 cm. tungsten wire stretched across the diameter.

The gas filling was a mixture of argon (96 per cent) and carbon dioxide (4 per cent) at a total pressure of 52 cm. of Hg and the operating voltage was about 2 kilovolts.

Each of the counters was connected to a linear amplifier channel (fig. 2) with a high frequency response up to 1·5 Mc./s., consisting of a head amplifier feeding through about 50 yards of correctly terminated coaxial cable to a main amplifier in a remote counting room. A differentiation time constant of 0·6 microseconds was used and all coupling time constants in the later stages of the amplifier were kept short to reduce the dead time following a large background pulse. With the actual neutron background encountered there was no difficulty from dead time effects.

The output pulses of the main amplifiers were mixed in a standard triple coincidence unit Type 1036A. The " tuning " of this coincidence unit was carried out in the usual way, by adjusting gate-open times and delay times in the individual channels until all real coincidences were counted ; the gate-open times finally used were 0·5 microseconds. The amplifier and discriminator were adjusted to register a count on the arrival of 10,000 electron charges in a pulse. Standard scaling units type 1009A were used to register the mixed pulses and the counts in each channel.

Fig. 2.

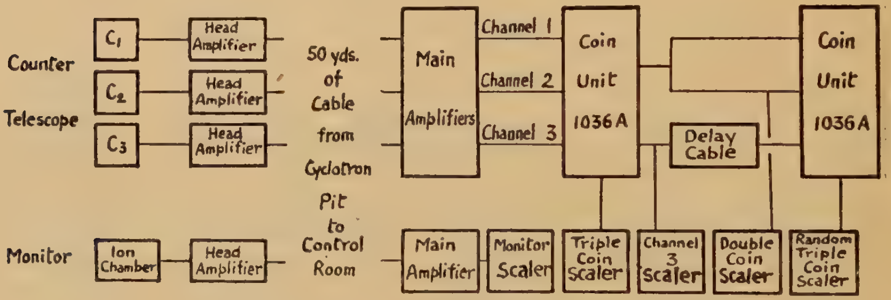

Block diagram of counting apparatus.

A second triple coincidence unit enabled the accidental coincidences to be measured during the normal counting runs. Double coincidences between channels 1 and 2 were fed into the final mixer stage of the second coincidence unit, and mixed with the single pulses from channel 3. The pulses from channel 3 were delayed by $2\frac{1}{2}$ microseconds in a coiled inner coaxial line, so that no genuine coincidences could be recorded. There was a considerable counting rate of genuine double coincidences caused by recoil protons which had sufficient energy to pass through the first two counters, but were brought to rest in the absorber A_2 between the second and third counters. Thus the background consisted of accidental coincidences between the mixed channel 1 and 2 pulses and the random counts of channel 3 caused by relatively slow neutrons emerging from the shielding walls.

All three counter voltages were adjusted to be on a plateau of triple coincidence counting rate against voltage in any arrangement used, thus ensuring that the fastest protons were being counted and that any slight drifts of voltage had a negligible effect on the counting rate.

The Neutron Attenuators.

A revolving drum (D, fig. 1), carrying four tubes 1·6 metres long and 6·3 cm. inside diameter, was slung between the second and third shielding walls, about 8 metres in front of the neutron detector. A carbon attenuator, 120·23 gm./cm.^{2}, was mounted in one tube and a polythene $((CH_2)_n)$ attenuator containing 136·93 gm./cm.^{2} of polythene in another. One tube was left empty, and a copper bar, sufficiently long to remove virtually all the neutrons from the beam, was fixed in a fourth position. The drum could be driven by remote control from the counting room, so that measurements in the various positions could be made in rapid succession. Impurities in the carbon and polythene were such as to have a negligible effect on the attenuation. A second pair of attenuators, containing 70·76 gm./cm.^{2} of carbon and 82·41 gm./cm.^{2} of polythene respectively, was also used.

THE EFFECTIVE NEUTRON ENERGY.

The triple coincidence telescope detected neutrons in two distinct ways, since protons were ejected from both the hydrogen and the carbon content of the polythene radiator. A test with a graphite radiator showed that during the total cross-section measurements 93 per cent of the counts arose from hydrogen recoils and 7 per cent from nuclear reactions in carbon. The hydrogen recoils were elastic so that neutron energies could be inferred directly from the energies of the protons actually detected. On the other hand, only a lower limit could be placed on the energy of the neutrons detected through nuclear reactions in the carbon. This lower limit was fortunately rather high, because of the $^{12}C(n, p)^{12}B$ threshold of 13·2 MeV.

Throughout the total cross-section measurements the absorbers A_1 and A_2 were kept equal to 11·26 and 3·35 gm./cm.^{2} respectively. The carbon equivalent of all the copper windows of the counters, together with the air separating them, was 0·21 gm./cm.^{2}. A further 1·00 gm./cm.^{2} of carbon equivalent was added because the protons, on the average, traversed half the thickness of the polythene radiator. With the help of the range-energy relation in carbon (Taylor 1950) the minimum mean proton energy detected was found to be 145 MeV. Since the telescope was set an at angle of 10° to the neutron beam the minimum neutron energy detected was, on the average, 149 MeV. Now, the energy of the primary protons in the cyclotron was 171 MeV., so that there were no neutrons of energy greater than 169 MeV. The effective energy of the experiment was thus quite closely defined from the outset.

If the total cross-sections measured are assumed not to vary rapidly with energy, then the effective energy can be fixed still more accurately. First, the effective energy E^{H}_{eff} of the neutrons detected through hydrogen recoils was found by means of the following subsidiary experiment. The absorber A_2 in the telescope was increased in steps to a maximum of 9·15 gm./cm.^{2} and the triple coincidence rate determined at each setting, first with a polythene radiator and then with a carbon radiator. The integral spectrum of the hydrogen recoils (fig. 3) was then found from the difference between these two sets of results. Small corrections of the order of 2 per cent had to be applied to allow for the increased nuclear absorption of the protons in the extra absorber. After translating hydrogen recoil energies into neutron energies, E^{H}_{eff} was found to be 155±3 MeV.

Fig. 3.

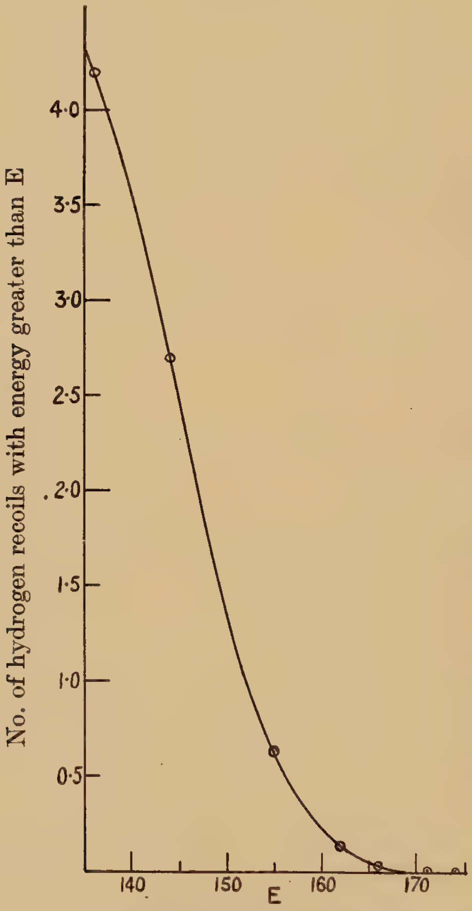

Hydrogen recoil energy in MeV.
Integral spectrum of hydrogen recoils.

The effective energy E^C_{eff} of the neutrons detected through nuclear reactions in carbon could not be found experimentally. This did not matter greatly because only 7 per cent of the protons came from this source.

The high n, p threshold in carbon restricted the corresponding neutron energies to the comparatively narrow range from 162 to 169 MeV. The value of E^C_{eff} was guessed to be 165±2 MeV.

Giving E^H_{eff} 93/7 times the weight of E^C_{eff}, the overall effective energy of the experiment was found to be 156±3 MeV. This value has been slightly revised from that given in our earlier report.

The estimated error of the effective energy includes some allowance for possible inaccuracies in the range-energy relation. The results displayed in fig. 3 show clearly that this source of error was small. The maximum neutron energy was 169 MeV., so that the maximum possible hydrogen recoil energy was 164 MeV. The curve of fig. 3 should therefore reach the energy axis at 169 MeV., remembering that half the radiator thickness has been added in arriving at the energy scale. In fact, the experimental intersection is at 169±2 MeV.

THE BEAM MONITOR.

The neutron output of the cyclotron was monitored by counting the pulses in an ionization chamber placed in a standard position behind the second shielding wall (fig. 1), where it was not affected by changing the neutron attenuator. Tests showed that the monitor counting rate was proportional to the cyclotron beam current.

EXPERIMENTAL PROCEDURE.

A complete cycle consisted of three successive measurements of the ratio of triple coincidence counts to the monitor counts with a polythene attenuator, a carbon attenuator and finally with no attenuator. The duration of counting was so arranged that about 300 triple coincidences were recorded in each run, and with a proton beam of 1 microampere mean current a complete cycle could be completed in about half an hour. Occasionally, between cycles, a blank run was performed with the long copper attenuator. In all, 19 cycles of readings were taken with the longer carbon and polythene attenuators, and 6 cycles with the shorter ones as a test for “ hardening ” and other effects which might have introduced errors.

Accidental triple coincidences represented a background which had to be subtracted from the counts observed during the experiment; they were measured by the method described above. Although the single channel counting rates were all far greater than the real triple coincidence counting rate, the background was only about 1 per cent with an attenuator in position. The background represented by the counting rate behind the long copper attenuator was negligibly small, showing that there were no serious leaks in the shielding.

RESULTS.

The measure of the incident neutron beam upon the counter telescope has been taken as the number of real triple coincidences divided by the monitor counts.

Calling the ratio T_0, T_c, T_p where the subscripts refer to the beam unattenuated, and attenuated by carbon and polythene respectively, then :

$$\ln T_0/T_c = (N\sigma)_c$$

and

$$\ln T_0/T_p = (N\sigma)_p,$$

where N is the number of atoms per cm.^{2} of attenuator and σ their cross-section. Hence

$$\ln T_c/T_p = (N\sigma)_p - (N\sigma)_c.$$

If $(\Delta N\sigma)_c$ represents the excess of carbon in the polythene over that in the carbon attenuator, then :

$$(N\sigma)_H = \ln T_c/T_p - (\Delta N\sigma)_c,$$

where the subscript H refers to the hydrogen content of the polythene. The results are presented as the ratios of T_0/T_c and T_c/T_p for each cycle of the experiment. The mean value of these ratios then is used and the standard deviation quoted is that determined from the deviations from this mean. The values of the standard deviations so found differ little from the values expected from the total number of counts in the whole experiment.

TABLE I.

Short Attenuator.

Cycle	T_c/T_p	T_0/T_c
A	1·360	3·780
B	1·436	2·981
C	1·320	2·919
D	1·413	3·598
E	1·312	3·373
F	1·412	2·890

From the results in Table I, the values of T_c/T_p and T_0/T_p are $1{\cdot}376 \pm 0{\cdot}025$ and $3{\cdot}257 \pm 0{\cdot}182$ respectively ; the standard deviations expected from the total number of counts are 0·044 and 0·104 respectively. With these values the total cross-sections σ_C, σ_H for carbon and hydrogen are :

$$\sigma_C = 0{\cdot}333 \pm 0{\cdot}016 \times 10^{-24} \text{ cm.}^2$$

$$\sigma_H = 0{\cdot}0454 \pm 0{\cdot}0025 \times 10^{-24} \text{ cm.}^2$$

From the results in Table II. the mean values of T_c/T_p and T_0/T_c are $1{\cdot}649 \pm 0{\cdot}0242$ and $7{\cdot}310 \pm 0{\cdot}127$ respectively, the standard deviations expected from the total number of counts being 0·0271 and 0·098 respectively. The total cross-sections with these values are :

$$\sigma_C = 0{\cdot}330 \pm 0{\cdot}003 \times 10^{-24} \text{ cm.}^2$$

$$\sigma_H = 0{\cdot}0467 \pm 0{\cdot}0014 \times 10^{-24} \text{ cm.}^2$$

The weighted means of these results are :

$$\sigma_C = 0{\cdot}330 \pm 0{\cdot}003 \times 10^{-24} \text{ cm.}^2$$

$$\sigma_H = 0{\cdot}0464 \pm 0{\cdot}0012 \times 10^{-24} \text{ cm.}^2$$

TABLE II.

Long Attenuator.

Cycle	T_c/T_p	T_0/T_c
A	1·714	7·810
B	1·596	7·364
C	1·913	7·139
D	1·779	7·682
E	1·402	8·406
F	1·845	6·747
G	1·547	6·915
H	1·625	7·674
I	1·750	6·765
J	1·640	6·807
K	1·622	6·724
L	1·672	7·235
M	1·675	6·808
N	1·600	7·431
O	1·629	6·866
P	1·558	7·812
Q	1·515	7·739
R	1·650	7·955
S	1·493	7·004
T	1·683	
U	1·715	

CONCLUSION.

This value of the hydrogen cross-section is in line with the results of experiments at Berkeley (Hadley *et al.* 1949, Kelly *et al.* 1949, De Juren and Moyer 1950, De Juren and Knable 1950). However, it is too low to be compatible with the theoretical total cross-sections calculated with the interactions suggested by present meson theories (Burhop and Yadav 1949, Christian and Hart 1950).

ACKNOWLEDGMENT.

We wish to thank the cyclotron operating crew for their cooperation throughout these experiments. This paper is published by permission of the Director of the Atomic Energy Research Establishment, Harwell.

REFERENCES.

BURHOP, E. H. S., and YADAV, H. N., 1949, *Proc. Roy. Soc.* A, **197,** 505.
CHRISTIAN, R. S., and HART, E. W., 1950, *Phys. Rev.*, **77,** 441.
DE JUREN, J., and KNABLE, N., 1950, *Phys. Rev.*, **77,** 606.
DE JUREN, J., and MOYER, B. J., 1950, *Bull. Am. Phys. Soc.*, **25,** 4, J. 8.
HADLEY, J., KELLY, E., LEITH, C., SEGRÈ, E., WIEGAND, C., and YORK, H., 1949, *Phys. Rev.*, **75,** 351.
KELLY, E., LEITH, C., SEGRÈ, E., and WIEGAND, C., 1950, *Phys. Rev.*, **79,** 96.
PICKAVANCE, T. G., ADAMS, J. B., and SNOWDEN, M., 1950, *Nature*, **165,** 90.
TAYLOR, A. E., PICKAVANCE, T. G., CASSELS, J. M., and RANDLE, T. C., 1950, *Nature*, **165,** 967.
TAYLOR, A. E., 1950, *Phil. Mag.*, **41,** 966.

III. *The Interaction between an Oblique Shock-wave and a Turbulent Boundary-layer.*

By O. Bardsley and W. A. Mair,
Fluid Motion Laboratory, University of Manchester *.

[Received October 10, 1950.]

[Plates I. to IV.]

Summary.

Schlieren photographs have been taken to show the reflection of oblique shock-waves of different strengths at the turbulent boundary-layer on the wall of a supersonic wind-tunnel. A weak shock-wave is reflected as a compression followed by an expansion; this is in agreement with Lighthill's theory in which the boundary-layer is replaced by a non-turbulent inviscid layer with the same velocity distribution as a turbulent boundary-layer. For stronger incident shock-waves the reflected wave moves upstream of the incident one to a point where the boundary-layer starts to thicken. Thus the incident and reflected shock-waves cross outside the boundary-layer. Near the point where the incident shock-wave meets the boundary-layer, the rate of growth of the boundary-layer suddenly decreases and an expansion occurs. For very strong shock-waves a Mach type of interaction occurs, with a short normal shock-wave between two intersections.

The supersonic wind-tunnel and optical system used for these experiments are briefly described.

§ 1. Introduction.

The experiments were made in a small intermittent supersonic wind-tunnel at a Mach number of 1·965, using a wedge to produce an oblique shock-wave. The strength of the shock-wave was varied by changing the angle of incidence of the wedge. The interaction between the shock-wave and the turbulent boundary-layer on the tunnel wall was investigated by schlieren photography.

§ 2. Notation.

p_1=static pressure before incident shock-wave.
p_2=static pressure after incident shock-wave.
$\chi=\frac{p_2-p_1}{p_1}$=strength of incident shock-wave.
δ=stream deflection produced by incident shock-wave.

---

* Communicated by the Authors.

α_0=theoretical angle between undisturbed stream and incident shock-wave, calculated from a given value of δ.

α_1=angle between undisturbed stream and incident shock-wave, measured at upstream edge of "fan" in photograph.

α_2=angle between undisturbed stream and incident shock-wave, measured at downstream edge of "fan" in photograph.

§ 3. DESCRIPTION OF WIND-TUNNEL.

The arrangement of the wind-tunnel is shown in fig. 1. The large reservoir M consists of three modified Lancashire boilers having a total capacity of about 130 cu.m. This reservoir is connected to the other parts of the wind-tunnel by the quick-operating valve L. Before starting the wind-tunnel the reservoir is evacuated to an absolute pressure of about 0·1 atmosphere. The valve L is then opened and air enters the intake A from the atmosphere, is dried by the silica gel C and passes through the contraction E to the working section F. The working section is rectangular, with a height of 12·7 cm. and a width of 10·2 cm., the shaped nozzle blocks being at the top and bottom, with parallel glass plates at the sides. Downstream of the working section there is a gradually expanding passage G, in which the supports for the models are fixed. This is followed by a transition to a circular section H and a subsonic diffuser K leading to the valve L.

Fig. 1.

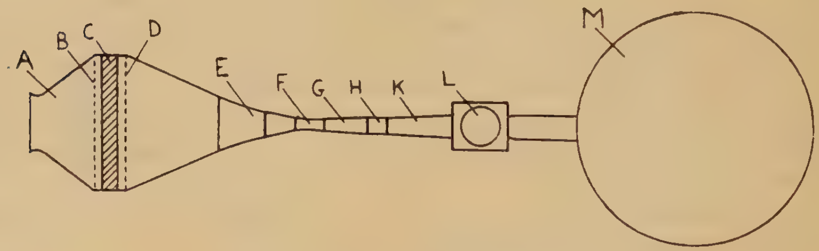

Intermittent supersonic wind tunnel.

In the drier the silica gel bed C is 19 cm. thick and has a frontal area of 2·65 sq. m. With a Mach number of 1·965 in the working section (area 129 sq. cm.) the mean velocity of the air passing through the silica gel is only 0·58 m. per sec. This small velocity makes it possible to use a cotton-wool filter B to clean the incoming air and so prevent contamination of the silica gel by dirt from the atmosphere. A wire gauze D is placed after the silica gel to reduce the turbulence caused by the structure supporting the silica gel compartment. The total pressure drop caused by the cotton-wool, silica gel, and wire gauze is about 15 cm. of water.

A small centrifugal fan and a 12 Kw. electric heater are provided for regenerating the silica gel as required by blowing hot air through it. The maximum duration of each run of the wind-tunnel is about 45 seconds. For many purposes a much shorter time is sufficient, and several runs can then be made with one evacuation of the reservoir. At a Mach number of 1·965 the pressure in the reservoir when the normal shock-wave begins to move upstream into the working section is 0·665 times the stagnation pressure upstream of the throat. The diffuser efficiency may be defined as the work done in isentropic compression, between the condition before and the pressure after the diffuser, divided by the decrease of kinetic energy in the diffuser. Using this definition the efficiency is 0·75, a value consistent with the results obtained by Neumann and Lustwerk (1949) for a similar type of diffuser.

The distribution of static pressure along the centre line of one side of the working section was measured, using a brass side-plate fitted with pressure holes instead of the usual glass window. From these static pressures the corresponding Mach numbers were calculated, assuming that the stagnation pressure was equal to the static pressure in the drier immediately after the gauze D. (Measurements with a pitot tube at high subsonic speeds have shown that this assumption is correct, outside the boundary-layer, within 0·2 per cent of the dynamic pressure.) The distribution of Mach number obtained in this way is shown in fig. 2; for the purpose of the present experiments the mean Mach number is assumed to be 1·965.

Fig. 2.

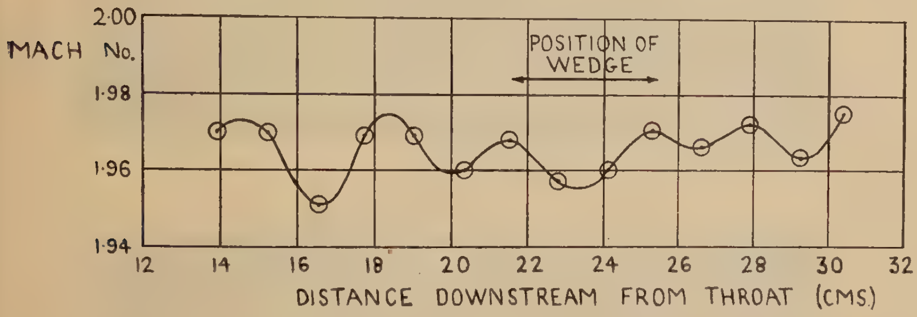

Distribution of Mach No. along centre line.

§ 4. Humidity Measurements.

The humidity of the air passing through the wind-tunnel cannot be measured in the limited time available while the tunnel is running, and an indirect method is therefore necessary. The tunnel is run about three times, starting with an absolute pressure of about 0·1 atmosphere in the reservoir and continuing each run until the pressure in the reservoir is atmospheric. When this has been done nearly all the air in the reservoir has passed through the drier, and a sample of air from the reservoir is therefore representative of the air passing through the wind-tunnel. A compressor is then used to pump air from the atmosphere through the silica gel drier into the reservoir, so that the pressure is slightly greater than atmospheric. A steady stream of air from the reservoir is then passed through a frost-point hygrometer of the type described by Brewer, Cwilong and Dobson (1948).

When the silica gel has just been regenerated the water vapour content of the dried air passing through the wind-tunnel is always less than 1 part in 5000 by weight, and is sometimes very much lower. Normally, the silica gel is regenerated when the water content of the dried air has risen to about 1 part in 2500 by weight.

§ 5. OPTICAL SYSTEM.

The optical apparatus used for the schlieren photographs was a conventional two-mirror system as shown in fig. 3. The two spherical concave mirrors M_1 and M_2 have a focal length of 152 cm. and a diameter of 12·7 cm. L_1 is a condenser lens and L_2 is a long-focus achromatic object lens. For setting up and adjusting the apparatus, and for visual observation of the schlieren image on a screen, a " compact source " mercury vapour lamp is used. The very high brightness of this lamp gives good illumination on the screen, even when the second knife-edge is very close to the position giving complete cut-off. This facilitates exact adjustment of the knife-edges and mirrors.

Fig. 3.

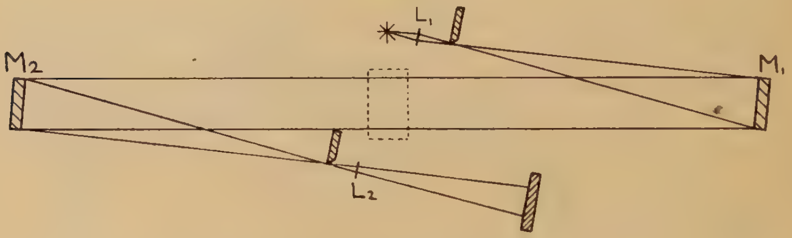

Schlieren optical system.

§ 6. PHOTOGRAPHS OF OBLIQUE SHOCK-WAVES.

The wedge used to produce the shock-waves was 3·8 cm. long in the direction of the stream, had an apex angle of 10·1°, and was made of hardened high-carbon steel. It was ground and lapped to give a constant angle with as sharp an edge as possible ; the thickness of the leading edge was measured and found to be between 2·5 and 12μ. The wedge extended across the whole width of the working section and was supported by two arms on the downstream side.

Fig. 4.

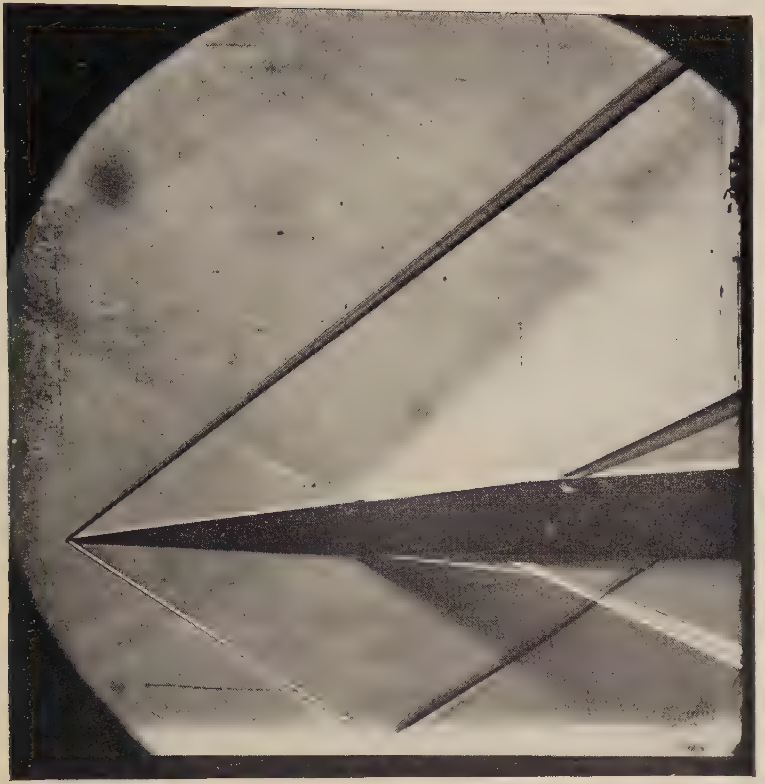

Fig. 5.

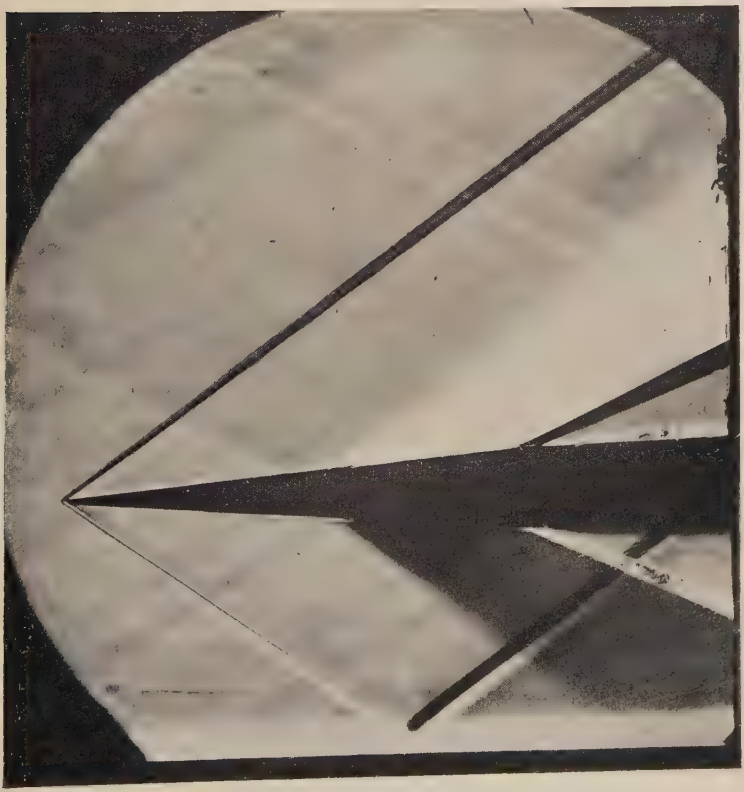

Fig. 6.

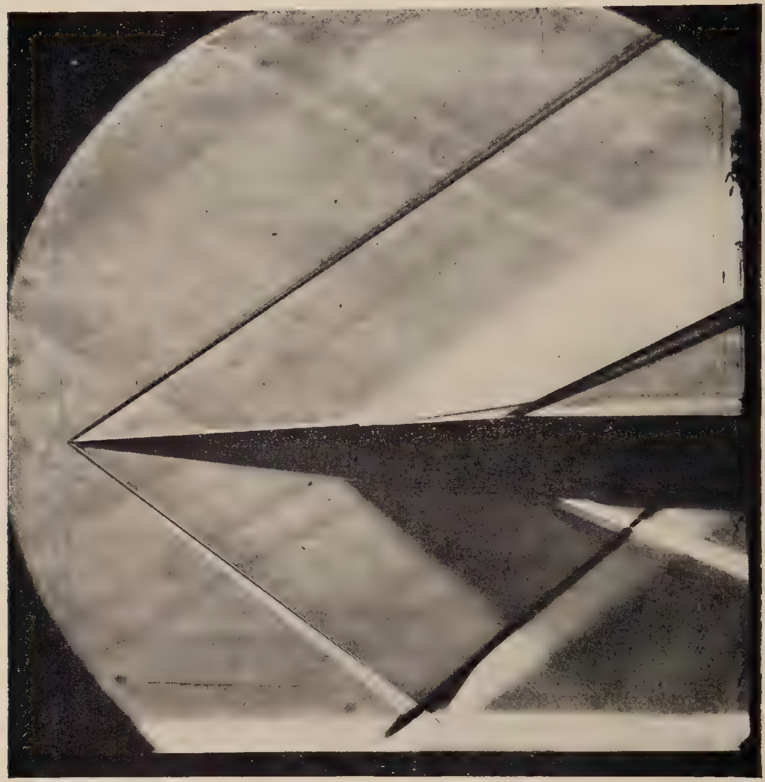

Fig. 7.

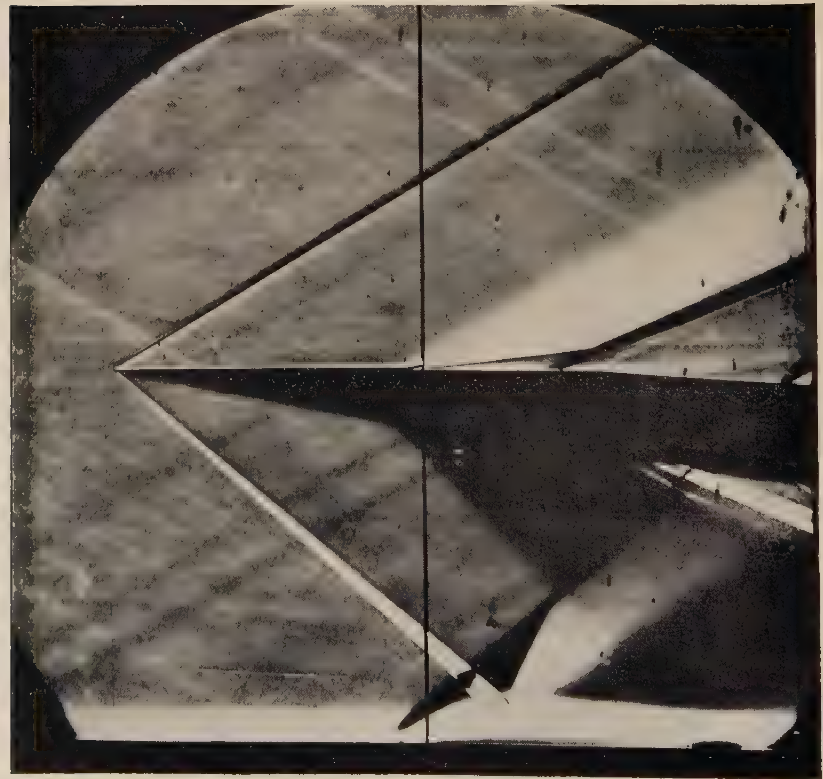

Fig. 8.

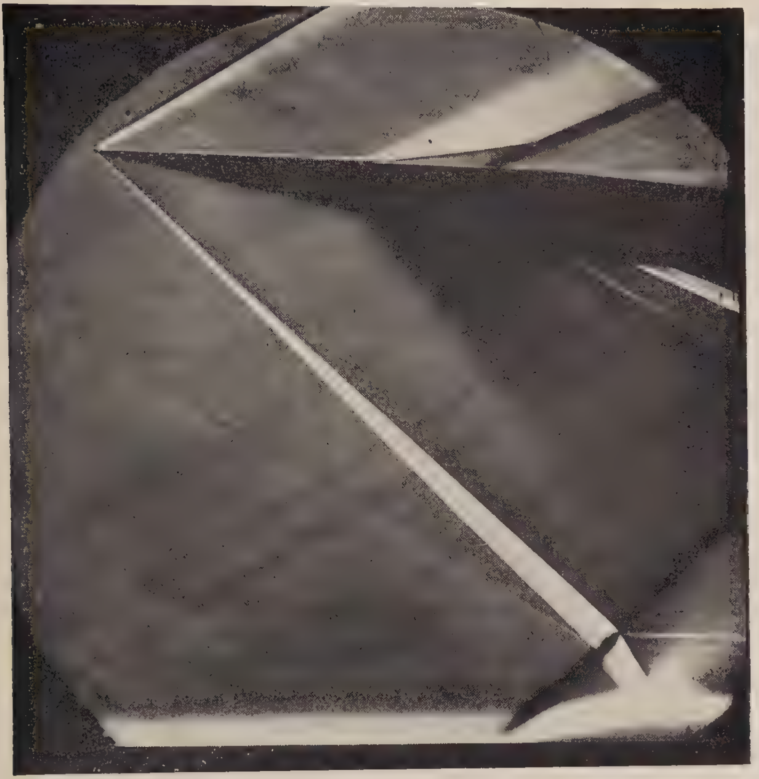

Fig. 9.

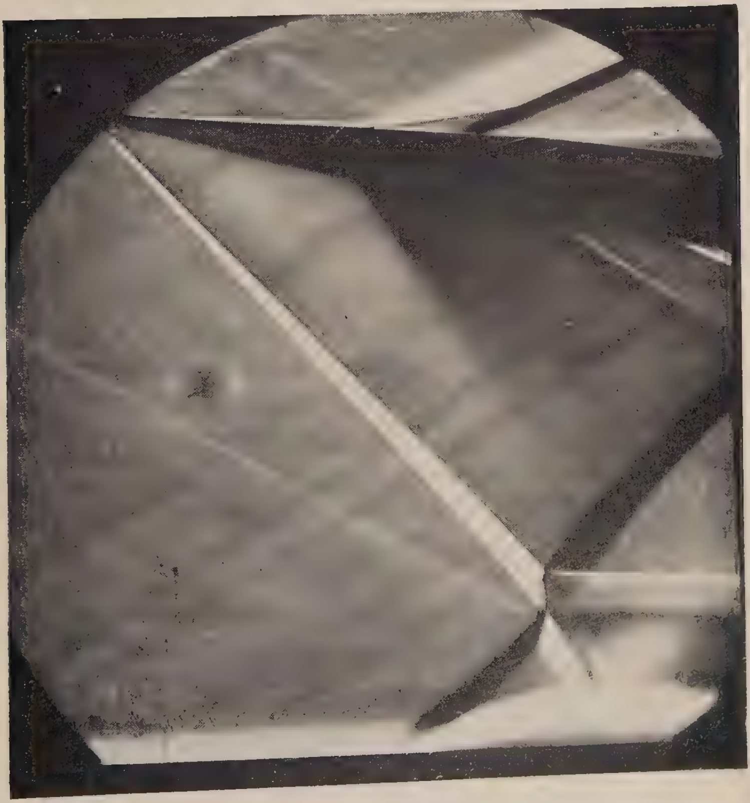

FIG. 10.

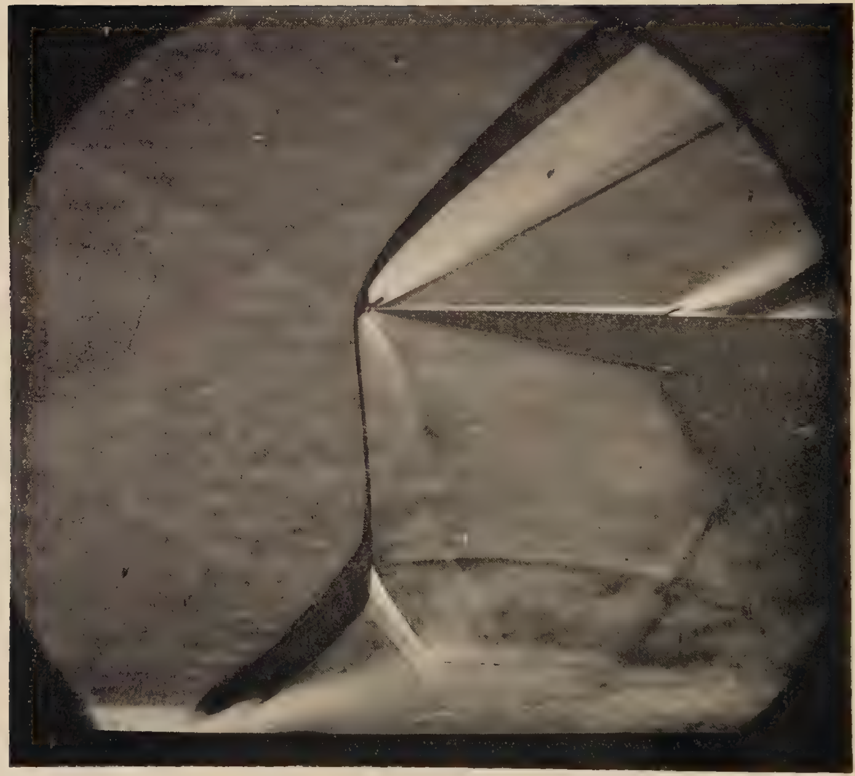

The schlieren system was arranged with horizontal knife-edges so that increasing air density in an upward direction corresponded to a light region in the photograph.

Preliminary visual observations showed that the flow was steady, so that a relatively long exposure ($\frac{1}{20}$th second) could be used for the photographs. The mercury vapour lamp gave considerably more light than was necessary for photography, and a slow "process" film was used, with a yellow filter to reduce its effective speed. This arrangement was convenient, as it enabled a single light source to be used for visual observation and photography. Figs. 4 to 9 (Pls. I. to IV.) are photographs of the flow for positions of the wedge giving deflection angles (δ) of 2·9°, 5·0°, 7·3°, 9·8°, 12·1° and 15·2°. In each case the flow is from left to right. Table I. gives the strengths (χ) of the incident shock-waves, calculated from the values of δ.

§ 7. DISCUSSION OF PHOTOGRAPHS.

The arms suporting the wedge continue downstream beyond the edge of the field of view. The position of the back of the wedge is revealed by the two large expansion regions. The joints in the supporting arms produce two shock-waves at the right-hand side of each photograph. In addition, several wavelets from the liners are visible and a scratch on one of the glass walls may be seen in the bottom left-hand corner of each photograph. In fig. 7 the vertical black line across the middle of the photograph is a reference mark to show the position of the wedge in the tunnel.

The thickness of the light region representing the boundary-layer on the tunnel wall is about 4 mm. at a point 24 cm. downstream of the throat. This indicates that the boundary-layer was turbulent, as would be expected at such a high Reynolds number ($1{\cdot}34 \times 10^5$ per cm. in the working section). In all cases the tunnel wall was flat at the point of incidence of the shock-wave.

In each photograph the thickness of the line representing the incident shock-wave increases with distance from the leading edge of the wedge. This is probably because the flow is not two-dimensional, so that the shock-wave is not plane over the whole section of the tunnel. The reduced velocity in the outer part of the turbulent boundary-layer on each glass wall increases the shock-wave angle in that region and hence explains this fan-shaped appearance. Thus the downstream side of the "fan" represents the true position of the shock-wave outside the boundary-layer. This explanation is supported by fig. 4, showing the weakest incident shock-wave, in which the fan-shaped region is very faint except at the downstream edge. Similarly, in figs. 4 to 7, the same effect can be seen in the fan-shaped region representing the shock-wave on the upper surface.

In Table I. the stream deflections and shock-wave angles are considered. For a given stream deflection angle (δ) the theoretical value of the shock-wave angle (α_0) has been calculated and compared with the measured angles at the upstream and downstream edges of the fan (α_1 and α_2). It can be seen that α_0 agrees much better with α_2 than with α_1, again showing that the downstream edge of the fan corresponds to the position of the shock-wave outside the boundary-layer. Part of the difference between the values of α_0 and α_2 may be explained by the growth of the boundary-layer on the wedge, causing an increase in the effective value of δ.

In the light fan-shaped region representing the incident shock-wave in figs. 4 to 7, there is a dark line near the downstream edge. The reason for this is not understood but further work is being done to investigate the flow at the sharp leading edge of a wedge.

TABLE I.

Fig. no.	δ	χ	α_0	α_1	α_2
4	2·9°	0·17	33·0°	—	33·6°
5	5·0°	0·31	34·9°	37·4°	35·6°
6	7·3°	0·48	37·2°	39·5°	37·8°
7	9·8°	0·68	39·8°	42·1°	40·1°
8	12·1°	0·90	42·6°	45·9°	43·4°
9	15·2°	1·20	46·6°	49·4°	47·1°

Figs. 4 and 5 show that a weak shock-wave is reflected as a compression followed by an expansion, *i. e.* as a pressure *ridge*. The dark region after the expansion indicates that there is a further compression there, with a smaller density gradient than in the first compression. The expansion appears to get weaker with increasing distance from the boundary; this would be expected as a result of interaction with the compression waves. At a sufficient distance from the boundary the expansion probably disappears completely, and the reflection of a weak shock-wave is then simply another shock-wave. These conclusions are in agreement with Lighthill's theory (1950) in which the boundary-layer is replaced by a non-turbulent inviscid layer with the same velocity distribution as a turbulent boundary-layer.

The above description applies to incident shock-waves with strengths (χ) up to about 0·4. For these strengths there is no appreciable thickening of the boundary-layer upstream of the shock-wave and no separation. When the strength of the shock-wave is more than about 0·4, however (figs. 6 to 9, Pls. II. & III.), the boundary-layer begins to thicken and separate on the upstream side of the incident wave and the reflected shock-wave moves up to this point. Thus the incident and reflected shock-waves cross at a point outside the boundary-layer. As the incident shock-wave becomes stronger the foot of the reflected wave moves further upstream and the point of intersection moves further away from the boundary. An expansion still occurs after the reflected shock-wave, but this remains near the point where the incident shock-wave meets the boundary-layer. In this region the rate of growth of the boundary-layer suddenly decreases, and there is a corresponding deflection of the stream due to the expansion. In figs. 6 and 7 there is a dark region after the expansion, indicating a further gradual compression similar to that occurring with the weaker shock-waves. The concave shape of the outer edge of the boundary-layer in this region can be seen clearly in fig. 7. The boundary-layer must always have a concave shape where there is a compression region, but it is not easily seen in the other photographs. The second compression would be expected to occur also for the stronger shock-waves in figs. 8 and 9 but in these photographs it is almost outside the field of view. (The dark region representing the compression after the expansion in figs. 6 and 7 should not be confused with the dark expansion region caused by the back of the wedge.)

Fig. 11.

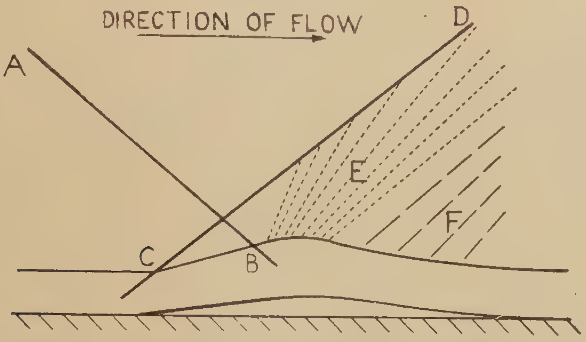

Reflection of oblique shock-wave of medium strength $(0{\cdot}5<\chi<0{\cdot}9)$.

The dark region near the tunnel wall in figs. 7 to 9 shows that the boundary-layer has separated near the foot of the reflected shock-wave. This dark region is just visible in fig. 6 ($\chi=0{\cdot}48$), suggesting that separation of the boundary-layer occurs if χ is more than about 0·45. Figs. 6 and 7 show a re-attachment of the boundary-layer further downstream. This probably occurs in all cases, but in figs. 8 and 9 the point of re-attachment is outside the field of view.

Fig. 11 is a diagram showing the typical configuration for incident shock-waves of strength (χ) between 0·5 and 0·9. AB is the incident shock-wave entering the boundary-layer at B. The boundary-layer separates and begins to thicken at C, and the reflected shock-wave CD passes through this point. At a short distance downstream of B there is an expansion region E where the rate of growth of the boundary-layer decreases rapidly through zero. After the expansion the outer edge of the boundary-layer becomes concave and this causes a gradual compression in the region F.

In fig. 9 the strength of the incident shock-wave is so great that its interaction with the reflected wave is of Mach type, with a short normal shock-wave between two intersections. Experiments by Fage and Sargent (1947) have shown that a strong normal shock-wave has a bifurcated foot where it enters a turbulent boundary-layer. It is suggested that the bifurcation at the foot of the Mach shock-wave in fig. 9 is similar to that of any normal shock-wave interacting with a turbulent boundary-layer at this Mach number, since the conditions at the upper end of the Mach shock-wave should not have much effect on the bifurcation at the lower end. For example, a similar configuration was observed with the wedge set at an incidence so high that the tunnel was choked and the normal starting shock-wave remained in the working section (fig. 10). (For this photograph a short-duration flash was used, as the flow was not quite steady.) The bifurcation of the normal shock-wave in this case is similar to that shown at the foot of the Mach shock-wave in fig. 9.

This means that for any oblique shock-wave with $\chi > 1{\cdot}2$ the bifurcated foot of the Mach shock-wave and the separating boundary-layer would be generally similar to figs. 9 and 10.

It is perhaps of interest to point out the vortex sheets that arise at the intersections of the shock-waves in figs. 8, 9 and 10.

At lower Mach numbers than in these experiments (*i. e.* $M < 1{\cdot}965$) Mach reflection would occur for weaker incident shock-waves. Thus the upper limit of shock-wave strength giving a cross formation similar to fig. 11 (without a Mach shock-wave) would decrease with Mach number. At the same time the lower limit of shock-wave strength giving this configuration would probably not change much with Mach number, since it depends on the separation or thickening of the boundary-layer caused by the shock-wave. Thus the range of shock-wave strengths giving a cross formation, without a Mach shock-wave, would become more restricted with decreasing Mach number. This means that for sufficiently low Mach numbers this formation would not occur for a shock-wave of any strength. Weak shock-waves would give reflections like figs. 4 and 5 and stronger ones would give Mach reflection, either with or without a bifurcated foot. This probably explains why Fage and Sargent (1947) did not find configurations like figs. 6, 7 and 8.

References.

Brewer, A. W., Cwilong, B., and Dobson, G. M. B., 1948, *Proc. Phys. Soc.*, **60,** 52–70.

Fage, A., and Sargent, R. F., 1947, *Proc. Roy. Soc.* A, **190,** 1–20.

Lighthill, M. J., 1950, *Quart. Journ. Mech. App. Math.* (in press).

Neumann, E. P., and Lustwerk, F., 1949, *Journ. App. Mech.*, **16,** 195–202.

IV. *Collision broadening at Microwave Frequencies.*

By D. C. M. Leslie, M.A.,
Clarendon Laboratory, Oxford *.

[Received September 14, 1950.]

Summary.

A theoretical formula is deduced for the broadening and shift of spectral lines due to collisions; this formula is valid in the microwave region, for gases at low pressures. It is assumed that the partial collision amplitudes f for the bimolecular collision problem are known, and using these, the equation of motion of the two-molecule density matrix is found. A formula for the line broadening and shift follows from this.

Using the equation of motion of the density matrix, it is also shown that a Boltzmann distribution is the only equilibrium one.

§1. Introduction.

There are three causes of the broadening of the spectral lines emitted by a gaseous radiator, namely, radiation damping, Doppler broadening, and effects due to intermolecular interactions. These effects are very complicated, and it is only at low pressures, where bimolecular collisions are the dominant interaction mechanism, that a detailed theoretical treatment is feasible. The low-pressure effect is called collision broadening.

Reducing the gas pressure naturally reduces the pressure broadening, and in the optical region, this effect is obscured by Doppler broadening. However, Doppler broadening is proportional to the radiated frequency ω, while collision broadening is independent of ω; hence, at sufficiently low frequencies, collision broadening must predominate. It turns out that this is the case in the microwave region ($\lambda \sim 1$ cm.).

Since the war, a number of accurate experiments have been done on collision broadening in the microwave region—notably those of Bleaney and Penrose (1947) on the inversion spectrum of NH_3—and this has stimulated theoretical work on the subject.

Karplus and Schwinger (1948) have taken the important step of transcribing the classical theories of Van Vleck and Weisskopf (1945) and Fröhlich (1946) into quantum form; they are then able to account for saturation. They show that the correct tool for this type of calculation is von Neumann's density matrix; its equation of motion may be written

$$\frac{\partial U}{\partial t} = \frac{1}{i\hbar}(H^0U - UH^0) + \frac{\partial_e U}{\partial t}, \quad . \quad . \quad . \quad . \quad . \quad . \quad (1.1)$$

---

* Communicated by Professor M. H. L. Pryce.

where H^0 is the internal Hamiltonian of one molecule, and $\partial_e/\partial t$ denotes the rate of change of an operator due to collisions. Their assumption is equivalent to setting

$$\frac{\partial_e U}{\partial t} = -\sigma(U - U_e), \qquad \text{(1.2)}$$

where U_e is the equilibrium statistical matrix (we use the terms "density" or "statistical" matrix indifferently). The original collision-broadening theory of Lorentz was equivalent to setting

$$U_e = \text{const.} \exp(-H^0/kT).$$

Van Vleck and Weisskopf (1945) pointed out that in the microwave region, the oscillating electric field applied to the gas (such measurements are always made in absorption) was essentially "slow," *i.e.*, that the collisions would attempt to maintain an instantaneous Boltzmann distribution.

$$U_e = \text{const.} \exp\{-(H^0 - \boldsymbol{\mu}.\mathbf{F}\cos \nu t)/kT\}$$

ν being the frequency of the applied field. Owing to the rapid variation of this field, the actual statistical matrix will be different from U_e. This assumption gives a line shape in agreement with experiment.

However, this phenomenological approach does not give any theoretical connection between the line width σ and the intermolecular potential $V(\mathbf{r})$. A theory due to Anderson (1949) has had considerable success in this direction, but it contains a number of assumptions which can be avoided. The theory presented below is restricted only by fundamental physical assumptions, namely that the gas pressure is small, and the applied field slow, in the sense explained above : this is believed to be true in the microwave region.

§ 2. CALCULATION OF $\partial_e U/\partial t$.

Karplus and Schwinger's equation (1.2) is certainly too restrictive, but for a U not far removed from equilibrium, the equation

$$\left\langle a \left| \frac{\partial_e U}{\partial t} \right| b \right\rangle = \sum_{cd} L(ab, cd)\langle c | U - U_e | d \rangle, \qquad \text{(2.1)}$$

must hold, since the definition of equilibrium is

$$\frac{\partial_e U_e}{\partial t} = 0.$$

The object of this section is to calculate the coefficients $L(ab, cd)$ in terms of known quantities.

We have explained that we are taking bimolecular collisions to be the only mechanism producing broadening, and we therefore want to investigate the effect of bimolecular collisions on S, the statistical matrix of an individual molecule (U is an averaged statistical matrix). We shall have to use a generalized statistical matrix D describing the external, as well as the internal, motions of the molecule. The external coordinates are continuous, and hence, in a coordinate representation, D will be a matrix in the internal coordinates, with each element a function of two external vector variables **r** and **r**′ (such a representation was first discussed by Born and Green, 1947).

S is very simply related to D, being its external trace;

$$\mathrm{S}=\iint \mathrm{D}(\mathbf{r}, \mathbf{r}') \,.\, \delta(\mathbf{r}-\mathbf{r}') \,.\, d^3\mathbf{r} \,.\, d^3\mathbf{r}'=\int \mathrm{D}(\mathbf{r}, \mathbf{r}) \,.\, d^3\mathbf{r}, \quad . \quad . \quad . \quad (2.2)$$

the integral being taken over unit volume. As a simple example, the matrix

$$\mathrm{D}=\mathrm{S} \exp [i\mathbf{k} \,.\, (\mathbf{r}-\mathbf{r}')],$$

describes a plane wave in a specified internal condition S.

To discuss bimolecular collisions, we must work in a 2-molecule Hilbert space, which is the direct product of two one-molecule spaces.

$$\mathscr{H}_2=\mathscr{H}_1^{(1)}\times\mathscr{H}_1^{(2)}.$$

As long as there is no correlation between molecules about to collide, which is certainly true in dilute gases, D_2 the density matrix in $\mathscr{H}_2$, is given before collision, by

$$\mathrm{D}_2=\mathrm{D}_1^{(1)}\wedge\mathrm{D}_1^{(2)},$$

where the symbol $\wedge$ denotes the Kronecker product of two matrices. D_2 has to describe the external motion of two molecules, and will therefore be a function of four vector variables, $\mathrm{D}_2(\mathbf{r}_1, \mathbf{r}_2 ; \mathbf{r}_1', \mathbf{r}_2')$. S_2, the two-molecule internal density matrix, is obtained from D_2 by a process analogous to (2.2)

$$\mathrm{S}_2=\iint \mathrm{D}_2(\mathbf{r}_1, \mathbf{r}_2 ; \mathbf{r}_1, \mathbf{r}_2) \,.\, d^3\mathbf{r}_1 \,.\, d^3\mathbf{r}_2, \quad . \quad . \quad . \quad . \quad (2.2\,a)$$

S_1, the one-molecule internal density matrix, is then found from

$$\mathrm{S}_1^{(1)}=Tr_2(\mathrm{S}_2). \quad . \quad . \quad . \quad . \quad . \quad . \quad . \quad . \quad (2.2\,b)$$

Tr_2 denoting the operation of taking the trace over the internal coordinates of molecule 2.

We shall suppose that we have, as a basis for $\mathscr{H}_1$, a complete normal orthogonal sequence (c.n.o.s.) $\{|y\rangle\}$ of eigenvectors of H^0, the internal Hamiltonian of one molecule, corresponding to energies $\{\mathrm{E}_y\}$. A suitable basis for $\mathscr{H}_2$ is then the c.n.o.s.

$$\{|a\rangle\}=\{|y\rangle|z\rangle\},$$

whose energies are $\{\mathrm{E}_a\}$, $\mathrm{E}_a=\mathrm{E}_y+\mathrm{E}_z$.

The Hamiltonian of a system of two interacting molecules is

$$\mathrm{H}_2=\mathrm{H}^0(1)+\mathrm{H}^0(2)+\frac{1}{2m}(p_1^2+p_2^2)+\mathrm{V},$$

where $H^0(1)$ and $H^0(2)$ are the internal Hamiltonians of the molecules (1) and (2), $\mathbf{p}_1$ and $\mathbf{p}_2$ their momenta, and V the interaction potential between them. Since we are assuming the electric field to be slow, we do not need to consider it while discussing collisions. We set

$$H^0(1)+H^0(2)=H_2^0,$$

the two-molecule internal Hamiltonian, which satisfies

$$H_2^0|a\rangle=E_a|a\rangle.$$

We also set

$$\mathbf{r}=\mathbf{r}_1-\mathbf{r}_2\ ,\ \mathbf{R}=\tfrac{1}{2}(\mathbf{r}_1+\mathbf{r}_2),$$

and similarly with $\mathbf{r}_1'$, $\mathbf{r}_2'$; then

$$H_2=H_2^0-\frac{\hbar^2}{m}(\nabla_r^2+\tfrac{1}{4}\nabla_R^2)+V(\mathbf{r}). \qquad (2.3)$$

The equation of motion of D_2 is

$$i\hbar\frac{\partial D_2}{\partial t}=H_2D_2-D_2H_2,$$

and with H_2 in the form (2.3), this can be separated. We write

$$H_2=H_2'-\frac{\hbar^2}{4m}\nabla_R^2,\ \text{where}\ H_2'=H_2^0-\frac{\hbar^2}{m}\nabla_r^2+V(\mathbf{r})$$

and

$$D(\mathbf{r},\mathbf{R};\mathbf{r}',\mathbf{R}')=\rho(\mathbf{r},\mathbf{r}').J(\mathbf{R},\mathbf{R}'),$$

ρ and J must then satisfy

$$i\hbar\frac{\partial\rho}{\partial t}=H_2'\rho-\rho H_2' \qquad (2.4\,a)$$

and

$$i\hbar\frac{\partial J}{\partial t}=-\frac{\hbar^2}{4m}(\nabla_R^2-\nabla_R'^2)J(\mathbf{R},\mathbf{R}'), \qquad (2.4\,b)$$

ρ is therefore a matrix in the internal variables, but J is a function of $\mathbf{R}$ and $\mathbf{R}'$ only. A particular solution of (2.4 *b*) is

$$J(\mathbf{R},\mathbf{R}')=\exp\{i\varkappa.(\mathbf{R}-\mathbf{R}')\},$$

representing uniform motion of the centre of gravity of the two-molecule system. A more general solution of this type is

$$J(\mathbf{R},\mathbf{R}')=\int f(\varkappa)\exp\{i\varkappa.(\mathbf{R}-\mathbf{R}').\,d^3\varkappa,$$

where $f(\varkappa)$ is a normalized function giving the distribution of velocities of the centres of gravity of the two-molecule systems. At equilibrium, $f(\varkappa)$ will be a Maxwellian distribution, since the oscillating electric field will not influence the external motion of the molecules.

We cannot solve (2.4 *a*) in the same way, since as we shall explain shortly, $V(\mathbf{r})$ must be taken to be time-dependent. S_2 is then given by

$$S_2 = \iint \rho(\mathbf{r}, \mathbf{r}) J(\mathbf{R}, \mathbf{R}) . \, d^3\mathbf{r} \, d^3\mathbf{R},$$

(since $d^3\mathbf{r}_1 . d^3\mathbf{r}_2 = d^3\mathbf{r} . d^3\mathbf{R}$)

$$= \iint \rho(\mathbf{r}, \mathbf{r}) f(\varkappa) . \, d^3\mathbf{r} . d^3\varkappa = \int \rho(\mathbf{r}, \mathbf{r}) . d^3\mathbf{r}.$$

The coordinate **R** does not, therefore, enter into the problem, and we have only to find a suitable solution of (2.4 *a*).

Now if we were to solve the ordinary static collision problem, we should only find the effect of one collision on a molecule. To attempt to find the effect of repeated collisions using a time-independent V would mean solving a many-body dynamical problem.

This can be avoided by solving a two-molecule time-dependent problem (it is our assumption that binary collisions are the only important interaction mechanism that makes this simplification possible). We take the potential to be given by

$$V(\mathbf{r}, t) = V(\mathbf{r}) \text{ if } T - \tau \leqslant t \leqslant T \qquad (T > 0),$$
$$= 0 \text{ otherwise},$$

$V(\mathbf{r})$ being the given time-independent interaction potential. The initial condition is that at time $t=0$

$$\rho(\mathbf{r}, \mathbf{r}') = \int S_2 g(\mathbf{k}) \exp \{ i\mathbf{k} . (\mathbf{r} - \mathbf{r}') \} . d^3\mathbf{k},$$

corresponding to a superposition of plane waves ; $g(\mathbf{k})$ is a velocity distribution function which we shall later be able to show to be Maxwellian. We shall show how the solution of this problem can be used when we have obtained it.

We shall assume that the asymptotic solution of the time-independent two-molecule collision problem is known in wavefunction form. In detail, we shall know that if the incident wave is given by

$$\langle a, \mathbf{r} | I \rangle = [\exp (i\mathbf{k} . \mathbf{r})] \delta_{am}, \quad \ldots \ldots \quad (2.5\ a)$$

(representing a wave with momentum $\hbar k$ incident on a scatterer in state $|m\rangle$), then the asymptotic scattered wave will be given by

$$\langle a, \mathbf{r} | S \rangle = \frac{\exp (ik_{ma} r)}{r} \langle a | f(\mathbf{k}, \mathbf{k}_{ma}) | m \rangle, \quad \ldots \quad (2.5\ b)$$

where

$$k_{ma}^2 = k^2 + \frac{m}{\hbar^2} (E_m - E_a). \quad \ldots \ldots \quad (2.6)$$

The coefficients f all being known. The complete asymptotic solution of the collision problem is then

$$|C\rangle = |I\rangle + |S\rangle. \quad \ldots \ldots \quad (2.5\ c)$$

All states occurring in formula (2.5) are two-molecule states. The ket $|\,\mathrm{C}\rangle$ is usually thought of as being given by Schrödinger's equation—a differential equation—but it can equally well be regarded as being determined by the integral equation

$$\langle a, \mathbf{r}\,|\,\mathrm{S}\rangle = -\frac{m}{4\pi\hbar^2}\sum_b \int \frac{\exp\,(ik_{ma}\sigma)}{\sigma}\,\langle a\,|\,\mathrm{V}(\mathbf{s})\,|\,b\rangle\langle b,\,\mathbf{s}\,|\,\mathrm{C}\rangle\,.\,d^3\mathbf{s}, \quad . \quad (2.7)$$

where $\boldsymbol{\sigma}=\mathbf{r}-\mathbf{s}$.

The determination of the f's in the case of inelastic scattering is always very difficult, and it is made doubly so in these collision-broadening problems by the fact that we are usually dealing with non-central potentials. The Born approximation is not satisfactory, since the thermal motions with which we are concerned are quasi-classical (see Anderson, 1949). This problem is quite distinct from the statistical problem now under discussion, but it is hoped to take it up in a later paper.

The scattered wave (2.5 *b*) has the form of a spherical wave in free space ; this form can therefore only be valid at large distances from the scattering centre, where the interaction potential is inappreciable (this is what we mean when we call it an asymptotic solution). A solution of this kind will only tell us about that part of the line broadening due to " permanent " changes in the molecules produced by collisions ; this type is referred to as " impact " broadening, and will plainly depend on the intermolecular velocity.

The other type, called " statistical " broadening, is due to transient changes in the molecules, which disappear as they move apart. Statistical broadening may be pictured as being due to changes in the energy levels of molecule (1) due to the influence of molecule (2). This will alter the radiated frequency, and the aggregate effect is to broaden the lines of the spectrum. These two types of broadening have been carefully discussed by Margenau and Watson (1936).

The actual broadening will be due to a mixture of the two types, but it is generally thought that the collision broadening of microwave lines is mainly of the impact type : this is because collisions only last for a fraction of a cycle of the applied electric field. Recently, Howard and Smith (1950) have measured the temperature dependence of a prominent line in the inversion spectrum of $\mathrm{NH_3}$; their measurements support this view.

We must now consider the solution of (2.4 *a*). It may be written in the form

$$\rho(t)=\mathrm{R}(t)\rho(0)\mathrm{R}^*(t),$$

where the unitary operator R satisfies

$$i\hbar\frac{\partial\mathrm{R}}{\partial t}=\mathrm{H}_2'\mathrm{R}. \quad . \quad . \quad . \quad . \quad . \quad . \quad . \quad . \quad (2.8)$$

Because of the form of $\rho(o)$, the equation for $\rho(t)$ is equivalent to

$$\langle a, \mathbf{r} | \rho(t) | b, \mathbf{s} \rangle = \sum_{cd} \int g(\mathbf{k}) \, . \, d^3\mathbf{k} \, . \, \langle a | \phi(\mathbf{r}, t) | c \rangle \langle c | \mathrm{S}_2(\mathrm{O}) | d \rangle \langle d | \phi^*(\mathbf{s}, t) | b \rangle, \quad . \quad . \quad . \quad (2.9)$$

where ϕ is defined by

$$\langle a | \phi(\mathbf{r}, t) | b \rangle = \int \langle a, \mathbf{r} | \mathrm{R}(t) | b, \mathbf{s} \rangle \exp(i\mathbf{k} \, . \, \mathbf{s}) \, . \, d^3\mathbf{s}.$$

We shall now show that ϕ can be simply expressed in terms of the f's.

We write

$$\mathrm{H}_2' = \mathrm{H}_0 + \mathrm{V}(\mathbf{r}, t),$$

where H_0, the " non-interaction " part of H_2', is defined by

$$\mathrm{H}_0 = \mathrm{H}_2^0 + \frac{1}{m} p^2.$$

Later, we shall need the symbol H_0 to denote $\mathrm{H}^0 - \boldsymbol{\mu} \, . \, \mathbf{F} \cos \nu t$: this sort of duplication is inevitable if we wish to use " H " for all the Hamiltonians occurring in the problem.

(2.8) is equivalent to the integral equation

$$\mathrm{R} = \exp(\mathrm{H}_0 t / i\hbar) + \frac{1}{i\hbar} \int_{\mathrm{T}-\tau}^{\mathrm{T}} \exp\{\mathrm{H}_0(t-t')/i\hbar\} \mathrm{V} \, . \, \mathrm{R}(t') \, dt'.$$

From this, we deduce that ϕ satisfies

$$\langle a | \phi(\mathbf{r}) | m \rangle = [\exp(i\mathbf{k} \, . \, \mathbf{r})] \, . \, \delta_{am} \, . \, \exp \frac{(\mathrm{E}_m + \hbar^2 k^2/m)t}{i\hbar}$$

$$+ \frac{1}{i\hbar} \sum_{bc} \int_{\mathrm{T}-\tau}^{\mathrm{T}} \int \langle a, \mathbf{r} | \exp\{\mathrm{H}_0(t-t')/i\hbar\} | b, \mathbf{s} \rangle \, d^3\mathbf{s}$$

$$\times \langle b | \mathrm{V}(\mathbf{s}) | c \rangle \langle c | \phi(\mathbf{s}) | m \rangle \, dt'.$$

The interpretation of the representative

$$\langle a, \mathbf{r} | \exp\{\mathrm{H}_0(t-t')/i\hbar | b, \mathbf{s} \rangle\}$$

is not immediately obvious, but, by transforming from a momentum representation, we find that it is equal to

$$\frac{\delta_{ab}}{(2\pi\hbar)^3} \left(\frac{\pi}{ix}\right)^{3/2} \exp\left\{i\left(\frac{\sigma^2}{4x\hbar^2} - m\mathrm{E}_a x\right)\right\},$$

where $x = (t - \mathrm{t}')/m\hbar$ and $\boldsymbol{\sigma} = \mathbf{r} - \mathbf{s}$. Now for $t < \mathrm{T} - \tau$, $\phi | m \rangle$ varies with t according to

$$\exp \frac{(\mathrm{E}_m + \hbar^2 k^2/m)t}{i\hbar}.$$

showing that it is a ket-vector corresponding to a state of energy $(\mathrm{E}_m + \hbar^2 k^2/m)$. Now the system we are considering is conservative, so that its energy will be the same for $t > \mathrm{T} - \tau$. Hence, if we define ψ by

$$\langle a | \phi(\mathbf{r}, t) | m \rangle = \langle a | \psi(\mathbf{r}, t) | m \rangle \exp \frac{(\mathrm{E}_m + \hbar^2 k^2/m)t}{i\hbar},$$

ψ will not have any oscillatory dependence on t. It will satisfy the integral equation

$$\langle a|\psi(\mathbf{r})|m\rangle=\delta_{am}\exp(i\mathbf{k}\,.\,\mathbf{r}+\frac{m}{i(2\pi\hbar)^3}\sum_b\int\langle a|\mathrm{V}(\mathbf{s})|b\rangle\,d^3\mathbf{s}$$
$$\times\int_{x_1}^{x_2}\left(\frac{\pi}{ix}\right)^{3/2}\left\{\exp i\left(\frac{\sigma^2}{4x\hbar^2}+\hbar^2k_{ma}^2x\right)\right\}.\langle b|\psi(\mathbf{s})|m\rangle\,dx,$$

where $$x_1=\frac{t-\mathrm{T}}{m\hbar}\quad\text{and}\quad x_2=\frac{t-\mathrm{T}+\tau}{m\hbar}.$$

The x-integral may be evaluated by the method of stationary phases (see Jeffreys and Jeffreys, 1946, p. 474). The asymptotic form of the equation turns out to be

$$\langle a|\psi(\mathbf{r})|m\rangle=\delta_{am}\exp(i\mathbf{k}\,.\,\mathbf{r})-\frac{m}{4\pi\hbar^2}\mathrm{Q}(r)\sum_b\int\frac{\exp(ik_{ma}\sigma)}{\sigma}$$
$$\times\langle a|\mathrm{V}(\mathbf{s})|b\rangle\langle b|\psi(\mathbf{s})|m\rangle\,d^3\mathbf{s},$$

where $$\mathrm{Q}(r)=1\ \psi\ \frac{2\hbar k_{ma}(t-\mathrm{T})}{m}\leqslant r\leqslant\frac{2\hbar k_{ma}(t-\mathrm{T}+\tau)}{m}$$
$$=0\text{ otherwise}$$

Hence, by comparison with (2.7), we infer that

$$\langle a|\psi(\mathbf{r})|m\rangle=\delta_{am}\,.\exp(i\mathbf{k}\,.\,\mathbf{r})+\mathrm{Q}(r)\frac{\exp(ik_{ma}r)}{r}\langle a|f\mathbf{k},\,\mathbf{k}_{ma})|m\rangle.$$

Hence in this problem, the " scattered wave " (represented by the second term) is the same as in the time-independent problem inside a shell of radii

$$\frac{2\hbar k_{ma}(t-\mathrm{T})}{m}\qquad\frac{2\hbar k_{ma}(t-\mathrm{T}+\tau)}{m}$$

and zero outside this shell. This shell is just the region which is classically accessible to the molecules, so that this equation is what we would expect on classical grounds. Using it, we can calculate $\rho(t)$, and hence $\mathrm{S}_2(t)$ by integration over the external coordinates. We find, asymptotically, that

$$\langle a|\mathrm{S}_2(t)|b\rangle=\exp(-i\omega_{ab}t)\{\langle a|\mathrm{S}_2(0)|b\rangle+\tau\sum_{cd}\mathrm{K}(ab,\,cd)\langle c|\mathrm{S}_2(0)|d\rangle\}.\qquad\text{. . . (2.10)}$$

where $\hbar\omega_{ab}=\mathrm{E}_a-\mathrm{E}_b$, and

$$\mathrm{K}(ab,\,cd)=\int g(\mathbf{k})\,d^3\mathbf{k}\left\{\frac{2\hbar k_{ca}}{m}\int\langle a|f(\mathbf{k},\,k_{ca}\mathbf{n})|c\rangle\overline{\langle b|f(\mathbf{k},\,k_{ca}\mathbf{n})|d\rangle}\,d\mathbf{n}\right.$$
$$\left.+\frac{4\pi\hbar}{im}[\langle a|f(\mathbf{k},\,\mathbf{k})|c\rangle\delta_{bd}-\overline{\langle b|f(\mathbf{k},\,\mathbf{k})|d\rangle}\delta_{ac}]\right\},\qquad\text{. . (2.11)}$$

n is the unit vector in the direction of **r**, and $d\mathbf{n}$ denotes integration over solid angle, *i. e.*, over all directions of scattering; $g(\mathbf{k})$ is the velocity distribution function. There are energy restrictions on the states occurring in the various terms of $\mathrm{K}(ab, cd)$; these are

$\omega_{ab}=\omega_{cd}$ for the first term
$\omega_{ac}=0$,, second ,,
$\omega_{bd}=0$,, third ,,

The first term represents the true scattered wave, while the second and third terms represent "shadow scattering" or loss from the incident wave due to the scattering process (we shall later justify this identification by classical analogy).

In the absence of the interaction V, the time development of the density matrix is given by

$$\langle a|\mathrm{Z}_2(t)|b\rangle=\exp(-i\omega_{ab}t)\langle a|\mathrm{S}_2(\mathrm{O})|b\rangle$$

(the symbol Z will always be used in this sense in future). Equation (2.10) can then be written

$$\langle a|\mathrm{S}_2(t)|b\rangle=\langle a|\mathrm{Z}_2(t)|b\rangle+\tau\sum_{cd}\mathrm{K}(ab, cd)\langle c|\mathrm{Z}_2(t)|d\rangle, \quad . \quad (2.10\,a)$$

which represents the effect of the interaction as a term proportional to τ, the time during which it is effective.

In future, the symbols $|a\rangle, |b\rangle, |c\rangle$, and $|d\rangle$ will be reserved for two-molecule states, and all other symbols will refer to one-molecule states. The quantity we are really interested in is not S_2, but S_1: now $\mathrm{S}_2=\mathrm{S}_1^{(1)}\wedge\mathrm{S}_1^{(2)}$, or, in representative form

$$\langle a|\mathrm{S}_2|b\rangle=\langle g|\mathrm{S}_1^{(1)}|h\rangle\langle y|\mathrm{S}_1^{(2)}|\mathrm{Z}\rangle.$$

Taking the trace of (2.10 *a*) over the coordinates of molecule (2), we get

$$\langle g|\mathrm{S}_1^{(1)}(t)|h\rangle=\langle g|\mathrm{Z}_1^{(1)}(t)|k\rangle \\ +\tau\sum_{ij,wx,y}\mathrm{K}(gy, hy;\ ij, wx)\langle i|\mathrm{Z}_1^{(1)}(t)|w\rangle\langle j|\mathrm{Z}_1^{(2)}(t)|x\rangle. \quad . \quad . \quad . \quad (2.12)$$

From a quantum-mechanical view-point, the molecule (1) must be regarded as interacting with all the (N−1) other molecules in unit volume. Thus equation (2.12) is incomplete, and should actually read

$$\langle g|\mathrm{S}_1^{(1)}(t)|h\rangle=\langle g|\mathrm{Z}_1^{(1)}(t)|h\rangle \\ +\tau\sum_{r=2}^{\mathrm{N}}\sum_{ij,wx,y}\mathrm{K}(gy, hy;\ ij, wx)\langle i|\mathrm{Z}_1^{(1)}(t)|w\rangle\langle j|\mathrm{Z}_1^{(r)}(t)|x\rangle.$$

The matrix U of §1 is defined by

$$\mathrm{NU}=\sum_{r=1}^{\mathrm{N}}\mathrm{S}_1^{(r)},$$

and similarly we may define

$$\mathrm{NW}=\sum_{r=1}^{\mathrm{N}}\mathrm{Z}_1^{(r)}.$$

Since N is very large, (2.12) can be written, with negligible error,

$$\langle g|\mathrm{S}_1^{(1)}(t)|h\rangle=\langle g|\mathrm{Z}_1^{(1)}(t)|h\rangle$$
$$+\mathrm{N}\tau\sum_{ij,\,wx,\,y}\mathrm{K}(gy,hy;\,ij,wx)\langle i|\mathrm{Z}_1^{(1)}(t)|w\rangle\langle j|\mathrm{W}(t)|x\rangle.$$

The same equation holds for any other molecule in the gas, *i. e.*

$$\langle g|\mathrm{S}_1^{(r)}(t)|h\rangle=\langle g|\mathrm{Z}_1^{(r)}(t)|h\rangle$$
$$+\mathrm{N}\tau\sum_{ij,\,wx,\,y}\mathrm{K}(gy,hy;\,ij,wx)\langle i|\mathrm{Z}_1^{(r)}(t)|w\rangle\langle j|\mathrm{W}(t)|x\rangle.$$

Summing this over all r, we have finally

$$\langle g|\mathrm{U}(t)|h\rangle=\langle g|\mathrm{W}(t)|h\rangle$$
$$+\mathrm{N}\tau\sum_{ij,\,wx,\,y}\mathrm{K}(gy,hy;\,ij,wx)\langle i|\mathrm{W}(t)|w\rangle\langle j|\mathrm{W}(t)|x\rangle,$$

and in particular

$$\langle g|\mathrm{U}(\mathrm{T})|h\rangle=\langle g|\mathrm{W}(\mathrm{T})|h\rangle$$
$$+\mathrm{N}\tau\sum_{ij,\,wx,\,y}\mathrm{K}(gy,hy;\,ij,wx)\langle i|\mathrm{W}(\mathrm{T})|w\rangle\langle j|\mathrm{W}(\mathrm{T})|x\rangle. \quad . \quad . \quad . \quad (2.13)$$

This formula is only true as long as the interval $(\mathrm{T}-\tau,\mathrm{T})$ is short, since it does not allow for the possibility of a molecule making more than one collision. But we are interested in the behaviour of $\mathrm{U}(t)$ over relatively long intervals of time; since we are assuming the applied field to be slow even one period is, for our purpose, a long time.

The second term on the right-hand side of (2.13) represents the redistribution of molecules among the various states by the collision process; this rearrangement is going on continually. In the problem we have, as it were, "frozen" the gas in the distribution $\mathrm{U}(0)$ up to time $t=\mathrm{T}-\tau$, and have then found the effect of single collisions on this distribution.

Now up to the time $t=\mathrm{T}-\tau$, when the interaction is switched on, $\mathrm{U}(t)=\mathrm{W}(t)$, so that we can subtract $\mathrm{U}(\mathrm{T}-\tau)=\mathrm{W}(\mathrm{T}-\tau)$ from both sides of (2.13), to give

$$\langle g|\mathrm{U}(\mathrm{T})-\mathrm{U}(\mathrm{T}-\tau)|h\rangle=\langle g|\mathrm{W}(\mathrm{T})-\mathrm{W}(\mathrm{T}-\tau)|h\rangle$$
$$+\mathrm{N}\tau\sum_{ij,\,wx,\,y}\mathrm{K}(gy,hy;\,ij,wx)\langle i|\mathrm{W}(\mathrm{T})|w\rangle\langle j|\mathrm{W}(\mathrm{T})|x\rangle.$$

This shows clearly that (2.13) represents an infinitesimal portion of the redistribution process, and must be regarded as a differential equation

$$\left\langle g\left|\frac{\partial\mathrm{U}}{\partial t}\right|h\right\rangle=\left\langle g\left|\frac{\partial\mathrm{W}}{\partial t}\right|h\right\rangle+\mathrm{N}\sum_{ij,\,wx,\,y}\mathrm{K}(gy,hy;\,ij,wx)\langle i|\mathrm{W}|w\rangle\langle j|\mathrm{W}|x\rangle,$$

since it is only true for every short time-intervals. Now from the definition of V

$$\frac{\partial \mathrm{W}}{\partial t}=\frac{1}{i\hbar}(\mathrm{H}^0\mathrm{W}-\mathrm{W}\mathrm{H}^0),$$

so that

$$\left\langle g\left|\frac{\partial \mathrm{U}}{\partial t}\right|h\right\rangle=\frac{1}{i\hbar}\langle g|\mathrm{H}^0\mathrm{W}-\mathrm{W}\mathrm{H}^0|h\rangle$$
$$+\mathrm{N}\sum_{ij,\,wx,\,y}\mathrm{K}(gy,\,hy;\,ij,\,wx)\langle i|\mathrm{W}|w\rangle\langle j|\mathrm{W}|x\rangle.$$

Since the interval τ is so small, the difference between U and V on the right-hand side of this equation may be neglected, and it may finally be written

$$\left\langle g\left|\frac{\partial \mathrm{U}}{\partial t}\right|h\right\rangle=\frac{1}{i\hbar}\langle g|\mathrm{H}^0\mathrm{U}-\mathrm{U}\mathrm{H}^0|h\rangle$$
$$+\mathrm{N}\sum_{ij,\,wx,\,y}\mathrm{K}(gy,\,hy;\,ij,\,wx)\langle i|\mathrm{U}|w\rangle\langle j|\mathrm{U}|x\rangle.$$

This interpretation of (2.13) as a differential equation is most easily grasped by thinking of the redistribution process as occurring in successive "rounds." If the initial density matrix is $\mathrm{V}=\mathrm{U}_0$, this will be reduced to U_1 by the first round of collisions. For the second round, we must then write $\mathrm{V}=\mathrm{U}_1$, and obtain as a solution $\mathrm{U}=\mathrm{U}_2$, and so on. Plainly, these rounds must be of infinitesimal length since, in a finite interval, there is always a finite possibility of a molecule making more than one collision. By comparison with (1.1), we see that

$$\left\langle g\left|\frac{\partial_e \mathrm{U}}{\partial t}\right|h\right\rangle=\mathrm{N}\sum_{ij,\,wx,\,y}\mathrm{K}(gy,\,hy;\,ij,\,wx)\langle i|\mathrm{U}|w\rangle\langle j|\mathrm{U}|x\rangle. \quad . \quad . \quad (2.14)$$

The equilibrium statistical matrix U_e is defined by $\partial_e\mathrm{U}_e/\partial t=0$, *i. e.*

$$\sum_{ij,\,wx,\,y}\mathrm{K}(gy,\,hy;\,ij,\,wx)\langle i|\mathrm{U}_e|w\rangle\langle j|\mathrm{U}_e|x\rangle=0.$$

We are interested in the value of $\partial_e\mathrm{U}/\partial t$ when U is fairly near equilibrium, *i. e.*, when

$$\mathrm{Y}=\mathrm{U}-\mathrm{U}_e$$

is small compared to U_e. Substituting this into (2.14) and neglecting the term of order Y^2, we get

$$\left\langle g\left|\frac{\partial_e \mathrm{U}}{\partial t}\right|h\right\rangle=\mathrm{N}\sum_{ij,\,wx,\,y}\mathrm{K}(gy,\,hy;\,ij,\,wx)[\langle i|\mathrm{U}_e|w\rangle\langle j|\mathrm{Y}|x\rangle$$
$$+\langle i|\mathrm{Y}|w\rangle\langle j|\mathrm{U}_e|x\rangle]$$
$$=\mathrm{N}\sum_{ij,\,wx,\,y}[K(gy,\,hy;\,ij,\,wx)+\mathrm{K}(gy,\,hy;\,ji,\,xw)]$$
$$\times\langle i|\mathrm{U}_e|w\rangle\langle j|\mathrm{Y}|x\rangle,$$

on rearranging the dummy indices on the second term. Comparing this last formula with (2.1), we see that

$$\mathrm{L}(gh,\, wx)=\mathrm{N}\sum_{i,j,y}\,[\mathrm{K}(gy,\, hy;\, iw,\, jx)+\mathrm{K}(gy,\, hy;\, wi,\, xj)]\times\langle i\,|\,\mathrm{U}_e\,|\,j\,\rangle, \quad . \quad . \quad . \quad (2.15)$$

the specific formula for the coefficients L which we wanted to find.

§3. The Derivation of U_e.

We should expect U_e to be a Boltzmann distribution

$$\langle i\,|\,\mathrm{U}_e\,|\,j\,\rangle=\frac{\exp\,(-\mathrm{E}_i/k\mathrm{T})}{\sum\limits_i \exp\,(-\mathrm{E}_i/k\mathrm{T})}\,\delta_{ij}. \quad . \quad . \quad . \quad . \quad . \quad (3.1)$$

but we have to show that this matrix satisfies the equation $\partial_e\mathrm{U}_e/\partial t=0$. We shall do this by showing that the solution of

$$\sum_{cd}\mathrm{K}(ab,\, cd)\langle c\,|\,\mathrm{S}_2\,|\,d\,\rangle=0$$

is
$$\langle c\,|\,\mathrm{S}_2\,|\,d\,\rangle=\frac{\exp\,(-\mathrm{E}_c/k\mathrm{T})}{\sum\limits_c \exp\,(-\mathrm{E}_c/k\mathrm{T})}\,\delta_{cd},$$

for the validity of (3.1) then follows by taking the trace of this equation with respect to the coordinates of molecule (2).

To justify this last equation, we need to prove a reciprocity theorem, analogous to the Lorentz theorem of electrodynamics, which states

$$\langle b\,|\,f(k\boldsymbol{\alpha},-k_{ba}\boldsymbol{\beta})\,|\,a\,\rangle=\langle a\,|\,f(k_{ba}\boldsymbol{\beta},-k\boldsymbol{\alpha})\,|\,b\,\rangle. \quad . \quad . \quad . \quad (3.2)$$

This is easy enough to prove for elastic scattering, but for inelastic scattering it becomes somewhat complicated, owing to the large number of coordinates involved. In order to keep the writing to a minimum, we shall only prove the theorem for the simplest possible case, that of the scattering of electrons by a hydrogen atom. The generalization of this to more complex cases is obvious enough, if rather tedious.

We take the proton as the centre of coordinates (assuming it to be so massive compared to the electrons that it does not move), and let the coordinates of the bound and free electrons be $\mathbf{r}_1$ and $\mathbf{r}_2$ respectively. We expand the overall wavefunction $\psi_1(\mathbf{r}_1,\, \mathbf{r}_2,\, t)$ in terms of the eigenfunctions $\{\phi_m(\mathbf{r}_1)\}$ of the scatterer

$$\psi_1(t)=\sum_n\phi_n(\mathbf{r}_1,\, t)\mathrm{F}_n(\mathbf{r}_2,\, t)$$

We also take another solution $\psi_2(t)$ of the equation of motion, and expand it in the form

$$\psi_2(-t)=\sum_m\phi_m^*(\mathbf{r}_1,\, t)\mathrm{G}_m(\mathbf{r}_2,\, -t)$$

[since $\phi^*_m(t)$ and $\phi_m(-t)$ have the same dependence on t]. We can thus show that F and G must satisfy the equation.

$$\sum_m \sum_n \phi^*_m(t)\phi_n(t)\left\{i\hbar\frac{\partial}{\partial t}[\mathrm{G}_m(-t)\mathrm{F}_n(t)]-\frac{\hbar^2}{2m}[\mathrm{G}_m\nabla^2\mathrm{F}_n-\mathrm{F}_n\nabla^2\mathrm{G}_m]\right\}=0,$$

the argument being much the same as that used to deduce the wave-mechanical current vector. We now integrate this over $d^3\mathbf{r}_1$, and since the $\{\phi_n\}$ form a c.n.o.s., we get

$$\sum_n\left\{i\hbar\frac{\partial}{\partial t}[\mathrm{G}_n(-t)\mathrm{F}_n(t)]-\frac{\hbar^2}{2m}[\mathrm{G}_n\nabla^2\mathrm{F}_n-\mathrm{F}_n\nabla^2\mathrm{G}_n]\right\}=0,$$

If ψ_1 and ψ_2 correspond to states of the same energy, the time-variations of F_n and G_n are equal and opposite, so that the first term is zero ; also the time factors cancel in the second term, giving

$$\sum_n(\mathrm{G}_n\nabla^2\mathrm{F}_n-\mathrm{F}_n\nabla^2\mathrm{G}_n)=0$$

or, by Green's theorem

$$\sum_n\int_{\mathrm{S}}(\mathrm{F}_n\nabla\mathrm{G}_n-\mathrm{G}_n\nabla\mathrm{F}_n)\,.\,d\mathbf{s}=0, \quad . \quad . \quad . \quad . \quad . \quad (3.3)$$

S being any closed surface. This equation is true for any inelastic scattering process.

In agreement with (2.5), we take F_n and G_n to be given asymptotically by

$$\mathrm{F}_n(\mathbf{r})=[\exp\,(ikr\mathbf{n}\,.\,\boldsymbol{\alpha})]\delta_{na}+\frac{\exp\,(ik_{na}r)}{r}\langle n|f(k\boldsymbol{\alpha},\,k_{na}\mathbf{n})|a\rangle$$

$$\mathrm{G}_n(\mathbf{r})=[\exp\,(ik_{ba}\mathbf{n}\,.\,\boldsymbol{\beta})]\delta_{nb}+\frac{\exp\,(ik_{nb}r)}{r}\langle n|f(k_{ba}\boldsymbol{\beta},\,k_{na}\mathbf{n})|b\rangle.$$

These refer to states of the same energy ; F represents a wave incident in direction $\boldsymbol{\alpha}$ on the scatterer in state $|a\rangle$, while G represents the scatterer in state $|b\rangle$ and the incident wave coming in direction $\boldsymbol{\beta}$. Substituting these into (3.3), and performing the integrations, the theorem (3.2) follows at once.

Another result which we need follows from the fact that the operator R introduced in equation (2.8) is unitary. This gives us the equation

$$\sum_c\int\langle a|\phi^*(\mathbf{r})|c\rangle d^3\mathbf{r}\langle c|\phi(\mathbf{r})|b\rangle=\delta_{ab}$$

and using our equation for ϕ, this reduces to

$$\sum_c k_{ac}\int\overline{\langle c|f(\mathbf{k},\,k_{ac}\mathbf{n})|a\rangle}\langle c|f(\mathbf{k},\,k_{ac}\mathbf{n})|b\rangle\,.\,d\mathbf{n}=-4\pi\mathrm{I}m\{\langle a|f(\mathbf{k},\,\mathbf{k})|b\rangle\}, \quad . \quad . \quad . \quad (3.4)$$

(subject to the restriction $w_{ab}=0$). (3.2) and (3.4) represent basic restrictions on any set of f's for a collision problem. (3.2) tells us that the cross-section for any given process is the same as the cross-section for the inverse process, while (3.4) is a consequence of the conservation of mass; any particles scattered must be compensated by losses from the incident "beam."

By repeated use of the reciprocity theorem, we can show that (3.4) is equivalent to

$$\Sigma \int k_{ca} g(\mathbf{k}_{ca})\, d^3\mathbf{k} \,.\int \langle a|f(\mathbf{k},\, k_{ca}\mathbf{n})|c\rangle \overline{\langle b|f(\mathbf{k},\, k_{ca}\mathbf{n})|c\rangle}\,.\, d\mathbf{n}$$

$$= -4\pi \mathrm{I}m\{\textstyle\int g(\mathbf{k})\, d^3\mathbf{k} \langle a|f(\mathbf{k},\, \mathbf{k})|b\rangle\}, \quad . \quad . \quad . \quad . \quad . \quad . \qquad (3.4\,a)$$

$g(\mathbf{k})$ being the velocity distribution function.

Our object is to find a value of S_2 which makes

$$\langle a|\mathrm{C}|b\rangle \sum_{cd} \mathrm{K}(ab,\, cd) \langle c|\mathrm{S}_2|d\rangle$$

zero, C being proportional to the two-molecule scattered wave. Now we know, on general statistical-mechanical grounds, that S_2 must be diagonal in an energy representation, so that we need only consider the diagonal elements $\mathrm{K}(aa, cc)$ of the array $\mathrm{K}(cd, ab)$ (this can be proved directly, using the reciprocity theorem). We then have

$$\langle a|\mathrm{C}|a\rangle = \sum_c \mathrm{K}(aa,\, cc) \langle c|\mathrm{S}_2|c\rangle$$

$$= \sum_c \int\int \frac{2\hbar k_{ca}}{m} |\langle a|f(\mathbf{k},\, k_{ca}\mathbf{n})|c\rangle|^2 d\mathbf{n}\,.\, d^3\mathbf{k}$$

$$\times \{g(\mathbf{k})\langle c|\mathrm{S}_2|c\rangle - g(\mathbf{k}_{ca})\langle a|\mathrm{S}_2|a\rangle\} \quad . \quad . \quad . \qquad (3.5)$$

from (3.4 *a*). (3.5) can be compared with the corresponding classical equation, for $\langle c|\mathrm{S}_2|c\rangle$ can be identified with ρ_c, the fraction of molecules in the state $|c\rangle$, while

$$\frac{k_{ca}}{k} |\langle a|f(\mathbf{k},\, k_{ca}\mathbf{n})|c\rangle|^2$$

is $\sigma_{ca}(\mathbf{n})$, the differential cross-section for a collision in which the scatterer goes from state $|c\rangle$ to state $|a\rangle$, the scattered particle going off in direction **n**. Remembering that $2\hbar k/m$ is just v, the relative molecular velocity before collision, (3.5) may be written

$$\langle a|c|a\rangle = \sum_c \int\int \mathrm{v}\,.\,\sigma_{ca}(\mathbf{n}) \{g(\mathbf{k})\rho_c - g(\mathbf{k}_{ca})\rho_a\}\, d^3\mathbf{k}\,.\, d\mathbf{n}.$$

This is identical with the classical expression obtained by direct physical arguments, which confirms the accuracy of our analysis. The first term represents the increase in the population of state $|a\rangle$ due to molecules being knocked into this state from other states; the second term represents losses in this population due to molecules being knocked out of this state. This argument identifies the terms of (2.11).

Now an argument, due originally to Boltzmann shows that $\langle a|C|a\rangle$ is zero if, and only if,

$$g(\mathbf{k})=\left(\frac{\hbar^2}{\pi mkT}\right)^{3/2}\exp\left(-\hbar^2k^2/mkT\right),$$

and
$$S_2=A\exp\left(-H_2^0/kT\right)$$

(A being a normalizing constant); *i. e.*, if $g(\mathbf{k})$ is a Maxwellian velocity distribution, and S_2 is a Boltzmann density matrix. Hence we have shown that

$$\langle i|U_e|j\rangle=\langle i|\rho_B|i\rangle\delta_{ij}$$

where
$$\langle i|\rho_B|i\rangle=\frac{\exp\left(-E_i/kT\right)}{\sum\limits_i\exp\left(-E_i/kT\right)},$$

(ρ_B thus being properly normalized). The formula (2.15) for $L(gh, wx)$ thus becomes

$$L(gh,\omega x)=N\sum_{i,y}\left[K(gy,hy;i\omega,ix)+K(gy,hy;\omega i,xi)\right]\langle i|\rho_B|i\rangle. \qquad (3.6)$$

§4. DEDUCTION OF A CLOSED FORMULA FOR σ.

In future, we shall use the symbol σ_{gh} to denote the "complex breadth" of the spectral line corresponding to the transition $g\rightarrow h$. By this, we mean that σ_{gh} is a complex number whose real and imaginary parts give the line breadth and shift respectively. We want to obtain an expression for σ in terms of the $L(gh, wx)$.

The equation of motion of S, including the effect of the applied electric field, is

$$\left\langle g\left|\frac{\partial S}{\partial t}\right|h\right\rangle=\frac{1}{i\hbar}\langle g|H_0S-SH_0|h\rangle+\sum_{wx}L(gh,wx)\langle w|S-S_e|x\rangle,$$

where

$$H_0=H^0-\boldsymbol{\mu}.\,\mathbf{F}\cos\nu t.$$

We solve this by making the weak-field approximation, putting

$$S=S_e+\mathbf{D}\,.\,\mathbf{F}$$

and ignoring terms in F^2. In the microwave region, all energy differences are $\ll kT$, so that

$$S_e\sim 1-\frac{H_0}{kT}+\frac{\boldsymbol{\mu}\,.\,\mathbf{F}}{kT}\cos\nu t.$$

This gives us the equation of motion

$$\left\langle g\left|\frac{\partial \mathbf{D}}{\partial t}\right|h\right\rangle=\frac{\nu\sin\nu t}{kT}\langle g|\boldsymbol{\mu}|h\rangle-i\omega_{gh}\langle g|\mathbf{D}|h\rangle+\sum_{wx}(Lgh,wx)\langle w|\mathbf{D}|x\rangle. \qquad (4.1)$$

Now rotational degeneracy must always be present. This is a consequence of the fact that, in an infinitesimal applied field such as we are considering here, all permitted orientations of the molecule have the same energy. We shall assume that there is no other form of degeneracy present; this is usually so, and when it is not the theory given below can easily be extended.

Hence any state must be labelled

$$|g, m_g\rangle,$$

where m_g is the magnetic quantum number; E_g is, of course, independent of m_g. We shall assume that there is no accidental degeneracy, that is that ω_{jk} cannot equal ω_{gh} unless $|j\rangle \equiv |g\rangle$ and $|k\rangle \equiv |k\rangle$. It seems likely that this assumption is correct for all actual atomic systems.

Suppose now that the applied field is in the z-direction; we shall then want to know D_z, and taking account of the orientational degeneracy, (4.1) may be written

$$\langle g, m_1 | \left(\frac{\partial}{\partial t} + i\omega_{gh}\right) D_z | h, m_2\rangle = \frac{\nu \sin \nu t}{kT} \langle g, m_1 | \mu_z | h, m_2\rangle$$
$$+ \sum_{w, m_3;\, x, m_4} L(g, m_1; h, m_2 : w, m_3; x, m_4) \langle w, m_3 | D_z | x, m_4\rangle.$$

Now since **D** . **F** is a scalar, **D** must transform like a vector; that is to say that **D** and **μ** transform in the same way under a rotation, so that

$$\langle g, m_1 | D_z | h, m_2\rangle = \langle g | \lambda | h\rangle \langle g, m_1 | \mu_z | h, m_2\rangle,$$

where the representatives $\langle g | \lambda | h\rangle$ are independent of the indices m. Then λ is given by

$$\langle g, m_1 | \mu_z | h, m_2\rangle \left\{ \langle g | \left(\frac{\partial}{\partial t} + i\omega_{gh}\right) \lambda | h\rangle - \frac{\nu \sin \nu t}{kT} \right\}$$
$$= \sum_{w, x} \langle w | \lambda | x\rangle \sum_{m_3, m_4} L(g, m_1; h, m_2 : w, m_3; x, m_4) \langle w, m_3 | \mu_z | x, m_4\rangle. \quad \ldots \quad (4.2)$$

The general solution of this equation is extremely complicated. However, in the case where the breadth of the lines is much less than their separation, we can derive a simple formula for σ. This is obviously the case of practical importance, since when the lines begin to overlap seriously, it will not be possible to measure their breadths.

The case not covered by this assumption is that of a very wide variation in the spacing of the lines. Thus, if two spectral lines were very close together, they might be merged while the spectrum was apparently well resolved. However, this line would probably have an anomalous shape, and if such an effect were found experimentally, it would be quite easy to check the above explanation.

In mathematical form, this assumption is equivalent to

$$\omega_{jk} - \omega_{mn} \gg L(gh, wx),$$

for any set of indices. We now suppose that ν, the frequency of the applied field, is near ω_{gh}, in the sense that $\omega_{gh}-\nu=\Delta$ is of the same order of magnitude as L. It is quite easy to show that, under these assumptions,

$$\langle j\,|\,\lambda\,|\,k\rangle \text{ is of magnitude } \frac{1}{k\mathrm{T}}\frac{\nu}{\omega_{jk}-\omega_{gh}}\ (j,\, k\neq g,\, h),$$

while

$$\langle g\,|\,\lambda\,|\,h\rangle \text{ is of magnitude } \frac{1}{k\mathrm{T}}\frac{\nu}{\Delta}.$$

Hence $\langle g\,|\,\lambda\,|\,h\rangle$ is much larger than the other representatives of λ, and therefore in the sum on the right-hand side of (4.2), only the terms containing $\langle g\,|\,\lambda\,|\,h\rangle$ need be retained. [This assumes that $\mathrm{L}(g,\, m_1\,;\, h,\, m_2 : g,\, m_3\,;\, h,\, m_4)$ is not much smaller than the other coefficients L; but this would give rise to a very narrow line, which would plainly be anomalous]. (4.2) then becomes a simple equation for $\langle g\,|\,\lambda\,|\,h\rangle$

$$\Bigg\{\left(\frac{\partial}{\partial t}+i\omega_{gh}\right)\langle g,\, m_1\,|\,\mu_z\,|\,h,\, m_2\rangle - \sum_{m_3,\, m_4}\mathrm{L}(g,\, m_1;\, h,\, m_2 : g,\, m_3;\, h,\, m_4)\langle g,\, m_3\,|\,\mu_z\,|\,h,\, m_4\rangle\Bigg\} \times\langle g\,|\,\lambda(\nu)\,|\,h\rangle=\frac{\nu\sin\nu t}{k\mathrm{T}}\langle g,\, m_1\,|\,\mu_z\,|\,h,\, m_2\rangle. \quad (4.3)$$

Since we know that $\langle g\,|\,\lambda\,|\,h\rangle$ is independent of the indices m, we clear them out, and at the same time convert (4.3) from a vector to a scalar equation, by multiplying both sides by

$$\langle h,\, m_2\,|\,\mu_z\,|\,g,\, m_1\rangle=\overline{\langle g,\, m_1\,|\,\mu_z\,|\,h,\, m_2\rangle},$$

and summing over m_1 and m_2. This gives us

$$\left(\frac{\partial}{\partial t}+i\omega_{gh}-\sigma_{gh}\right)\langle g\,|\,\lambda\,|\,h\rangle=\frac{\nu\sin\nu t}{k\mathrm{T}}, \quad (4.4)$$

where

$$\sigma_{gh}=\frac{\displaystyle\sum_{m_1m_2m_3m_4}\mathrm{L}(g,\, m_1;\, h,\, m_2 : g,\, m_3;\, h,\, m_4)\langle g,\, m_3\,|\,\mu_z\,|\,h,\, m_4\rangle\langle h,\, m_2\,|\,\mu_z\,|\,g,\, m_1\rangle}{\displaystyle\sum_{m_1m_2}|\langle g,m_1\,|\,\mu_z\,|\,h,\, m_2\rangle|^2}. \quad (4.5)$$

By comparison with the calculations of Karplus and Schwinger, we see that this corresponds to a line of Van Vleck-Weisskopf shape, with a complex breadth σ_{gh}. An equation substantially eqivalent to (4.5) has already been deduced by Anderson (1949), by a different method.

We have equations giving $L(gh, wx)$ in terms of $K(ab, cd)$ and $K(ab, cd)$ in terms of the f's, so that we can obtain a formula for σ_{gh} in terms of the f's. The details of the substitution are quite trivial, though rather tedious; the result is

$$\sigma_{gh} = \frac{N\int \Omega_{gh}(\mathbf{k}) g(\mathbf{k})\, d^3\mathbf{k}}{\sum\limits_{m_1 m_2} |\langle g, m_1 | \mu_z | h, m_2\rangle|^2}, \quad . \quad . \quad . \quad . \quad . \quad (4.6)$$

where $g(\mathbf{k})$ is the Maxwellian velocity distribution, and

$$\begin{aligned}
\Omega_{gh} = \frac{2\hbar}{m} \Bigg[& \sum_{i, m_i;\, y.\, m_y;\, m_1, m_3} \langle i | \rho_{\mathrm{B}} | i\rangle \langle g, m_1 | \mu_z | h, m_1\rangle \langle h, m_3 | \mu_z | g, m_3\rangle \\
& \times \int \overline{\{\langle h, m_3; y, m_y | f(\mathbf{k}, k_{iy}\mathbf{n}) | h, m_1; i, m_i\rangle} \\
& \times \langle g, m_3; y, m_y | f(\mathbf{k}, k_{iy}\mathbf{n}) | g, m_1; i, m_i\rangle \\
& + \overline{\langle h, m_3; y, m_y | f(\mathbf{k}, k_{iy}\mathbf{n}) | i, m_i; h, m_1\rangle} \\
& \times \langle g, m_3; y, m_y | f(\mathbf{k}, k_{iy}\mathbf{n}) | i, m_i; g, m_1\rangle\} \, d\boldsymbol{n} \Bigg] \\
& + \frac{4\pi\hbar}{im} \Bigg\{ \Bigg[\sum_{i, m_i;\, m_1} \langle i | \rho_{\mathrm{B}} | i\rangle |\langle g, m_1 | \mu_z | h, m_1\rangle|^2 \\
& \times (\overline{\langle h, m_1; i, m_i | f(\mathbf{k}, \mathbf{k}) | h, m_1; i, m_i\rangle} \\
& - \langle g, m_1; i, m_i | f(\mathbf{k}, \mathbf{k}) | g, m_1; i, m_i\rangle) \Bigg] \\
& + \Bigg[\sum_{m_1 m_3} \langle g, m_1 | \mu_z | h, m_1\rangle \langle h, m_3 | \mu_z | g, m_3\rangle \\
& \times (\langle g | \rho_{\mathrm{B}} | g\rangle \overline{\langle h, m_3; g, m_1 | f(\mathbf{k}, \mathbf{k}) | g, m_3; h, m_1\rangle} \\
& - \langle h | \rho_{\mathrm{B}} | h\rangle \langle g, m_3; h, m_1 | f(\mathbf{k}, \mathbf{k}) | h, m_3; g, m_1\rangle) \Bigg] \Bigg\},
\end{aligned}$$

$$. \quad . \quad . \quad . \quad (4.6\,a)$$

(the last two f terms are not necessarily equal, since f need not be Hermitian). This will, in general, be a complex quantity, so that we would expect collisions to shift lines as well as to broaden them. It is quite easy to show that if $E_i \ll kT$

$$\frac{\text{shift}}{\text{breadth}} = O\left(\frac{E_i}{kT}\right).$$

Hence in the microwave region, the shift will be a relatively small effect, and it is not surprising that it has not yet been detected.

The equation (4.6) is believed to be more accurate than that used by Anderson. However, using Anderson's equation, it is quite easy to calculate σ_{gh} from a known $V(\mathbf{r})$, while using this equation, it is very difficult because of the difficulty of determining the f's. It is therefore hoped to show, in a later paper, that Anderson's equation is a first approximation to our (4.6), and to estimate the error of this approximation (which will presumably be mainly due to neglect of inelastic collisions).

I am much indebted to Professor M. H. L. Pryce for the advice and encouragement he has given me during the course of this work, and to the D.S.I.R. for a maintenance grant.

REFERENCES.

ANDERSON, 1949, *Phys. Rev.*, **76**, 647.
BLEANEY and PENROSE, 1947, *Proc. Roy. Soc.* A, **189**, 358.
BORN and GREEN, 1947, *Proc. Roy. Soc.* A, **191**, 168.
FRÖHLICH, 1946, *Nature, Lond.*, **157**, 478.
HOWARD and SMITH, 1950, *Phys. Rev.*, **77**, 840.
JEFFREYS and JEFFREYS, 1946, *Methods of Mathematical Physics* (Cambridge: University Press).
KARPLUS and SCHWINGER, 1948, *Phys. Rev.*, **74**, 1020.
LORENTZ, 1906, *Proc. Amst. Acad. Sci.*, **8**, 59.
MARGENAU and WATSON, 1936, *Rev. Mod. Phys.*, **8**, 22.
VAN VLECK and WEISSKOPF, 1945, *Rev. Mod. Phys.*, **17**, 227.

V. *Anisotropy of Electrical Resistivity of Cold-Rolled Cubic Metals and Alloys.*

By T. Broom,
Division of Tribophysics, C.S.I.R.O., Melbourne, Australia *.

[Received September 11, 1950.]

Abstract

The electrical resistivity of cold-rolled copper, low carbon steel, brass and sterling silver has been found to vary with direction of measurement. The magnitude of the anisotropy may be qualitatively accounted for by considering the effect of oriented dislocations. The temperature coefficients of resistivity of these rolled metals are isotropic to within 0·5 per cent. These results indicate that deviations from Matthiessen's rule are to be expected.

§1. Introduction.

The effect of cold-work on the electrical resistivity of cubic metals and alloys has been studied mainly after wire-drawing (Boas 1947). However, the possibility of development of anisotropy of electrical resistivity by cold-work has generally been overlooked. Matsuda (1925), in a general investigation of the effect of cold-rolling on the physical properties of copper and aluminium and their alloys, found small but not systematic differences between the resistivities of longitudinal and transverse specimens Becker and Born (1925) showed that anisotropy of electrical resistivity in cold-rolled tungsten could not be greater than 5 per cent.

In the present paper experimental evidence is given for the existence of anisotropy in cold-rolled cubic metals, and an explanation of this effect is put forward.

§2. Experimental.

(i) *Materials.*

The six cubic metals selected for study were aluminium of commercial purity, tough-pitch copper, fine silver, low carbon (0·07 per cent) steel, $\alpha+\beta$ brass, and sterling silver ; their analyses are given in Table I.

Annealed strips of each metal, about 60 mm. wide and 2·5 mm. thick, were reduced 95 per cent in thickness (to 0·125 mm.) by cold-rolling. Specimens of about 60 × 2 mm. were cut from the strip at 0°, 45° and 90° to the rolling direction. Some of these specimens were then recrystallized by vacuum annealing.

---

* Communicated by Dr. W. Boas.

(ii) *Determination of Resistivity.*

A Kelvin Double Bridge was used for all measurements of electrical resistance and the conventional current and potential contacts were made using a system of four needle points on each specimen in turn. The resistance of the 20 mm. length between the potential needle contacts was measured while the specimens were immersed in a bath maintained at 1·0+0·3° C. The usual precautions were taken to eliminate errors due to parasitic E.M.F.s. Some resistance measurements were also made at 0° C. in melting ice and at − 183° C. in boiling oxygen in order to determine whether the temperature coefficients of resistivity were isotropic.

For the calculation of resistivities the average cross-section of each specimen was found by determining its weight and length and by assuming a value for the density*. As the thickness of the strips from which the specimens were cut was not uniform across the width, the average cross-section found for specimens cut at 45° and 90° to the direction of rolling was not that of the central 20 mm. over which the resistance measurements were made.

The difficulty in measuring the actual thickness of the central portion of specimens was avoided by remeasuring the resistance of the specimens of each orientation after they had received a suitable vacuum annealing treatment. The resistivity of annealed cubic metals is isotropic, so that differences in the results obtained from the annealed specimens of different orientations were attributed to the effect of non-uniformity of thickness. The value of resistivity found for specimens at 0° to the rolling direction was assumed to be free from this error. The test of anisotropy was whether the fractional change of resistivity on annealing varied with orientation. For this, a statistical treatment was developed.

(iii) *Statistical Treatment.*

In each of the three orientations, 10 specimens were taken and the resistivities x_{ij} ($i=1, 2, 3$; $j=1, 2, \ldots 10$) were measured. After annealing the specimens were found to have resistivities x'_{ij} ($i=1, 2, 3$; $j=1, 2, \ldots 10$). Let $x_{i\bullet}$, $x'_{i\bullet}$ ($i=1, 2, 3$) denote the mean resistivity for each set of ten specimens. We require to test whether the change in mean resistivity on annealing is dependent on orientation.

Assuming that the variation within each set of 10 measurements is due solely to random fluctuations, we have, as a pooled estimate, S^2, of the error variance,

$$S^2=\frac{\sum\limits_{i=1}^{3}\sum\limits_{j=1}^{10}(x_{ij}-x_{i\bullet})^2+\sum\limits_{i=1}^{3}\sum\limits_{j=1}^{10}(x'_{ij}-x'_{i\bullet})^2}{60-6},$$

---

* The assumed densities in evaluation of resistivity were : aluminium, 2·70 ; copper, 8·94 ; silver, 10·60 ; 0·07 per cent carbon steel, 7·80 ; 64/36 brass, 8·50 ; sterling silver, 10·31 gm./cm.^{3}.

The estimated error variance of the mean of 10 specimens is $S^2/10$ and as the variance of the difference of two variates is the sum of the variances of both variates, the difference $(x_{i\bullet}-x'_{i\bullet})$ is seen to have an estimated error variance of $S^2/5$. To compare the resistivity differences for any two orientations we therefore employ the standard error, $\sqrt{\frac{2}{5}}S$. In the present case, referring to the t-table, we have $t=2{\cdot}01$ for 54 degrees of freedom and probability $P=0{\cdot}05$. Hence, if the resistivity differences at two orientations differ by greater than 2·01 times the standard error, the effect of orientation is significant.

It was found convenient to express the difference between means of cold-worked and annealed specimens of any one orientation as a fraction of the "annealed" resistivity in that direction and accordingly, the standard errors were calculated as fractions of the annealed resistivity.

TABLE I.

Analyses of Materials Used.

Aluminium	0·5% Fe ; 0·2% Si ; traces of Mn, Mg, Cr and Cu.
Copper	0·12% O_2($1{\cdot}06\%$ Cu_2O) ; traces of Ag, Ni and Fe.
Fine Silver	Traces of Mg and Cd.
Mild Steel	0·07% C ; 0·21% Mn.
Brass	63·5% Cu ; 36·5% Zn ; traces of Ag, Mn and Fe.
Sterling Silver ..	92·8% Ag ; 7·2% Cu ; traces of Mg and Cd.

§3. RESULTS.

No changes in resistivity of the fine silver specimens were found after a "high" temperature annealing treatment, and it was assumed that the cold-rolled strip had previously recrystallized at room temperature. No results for silver are therefore reported.

The resistivities of the annealed metals used, determined at 1° C. on specimens at 0° to the rolling direction, are given in the second column of Table II. The fractional changes in resistivity, $\Delta\rho/\rho$, on annealing (and their standard errors) relative to the resistivities of the annealed specimens are also given in Table II. for each orientation. The last column gives the anisotropy of resistivity of the 95 per cent cold-rolled metals used, calculated as

$$\frac{1+(\Delta\rho/\rho)_0}{1+(\Delta\rho/\rho)_{90}}=\frac{(\rho_D/\rho_A)_0}{(\rho_D/\rho_A)_{90}},$$

where ρ_D, ρ_A are the resistivities of deformed and annealed specimens, respectively.

Table III. gives the values of the ratios of the resistances of specimens at −183° C. to those of the same specimens at 0° C. The ratios must be independent of orientation for the annealed specimens and the variation found gives an estimate of the experimental error. It will be seen that the ratios for the rolled materials are also independent of orientation within this error (~0·5 per cent).

§4. Discussion.

The average values for the increase of resistivity accord well with published results, except in the case of copper. Table III. shows that for steel, brass and sterling silver, the transverse resistivity was significantly less than that in the direction of rolling. The reverse was found for copper.

Table II.

Fractional Increase of Resistivity on Cold-Rolling (95 *per cent Reduction in Thickness*).

Metal	Resistivity at 1° C. ohm. cm $\times 10^{-6}$	$\Delta\rho/\rho \times 10^2$ (at 1° C.) Orientation to rolling direction 0°	45°	90°	Anisotropy of resistivity
Aluminium	2·63	1·58±0·41	2·07±0·41	1·86±0·41	0·998±0·008
Copper	1·74	4·03±0·46	3·93±0·46	5·04±0·47	0·990±0·009
Steel	9·86	3·63±0·40	2·32±0·40	2·65±0·40	1·010±0·008
Brass	6·42	25·13±0·31	23·46±0·31	23·07±0·32	1·018±0·006
Sterling Silver	1·76	20·19±0·45	19·34±0·44	17·88±0·44	1·020±0·008

Table III.

Change of Resistance with Temperature.

Metal	Condition	R_{183}/R_0 Orientation to rolling direction 0°	45°	90°
Aluminium	Annealed	0·198	0·201	0·202
	Rolled	0·214	0·217	0·215
Copper	Annealed	0·268	0·268	0·269
	Rolled	0·299	0·299	0·299
Steel	Annealed	0·187	0·187	0·185
	Rolled	0·205	0·206	0·204
Brass	Annealed	0·695	0·694	0·696
	Rolled	0·758	0·758	0·758
Sterling Silver. .	Annealed	0·327	0·328	0·329
	Rolled	0·437	0·438	0·434

This anomalous behaviour of copper may be attributed to the high oxide content, which may also be the cause of the high value of the increase in resistivity. The resistivities at 45° to the rolling direction were intermediate within experimental error, between the longitudinal and transverse resistivities. No significant effect of orientation was found for aluminium, but it should be noted that the error was high, relative to the increase of resistivity, and an effect of the magnitude found for the other metals would have been undetected.

The isotropy of the temperature coefficients of resistivity (Table III.) is, at first, surprising. However, Grüneisen and Goens (1924) found that the temperature coefficients of zinc and cadmium single crystals were isotropic, despite the pronounced anisotropy of resistivity.

The present results indicate that deviations from Matthiessen's Rule can be expected for a worked cubic metal in which the resistivity is anisotropic. Rutter and Reekie (1950) have recently found deviations which they interpreted in terms of an increase, due to cold-work, in the thermal component of resistivity. It is suggested that a part, at least, of the deviations found by them was due to the dependence of resistivity on the direction of measurement. From considerations given below it will be seen that anisotropy of resistivity is likely to be more marked in drawn wires (as used by Rutter and Reekie) than in rolled metals.

Three possible causes of the anisotropy of resistivity can be considered ; the effect of (i) a second phase, (ii) general lattice strains, and (iii) oriented dislocations.

(i) The effect of a second phase.

None of the metals used was single phase. However the anisotropy found appears to be independent of the estimated quantity of second phase (compare *e.g.* aluminium and steel). Again, the anisotropy developed in brass and sterling silver was similar, although in the case of brass, the second phase has higher hardness and lower resistivity than the matrix and in the case of sterling silver these properties are very similar for both phases. From this indirect evidence it is probable that the presence of second phases had little influence on the anisotropy of the metals used*.

(ii) The effect of general lattice strains.

Bridgman (1925) has studied the effect of tension, within the elastic range, on the transverse and longitudinal resistivities of annealed, flat specimens of several metals. The development of anisotropy was shown and found to vary approximately linearly with the applied load.

This behaviour was presumably due to deformation of the cubic lattice under the externally applied stress. In cold-rolled strip the sum of the internal stresses must be zero, and any effect depending linearly on the stress is therefore also zero. This condition holds approximately in the strip with a high degree of preferred orientation of the crystals. However, if the distribution of crystal orientations is such that the sum of the strains is not zero, owing to the anisotropy of elastic constants, an effect on the electrical resistivity may be expected.

---

* These considerations apply only when no cracks develop between the second phase and the matrix. It is tentatively suggested that in the present experiments the copper, which contained 1·1 per cent Cu_2O, had a higher transverse resistivity than longitudinal owing to the formation of longitudinal cracks.

A gross overestimate of the magnitude of this effect may be set by considering the application of a stress equal to the yield stress of the material used. For iron, Bridgman gives the values of $+1{\cdot}42\times10^{-6}$ for the longitudinal and $+0{\cdot}54\times10^{-6}$ for the transverse fractional changes of resistivity per kilogram per sq. cm. If we assume a value of 8000 kg /cm.^{2} for the yield stress, we have 1·007 for the maximum value of the anisotropy. For copper, assuming a value of 4000 kg. cm.^{2} for the yield stress, and using Bridgman's values of $+1{\cdot}75\times10^{-6}$ and $-2{\cdot}4\times10^{-6}$ per kg /cm.^{2} for the longitudinal and transverse coefficients respectively, we find the maximum anisotropy to be 1·015.

These values are comparable with those found in the present experiments, but it should be emphasized that the effect of internal stresses will be very much less than that of a uniaxial stress equal to the yield value. The effect of long-range internal stresses can therefore be regarded as unimportant.

(iii) The effect of oriented dislocations.

Recent calculations of Mackenzie and Sondheimer (1950) on the increase of resistivity produced by cold work lead to a prediction of anisotropy. They consider the scattering of conduction electrons by dislocations and show that the increase in resistance parallel to a dislocation axis is zero while the increase in the slip direction exceeds that normal to the slip plane by a factor of about 2, depending on Poisson's ratio.

During the rolling of polycrystalline metals, the dislocations introduced will not be oriented at random as slip will occur preferentially along favourably oriented slip directions. When cold-rolling has produced a preferred orientation, a complete calculation of the anisotropy would require an estimate of the relative abundance of dislocations perpendicular to each slip direction in each of the slip planes in the ideal preferred orientation produced by cold-rolling. Such a calculation is very sensitive to the distribution of dislocations among the various slip planes and of crystal orientations so that an estimate is not given here. However, it is clear that the present results for anisotropy of increase of resistivity $(\Delta\rho/\rho)_0/(\Delta\rho/\rho)_{90}$ (brass 1·195, silver 1·130, steel 1·370) can be explained by the above considerations if appropriate assumptions (suggested by the mode of deformation) are made.

Recent developments of dislocation theory by Cottrell and Bilby (1949) have led Bhatia (1949) to predict anisotropy of resistance change during strain ageing in iron single crystals. Interstitial solute atoms are assumed to form "atmospheres" around non-randomly oriented dislocations owing to the presence of local lattice strains. In such a case, the effect of dislocations alone, as considered above, would be enhanced. It is interesting to note that in the present experiments the highest value of anisotropy of resistivity increase (1·370), was found for steel. This suggests that the diffusion of carbon atoms to dislocations, as considered by Bhatia, had occurred and accentuated the purely dislocation effects.

From the above considerations it is concluded that the major cause of anisotropy of resistivity of cold-rolled cubic metals is the presence of oriented dislocations,

ACKNOWLEDGMENTS.

The author is indebted to the Goldsmiths' Company for a Dominions (Travelling) Scholarship and to the Division of Tribophysics, C.S.I.R.O., for laboratory facilities. The assistance given by Dr. W. Boas in many helpful discussions is gratefully acknowledged. Thanks are also due to the staff of the Defence Research Laboratories, Maribyrnong, for the analyses ; to Mr. E. J. Williams of the Section of Mathematical Statistics, C.S.I.R.O., for suggesting the statistical procedure ; and to Mr. E. D. Hondros for assistance in the experimental work.

REFERENCES.

BECKER, R., and BORN, F., 1925, *Zeit. f. Tech. Physik*, **6,** 356.
BHATIA, A. B., 1949, *Proc. Phys. Soc.* B, **62,** 229.
BOAS, W., 1947, *Introduction to the Physics of Metals.* Melbourne University Press, p. 124.
BRIDGMAN, P. W., 1925, *Proc. Amer. Acad. Arts Sci.*, **60** (8), 423.
COTTRELL, A. H., and BILBY, B. A., 1949, *Proc. Phys. Soc.* A, **62,** 49.
GRÜNEISEN, E., and GOENS, E., 1924, *Zeit. f. Physik*, **26,** 250.
MACKENZIE, J. K., and SONDHEIMER, E. H., 1950, *Phys. Rev.*, **77,** 264.
MATSUDA, T., 1925, *Sci. Rep. Tohoku Imp. Univ.*, **14,** 343.
RUTTER, J. W., and REEKIE, J., 1950, *Phys. Rev.*, **78,** 70.

VI. *The Origin of Cosmic Ray Stars.*

By J. B. HARDING,
Imperial College, London, S.W.7 *†.

[Received October 13, 1950.]

ABSTRACT.

Estimates for the energy and momentum lost by particles which produce stars when passing through the nuclei in a photographic emulsion support the conclusions reached in a previous paper that the majority of disintegrations are not produced by neutrons which are captured in a single nuclear encounter. The ratio of these two quantities, which have been obtained from the detailed statistical analysis of the various particles produced in nuclear disintegrations, suggests that nuclei are partially transparent to high energy neutrons which at 3600 m. have sufficient energy to produce a small number of stars.

INTRODUCTION.

IN a previous paper (Harding 1949 a) the nature of the radiation responsible for the production of cosmic ray stars has been discussed by considering the momentum and energy transfer from the incident particle to the excited nucleus. An estimate for the transfer of momentum was obtained from the angular distribution of the residual nuclei, or recoil fragments, which are left when the original nuclei have cooled down by particle emission. However, this analysis was carried out for stars formed in C2 " Nuclear Research " emulsion which is not capable of recording tracks left by protons of more than 50 MeV. It is therefore necessary to re-examine the former experimental data and to include further results obtained with electron sensitive plates in order to investigate the validity of the previous conclusion, viz., that the majority of nuclear disintegrations at 3600 m. are produced by nucleons, but that these are not absorbed catastrophically in a single encounter.

EXPERIMENTAL RESULTS.

(*a*) The angular and range distributions of recoil fragments are given in the previous paper, as is the size distribution of stars examined. In this paper the size of a star is denoted by the number of evaporation (black) tracks.

---

* Communicated by Sir George Thomson, F.R.S.

† Present address : Atomic Energy Research Establishment, Harwell.

(*b*) The variation of the α/p ratio with star size has been given by Perkins (1950) and Page (1950). The ratios assumed in this paper for stars in heavy elements (Ag, Br) are :

Star-size	2, 3 and 4	5–14	15
α/p ratio	0·4	0·5	0·45

(*c*) The particles responsible for the " grey " tracks in these stars are mainly protons of energies 30–350 MeV. (Harding 1950). In plates exposed at high altitudes, Camerini *et al.* (1950) have shown that about 5 per cent of such tracks are produced by mesons. In the following we assume that all " grey " tracks are produced by protons. (It would be easier to maintain our original conclusions were we to assume a certain percentage to be produced by mesons, as for a given momentum transfer the energy transfer would be greater than for protons.)

From an analysis of these " grey " tracks (see Appendix) we obtain the following :

Average energy (including binding energy) per particle = 90 MeV.
Average downward momentum per particle = 110 ± 20 MeV./*c*.

(*d*) It is intended to apply momentum and energy consideration to the heavy nuclei, but in the previous paper a certain number of stars arising through the disintegration of the light elements (C, O, N) were also observed. In order to allow for such stars we recall an experiment (Harding 1949 b) designed to give information on these light stars, *i. e.* on stars formed in layers of gelatin.

Having now observed 38 such stars, we estimate that 35 ± 6 per cent of a random sample of stars in C.2 emulsion arise through the disintegration of the light elements.

Assuming a cross-section for star production proportional to $A^{2/3}$ (which is approximately correct), we estimate that from these 38 stars we should expect a charge of 260*e* to be emitted. We have seen

62 protons (deuterons or tritons) : charge 62*e*,
54 α-particles (some may be due to heavier fragments but identification uncertain) : charge $\geqslant 108e$,
3 particles identified as having $Z \geqslant 3$: charge $\sim 10e$.

Estimated charge due to tracks of length *greater* than 10 μ, these tracks remaining in gelatin layers, *i. e.* " lost ", charge $\sim 10e$. In the Appendix we show that in a random sample of small stars there are three-quarters " grey " proton per star. We interpret these as " knock-on " protons, and they should therefore be produced in light nuclei, from which they should stand more chance of escaping than from heavy nuclei. We are therefore justified in assuming that at least three-quarters " grey " proton are produced per light star, *i. e.* emitted charge $\geqslant \frac{3}{4} . 38e = 29e$.

Therefore total emitted charge is $\geqslant 219e$.
Therefore missing charge per star is $< 41e/38$.

This must all go into tracks of $<10\,\mu$, and these must remain in the gelatin layer. It seems unreasonable, and is certainly not expected from evaporation theory, to suppose that we get one short proton per light star. Rather we *assume* that one-third of these stars have a "recoil" of average charge $3e$. As will become apparent later on, it will be easier to maintain the original conclusions, viz., stars are not produced by neutrons which are captured at the first nuclear collision, if we were to assume one-quarter or one-fifth of the light stars to have "recoils" of 4 or $5e$.

In the previous paper a random sample of 411 stars were examined, and hence 144 ± 25 are estimated to arise from light elements. A further 202 stars with six or more prongs, *i. e.* stars arising from heavy elements, were also included in the previous statistics. 279 recoils were observed, of which we assume $(144\pm25)/3=48\pm8$ are fragments from light nuclei.

FORMULATION OF THE SCHEME FOR STAR PRODUCTION.

We consider a star-producing particle ("primary" for shortness) of initial energy and momentum E_1, $\overline{P}_1$ respectively travelling at an angle γ to the downward vertical. It emerges from the nucleus with energy and momentum E_2, $\overline{P}_2$ in the laboratory system, and is accompanied by a small number of "knock-on" (grey) protons and neutrons which carry away energy and momentum E_3 and $\overline{P}_3$. In escaping from the nucleus, the knock-on particles will undergo further collisions which leave the nucleus, now of mass m, in an excited state and moving with a small velocity. Let V_1 be the downward component of this velocity. We can now apply the laws of conservation of energy and momentum:

$$\left.\begin{aligned} E_1-E_2 &= E_3+\mathscr{E} \qquad (=E,\text{ say}), \\ (\overline{P}_1-\overline{P}_2)\,.\,\overline{n} &= \overline{P}_3\,.\,\overline{n}+mV_1 \qquad (=P,\text{ say}). \end{aligned}\right\} \quad . \quad . \quad . \quad (1)$$

where $\mathscr{E}$ is the excitation energy of the nucleus—its kinetic energy is negligible—and $\overline{n}$ is unit vector in the downward direction.

While moving, this excited nucleus will evaporate α-particles, protons and neutrons. We assume that this process is isotropic in the centre of mass system of the excited nucleus. In general this excited nucleus does not possess sufficient energy to break up completely, and a residual nucleus, or recoil fragment, will be left. If this possesses sufficient energy it will be recorded as a short track. In fact we define a recoil track as one of less than $10\,\mu$, and it is now necessary to estimate the distribution in mass of recoil fragments by considering the numbers of "knock-on" and evaporated particles.

From the 613 stars analysed, 469 are estimated to arise through the disintegration of silver and bromine. We assume that the size distribution of the 144 light stars is similar to that of silver stars of two to five tracks. This is suggested by the size distribution of the gelatin stars. We have assumed silver and bromine stars to have similar size distribution. (The final result is very insensitive to the exact assumptions made about these size distributions.)

It can then be shown that for the heavy stars 1·6 "grey" protons are knocked on per star. Since a heavy nucleus contains about $1\frac{1}{4}$ neutrons per proton we assume that $1\frac{1}{4}\times 1{\cdot}6$ neutrons are also directly knocked on by the primary particle.. Therefore $3\frac{1}{2}$ fast nucleons are knocked on per star. (From the recent Berkeley results it would seem that the $n-n$ scattering cross-section is smaller than the $n-p$ cross-section, in which case we might expect fewer knock-on neutrons. As will become apparent later on, such an assumption would make it easier for us to maintain our original conclusions.)

Since we observe a β-ray in less than 5 per cent of the stars, we conclude that the recoils are generally stable fragments. As the average α/p ratio of ejected particles is $\sim 0{\cdot}5$ while the original neutron/proton ratio in a heavy nucleus is 1·25, it follows that 1·5 neutrons must be evaporated for each proton.

If we now assume that the ratio of silver to bromine stars depends on the ratio of their geometric cross-sections and their relative abundance in the emulsion, we can now estimate the distribution in mass of the heavy recoil fragments. Two peaks are observed in this distribution since we start with two groups of nuclei. From the point of view of further calculations it will be sufficiently accurate to consider two "average" recoil groups, one of mass 93, charge $41e$, and the other of mass 67, charge $30e$. These average recoils occur with relative frequencies 216 and 253 respectively. Range velocity curves for such fragments were obtained by the method discussed in the previous paper.

ESTIMATION OF THE ENERGY TRANSFER, E.

We have on average $3\frac{1}{2}$ nucleons knocked-on by the primary. Therefore from the experimental results our best estimate for E_3 is $90\times 3\frac{1}{2}=315$ MeV. It has here been necessary to assume that the angular and energy distribution of particles producing "grey" tracks is the same in light and heavy nuclei, for we use the distribution which was obtained for a random sample ($\sim\frac{1}{3}$ light stars) to estimate E_3, and later P_3 (see Appendix). For stars of medium size ($\sim$6 tracks) the distribution of energy of protons evaporated from an excited nucleus can be represented by

$$P(E)\, dE=\frac{E-V}{T^2}\exp\{(E-V)/T\}\, dE,$$

where V=5 MeV. and T=4 MeV. For neutrons we assume the same distribution, but with V=0 MeV. A similar distribution can be fitted to the α-particle spectrum with V=7 MeV.

Allowing 4 MeV. as binding energy of an α-particle and 8 MeV. for protons and neutrons, we estimate that, for the heavy stars examined, the average energy per star taken by α-particles, neutrons and protons is 40, 100 and 90 MeV. respectively. Thus $\mathscr{E}=230$ MeV.

Therefore our best estimate for E is 315+230=545 MeV.

ESTIMATION OF THE DOWNWARD MOMENTUM TRANSFER, P.

For the three and a half knocked-on nucleons our best estimate of P_3 is $3\frac{1}{2} \times 110 = 385$ MeV./*c*.

We have now to estimate the downward velocity V_1 of the excited nucleus, and for this we will use the angular distribution of the recoil fragments as given in paper I.

Assume that we can observe all recoils of range greater than 3 μ. This assumption is justified below. Our previous results gave 77 recoils observed to travel upwards and 133 downwards. We now believe that 48 of these could be produced from light elements, but unfortunately we have no information about their angular distribution. The greater the downward excess of recoils the greater the downward velocity of the excited nucleus. It is unreasonable to suppose that the light recoils are collimated upward. Therefore if we wish to determine the downward velocity of the heavy nuclei by subtracting from the observed angular distribution of recoils those due to light nuclei, we will obviously obtain the greatest downward excess of heavy recoils (and hence greatest velocity) by assuming that the light recoils are isotropic, *i. e.* if

$$R = \frac{\text{No. of heavy recoils travelling upwards}}{\text{No. of heavy recoils travelling downwards}},$$

$$R_{(\max)} = \frac{(77 \pm \sqrt{77}) - (24 \pm \sqrt{24})}{(133 \pm \sqrt{133}) - (24 \pm \sqrt{24})} = 0{\cdot}49 \pm 0{\cdot}1.$$

(This, then, is the most unfavourable case to take if we are trying to confirm our original conclusion.)

In any given star the velocity of a recoil in the laboratory system will be the vector sum of the downward velocity component V_1 and a velocity V_2, where

$$m_R V_2 = -P_E, \quad \ldots\ldots\ldots \quad (2)$$

m_R being the mass of the recoil fragment and P_E being the resultant momentum of the evaporated particles in the centre of mass system of the excited nucleus. In practice there is a distribution of P_E which can be calculated according to "Random Walk" theory. Let M_N be the number of stars with N prongs. If all particles carried off equal momentum P′ then the differential distribution $\rho_1(P_E)\,dP_E$ is given by Chandrasekhar (1943):

$$\rho_1(P_E)\,dP_E = K P_E^2 \left\{ \sum_N \frac{\exp(-3P_E^2/2NP'^2)}{(2\pi NP'^2/3)^{3/2}} M_N \right\} dP_E.$$

In practice there is also a distribution in the momentum carried off by the individual particles, *i. e.* a distribution $\rho_2(P')\,dP'$ which is calculated from the energy spectra of the particles. Therefore we obtain

$$\rho_1(P_E) = K' P_E^2 \int_{P=0}^{\infty} \left\{ \sum_N \frac{\exp(-3P_E^2/2NP'^2)}{(2\pi NP'^2/3)^{3/2}} M_N \right\} \rho_2(P')\,dP'.$$

From this distribution we can therefore obtain the velocity distribution $\rho(V_2)\,dV_2$ of the two groups of recoils in the centre of mass system of the excited nucleus by using equation (2).

If a recoil is observed to travel upwards with velocity V it must have been ejected upward in the centre of mass system with a velocity greater than V. Averaging over all recoils observed with velocity V in the top hemisphere we have that the average velocity $(\overline{V}_2)_{\text{up}}=Vf_1(V_1/V)$. Similarly, in the lower hemisphere, recoils with velocity V in the laboratory system must be ejected with velocities V_2 in the centre of mass system smaller than V. On the average $(\overline{V}_2)_{\text{down}}=Vf_2(V_1/V)$. The functions f_1 and f_2 can be obtained in an analytical form and their numerical values obtained for any given value V_1/V. It can now be shown that if V_A, V_B are recoil velocities in the laboratory system corresponding to ranges of 3 and 10 μ, then

$$\frac{\text{No. of recoils up}}{\text{No. of recoils down}}=R=\frac{\int_{V_Af_1}^{V_Bf_1}(1-V_1/V_2)\rho(V_2)\,dV_2}{\int_{V_Af_1}^{V_Bf_2}(1+V_1/V_2)\rho(V_2)\,dV_2}.$$

We assume a value for V_1, calculate the limits to the integrals and hence determine R by numerical integration. We can therefore plot a graph against V_1 and hence determine the value of V_1 for the experimental value of $R=0{\cdot}49$. The value so obtained is $0{\cdot}9\times10^8$ cm./sec.

Averaged over the silver and bromine we obtain $mV_1=270$ MeV./*c*.

Hence our best estimate for the downward momentum transfer P (for the assumption regarding the light recoils) is $270+385=655$ MeV./*c*. (Were we to assume that the light recoils were collimated downwards to the same extent as the heavy recoils, this analysis would give $V_1=0{\cdot}7\times10^8$ cm./sec., giving an estimate of 595 MeV./*c*. for P. Taking the other limiting hypothesis, in which all the light recoils are collimated downwards, our estimate for P would be 425 MeV./*c*.

Estimation of Range Distribution of Recoil Fragments.

We have assumed that we can observe all recoil fragments of range greater than 3 μ. To test this we calculate the expected range distributions of recoil fragments and compare them with the observed distributions in the upper and lower hemisphere.

It can be shown (see paper I.) that the differential velocity distributions $N(V)\,dV$ for recoils in the laboratory system are given by

(*a*) (Upper hemisphere)

$$N(V)=-\frac{V}{2V_1}\int_{\sqrt{V^2+V_1^2}}^{V+V_1}\frac{\rho(V_2)}{V_2}\,dV_2,$$

(*b*) (Lower hemisphere)

$$N(V)=-\frac{V}{2V_1}\int_{V-V_1}^{\sqrt{V^2+V_1^2}}\frac{\rho(V_2)}{V_2}\,dV_2.$$

These distributions have been worked out (taking $V_1 = 0{\cdot}9 \times 10^8$ cm./sec.) for the two groups ($A=93$, $Z=41$, and $A=67$, $Z=30$) of fragments. Using theoretical range-velocity curves, calculated according to the method given in the previous paper, the range distributions were obtained and are shown in fig. 1.

DISCUSSION OF ERRORS IN P AND E.

It is here convenient to discuss the errors arising from statistical consideration. We assume first that all energy measurements are correct, but because of the uncertainty of the angular distribution of the "grey" tracks, the estimated momentum of 110 MeV/*c* is only correct to ±20MeV./*c* (standard deviation—see Appendix). Due to the finite number of stars examined, there is an uncertainty in R (for any given assumption about light recoils). For $R = 0{\cdot}49 \pm 0{\cdot}1$ we obtain limits for the downward momentum of the excited nucleus of 205 and 330 MeV/*c*.

Fig. 1.

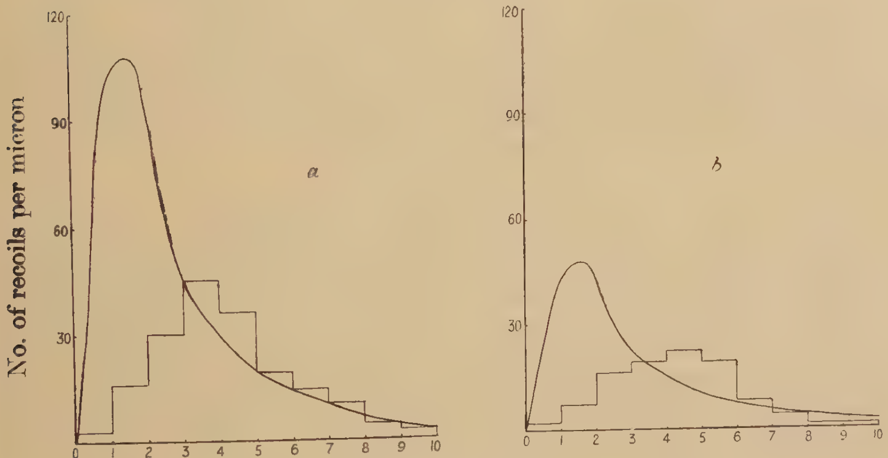

Range in microns.

Assuming these uncertainties in momentum can be represented by error distributions, it can be shown that the uncertainty in P can also be represented by an error distribution with a standard deviation of 75 MeV/*c*, *i. e.*, $P = 655 \pm 75$ MeV/*c*.

Due to uncertainties in the grain-counting technique, there must be an uncertainty in our estimate of E of the order of 10 per cent. However, if we overestimate E, we overestimate P and *vice versa*, and thus the error in the ratio P/E is not so important. Therefore, if in the further analysis we assume the 10 per cent error in E, the resultant error in the ratio will be slightly overestimated. Thus

$$P/E = \frac{655 \pm 75}{545 \pm 55} = 1{\cdot}20 \pm 0{\cdot}18.$$

(In these system of units c=unity.)

EFFECT OF AN ANGULAR DISTRIBUTION OF THE PRIMARIES.

So far we have estimated the downward momentum transfer. The true momentum transfer will be greater. We must now take an angular distribution of the primaries, $P(\gamma)d\gamma$, in order to estimate the true average magnitude of $\overline{P}_1-\overline{P}_2$.

Assume $P(\gamma)=\cos^2\gamma\sin\gamma$, where γ is the angle with the downward vertical. This distribution has been found for the hard component of cosmic rays by counter technique, and seems to hold for the angular distribution of the ionizing primaries of stars formed in electron sensitive emulsions (Coates 1949, Page 1950).

We will now investigate the hypothesis that the star primary is captured by the nucleus. In this case the resultant momentum transfer will be along the direction of the primary particle. Assuming that the energy distribution of the primaries is independent of their direction, it may be shown that for the above angular distribution, the downward component of the average momentum is three-quarters of the magnitude of the true momentum transfer.

Hence, if the primaries are captured, the ratio of the momentum to energy transfer is $4/3\times(1{\cdot}20\pm0{\cdot}18)=1{\cdot}6\pm0{\cdot}2_4$, and it is on the basis of this ratio that we test assumptions about the primary particles.

DISCUSSION OF RESULTS.

80 per cent of the stars at 3600 m. are formed by non-ionizing radiation (Brown *et al.* 1949). We will therefore assume neutrons of average energy 545 MeV. produce one star. In this case the momentum transfer will be 1150 MeV./*c*, and thus $P/E=2{\cdot}1$. The probability of experimental results being consistent with this value is 0·015, and we therefore see that, even with the most unfavourable assumptions about the angular distribution of recoil fragments from light elements, the hypothesis that neutrons are captured in a single encounter with a heavy nucleus is untenable. Taking $P/E=1{\cdot}6$ for a neutron defines its energy as 1200 MeV. The results are therefore consistent with neutrons producing a small number, $\sim1200/545\doteqdot2$, of stars.

In 9 per cent of the stars we observe one fast particle (if a proton its energy is above 350 MeV.) to be emitted in a downward direction. It is reasonable to suppose that this is the primary particle escaping from the nucleus, possibly after change of charge. A further 5 per cent of stars show showers of fast particles, the majority of which are known to be mesons (Camerini *et al.* 1950). From the point of view of the above momentum and energy considerations the ejection of fast mesons could take place as an alternative to the re-emission of the primary particle. Thus in 14 per cent of stars fast particles are observed to leave, and hence it is necessary to assume that in about $50-(9+5)=36$ per cent of stars fast neutrons capable of further star production must be emitted. Hence we should expect the absorption cross-section for the primaries to be less than the collision cross-section. Taking the latter quantity

Fig. 2.

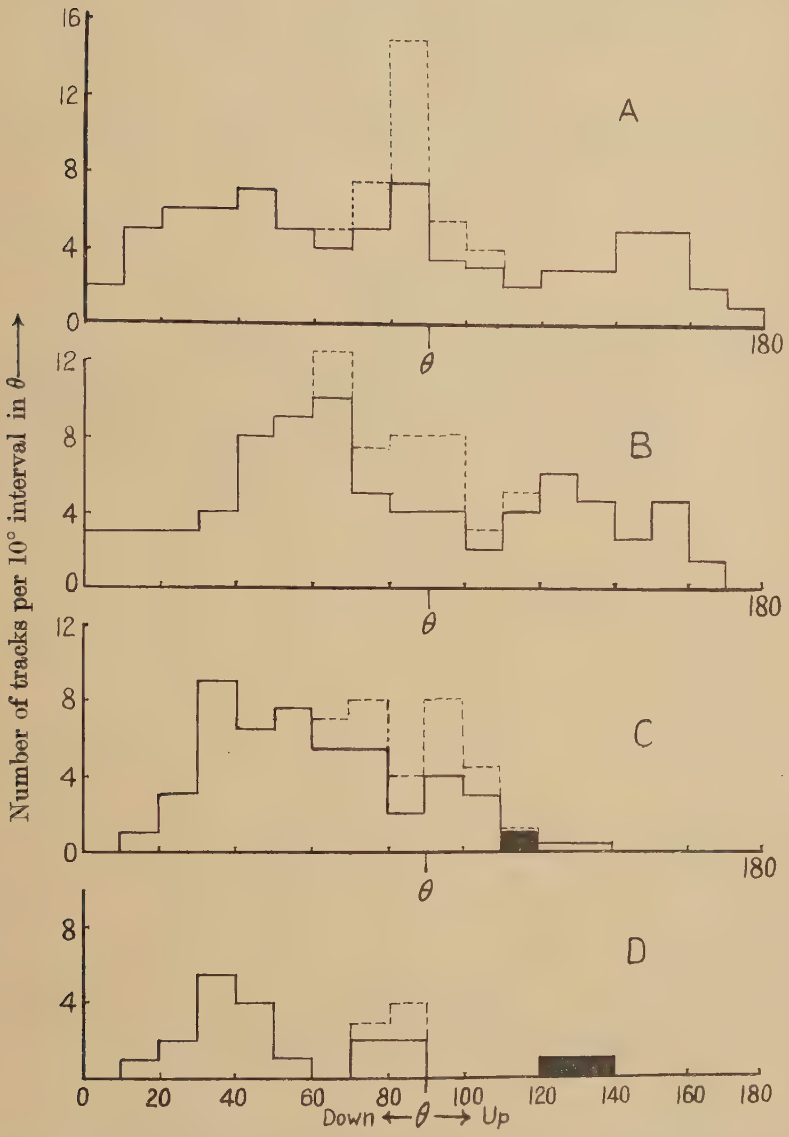

Distribution of the values of θ, zenith angle for "grey" tracks assumed to be produced by protons of energy

(*a*) 30– 50 MeV.
(*b*) 50–100 MeV.
(*c*) 100–200 MeV.
(*d*) 200–350 MeV.

The shaded portions represent tracks which are likely to have been produced by the star primary rather than by a particle ejected in the disintegration. The dotted lines represent corrections which have been applied for loss of steeply dipping tracks.

as determined by the geometrical nuclear cross-section we do in fact obtain a smaller value for the absorption cross-section for lead, aluminium, carbon, air and water (see Bernadini, 1950).

ACKNOWLEDGMENTS.

I wish to express my thanks to Professor Sir George Thomson for his helpful discussions on this problem.

APPENDIX.

A. *The Angular Distribution of the "Grey" Tracks.*

A random sample of 295 stars formed in electron sensitive emulsion exposed at 3600 m. have been analysed with the co-operation of Messrs. P. E. Hodgson and T. T. Li. The plates were calibrated by grain-counting on ρ-meson tracks and then the energies of the particles, assumed to be protons, which produce the "grey" tracks were obtained from grain-density measurements. In figs. 2 *a*, *b*, *c*, *d* we show the distribution in zenith angle of the tracks produced by protons 30–50, 50–100, 100–200,

Fig. 3.

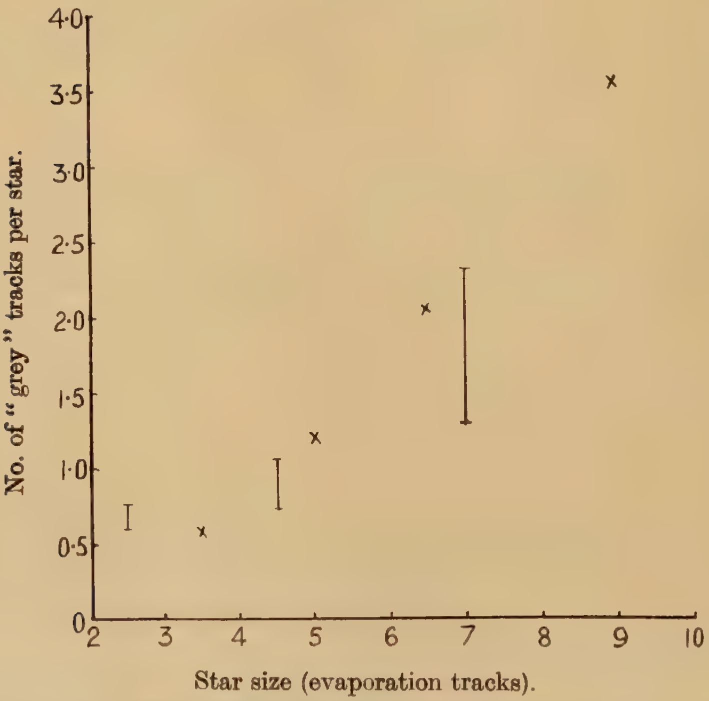

Average number of "grey" tracks as a function of the number of evaporation tracks. For comparison, × indicates results of Brown *et al.* 1949.

200–350 MeV. The variation in the number of such "grey" tracks with star size is shown in fig. 3. Good agreement is obtained with the results of Brown *et al.* (1949).

The statistics for the angular distributions are somewhat poor, and thus, if we take the energy measurements as correct, we estimate

(*a*) Average energy (K.E.+binding energy) per "grey" proton= 90 MeV.

(*b*) Average downward momentum per "grey" proton= 110±20 MeV./*c*.

REFERENCES.

BERNADINI, G., CORTINI, C., and MANFREDINI, A., *Phys. Rev.*, **76,** 1792.
BROWN, R. H., *et al.*, 19—, *Phil. Mag.*, **40,** 862.
CAMERINI, U., *et al.*, 1950, *Phil. Mag.*, **41,** 413.
CHANDRASEKHAR, S., 1943, *Rev. Mod. Phys.*, **15,** 1.
COATES, A. C., and HERZ, R. H., 1949, *Phil. Mag.*, **40,** 1088.
HARDING, J. B., 1949 a, *Phil. Mag.*, **40,** 530; 1949 b, *Nature, Lond.*, **163,** 440; 1950, *Nature, Lond.*, **165,** 273.
PAGE, N., 1950, *Proc. Phys. Soc.* A, **63,,** 250.
PERKINS, D. H., 1950, *Phil. Mag.*, **41,** 138.

VII. *On the Velocity of Second Sound in Liquid Helium II.*

By H. N. V. Temperley,
King's College Cambridge *.

[Received October 25, 1950.]

Abstract.

Some recent experiments by Atkins and Osborne (1950) in the Mond Laboratory give values for the velocity of second sound at very low temperatures in close agreement with Landau's (1941) predictions. It is shown that such results cannot be obtained from any theory of Tisza–London type, unless it is postulated that other states besides the very lowest one contribute to ρ_s, the density of superfluid. Landau's (1941) method of calculating ρ_s can be applied to any model and does imply such a postulate.

It is concluded that the experimental results only throw light on the correct method of calculating ρ_s and cannot be regarded as evidence in favour of Landau's quantum hydrodynamics. On the other hand, the fact that liquid He^3 does not show superfluid properties can no longer be regarded as evidence against Landau's theory, as the predictions of the Landau and Tisza–London types of theory are identical for both the perfect Bose–Einstein and the perfect Fermi–Dirac gases.

§1. Introduction.

Recent measurements, Pellam and Scott (1950), have confirmed that the velocity of "second sound" passes through a minimum value at about 1° K. and begins to rise rapidly at lower temperatures. Recent work by Atkins and Osborne in the Mond Laboratory (1950) confirms the existence of this rapid rise, and shows further that, at very low temperatures, the velocity approaches a value of the order of 150 metres/sec. This is in agreement with Landau's (1941) prediction that the ratio of the velocities of propagation of first and second sound should at very low temperatures tend to the value $\sqrt{3}$. In this paper, we shall show that such a result cannot be obtained from any theory which treats liquid helium II as a condensed Bose–Einstein assembly, the lowest state constituting the superfluid, but that this must not be taken to mean that the hypothesis of the essential connection between Bose–Einstein condensation and the properties of liquid helium II will have to be abandoned; nor can it be regarded as evidence for the soundness or otherwise of Landau's quantum hydrodynamics (the theoretical validity of which has been questioned by some workers). We shall also show that the difference

---

* Communicated by the Author.

between the two types of theory is not nearly as great as is usually thought, because both theories give precisely the same result when applied to the perfect gas model, and the absence of superfluidity in pure liquid He^3 can be understood on the basis of either theory.

§ 2. THE TWO-FLUID CONCEPTION.

The velocity of "second sound" can be shown; see, for example, Landau (1941) to be given by the expression

$$c_2^2 = \frac{\rho_s S^2}{\rho_n(\partial S/\partial T)},$$

where S is the entropy per unit mass.

This result follows according to either theory and can be derived independently of any physical model, making the assumptions that helium II consists of a solution or intimate mixture of two fluids, each having its own density and velocity field, the normal fluid with density ρ_n resembling an ordinary liquid, the superfluid with density ρ_s being unable to transport any entropy. This set of assumptions has been found to be capable of accounting for a large number of the experimental facts, and it is usually referred to collectively as the two-fluid theory. Now $\partial S/\partial T$ can be found directly from specific heat measurements, and S can be obtained from them by numerical integration following a reasonable extrapolation to absolute zero, so that a measurement of c_2 may also be regarded as a measurement of ρ_s/ρ_n. A quite independent measurement of this ratio can be made, Andronikashvili (1948), by measuring the angular momentum of a pile of disks on a common axis, oscillating in liquid helium II, and identifying the relative density of the superfluid with that fraction of the liquid not "carried round" by the disks. Agreement between these two methods is satisfactory down to 1·3° K.

§ 3. THE DIFFERENCE BETWEEN THE TWO THEORIES.

There seem to be two main differences between the two theories. The first difference, which is not a fundamental one, consists of the use by Landau (1941) of the Debye model, in which attention is fixed, not on the atoms themselves, but on the quantized sound waves that represent their relative motion. Tisza (1950), on the other hand, assumes that a satisfactory model of liquid helium can be obtained by modifying the energy spectrum appropriate to a gas of non-interacting helium atoms in a vessel. Evidently the true state of affairs in a liquid involves some compromise between these two models, one of which we may describe as "solid-like" while the other is "gas-like". They appear to have quite different statistical mechanical consequences, because the total number of material particles is fixed, while the total number of sound quanta may vary, but this difference is only apparent. Either type of model may be specified by the density of energy-levels as a function of energy, or, which amounts to the same thing, by the relationship between the energy and total momentum of an elementary excitation. Given a particular model of one kind, it seems to be almost always possible to devise a distribution of energy-levels so that a model of the other kind may give the same partition function, and the two types of model may, in a sense, be regarded as two different approximate descriptions of an assembly, rather than as embodying different physical assumptions.

The really important difference arises from the methods of calculating ρ_s/ρ. The most natural assumption to make in a theory of Tisza–London type is simply to put this ratio equal to the fraction of atoms occupying the very lowest state of the assembly, so that this method is obviously not directly applicable to a model of Debye type. Landau's (1941) method, which consists of imagining the assembly to be in statistical equilibrium with a body moving with a very small velocity and then calculating its mean momentum statistically, is applicable to a model of either type (irrespective of whether his quantum hydrodynamics is sound or not) so that a direct comparison of the two methods is possible. They give the same result for the perfect Bose–Einstein gas, and for the perfect Fermi–Dirac gas both methods predict that ρ_s should be zero, but, in general, the two methods give quite different results, and the experimental evidence thus indicates that Landau's method of calculating ρ_s/ρ is more correct than that suggested above for the Tisza–London type of theory, which is tantamount to saying, that if liquid helium II can be represented as a condensed Bose–Einstein assembly other states of the material particles besides the very lowest one contribute to ρ_s. Landau (1941) also considers, but does not actually use, an alternative method of calculating ρ_s/ρ by imagining the assembly set into rotation with a small angular velocity, calculating the mean angular momentum, and comparing it with the "rigid body" value. He assumes tacitly that the two methods give the same result. By considering the perfect gas model by both methods, we shall show that they are likely to give substantially the same results, though the "rotation" method is, logically, slightly preferable. There is a possibility that, at extremely low temperatures, the two methods might not agree for all models.

§4. THE CALCULATION OF c_2 ACCORDING TO THE LONDON–TISZA TYPE OF THEORY.

We shall consider only the behaviour of ρ_s/ρ_n and c_2 at very low temperatures (as it is already clear that there is no significant difference between the predictions of the two types of theory above 1° K.) for which purpose we need only specify the low-energy end of the spectrum relating energy and momentum of excitations. We assume for this region the following relation between the energy E and the length of the momentum vector p. $E=Ap^n$ where A and n are constants. Now an integration over phase space involves an integration over the three components of momentum, and the volume element in momentum space is $p^2\,dp \sin\theta\, d\theta\, d\phi$. If we change the variable from p to E, we see that the model is equivalent to assuming a density of energy-levels $4\pi A'E^t$ where $t=\dfrac{(3-n)}{n}$. We make the calculation, first by calculating the occupation number of the lowest state, then by Landau's method. For the assembly to be capable of a Bose–Einstein condensation, we must have $t>0$, *i. e.* $n<3$. In practice, since the energy of a particle obeying Schrödinger's equation will always contain a term $p^2/2m$, we probably have $n\leqslant 2$.

For the total occupation of all the states but the lowest

$$\mathrm{N}-\mathrm{N}_0=4\pi\mathrm{A}'\int_0^\infty d\mathrm{E}\ \mathrm{E}^t/[\exp(\mathrm{E}/k\mathrm{T}-1)] \text{ per unit volume.} \quad . \quad (1)$$

For sufficiently low temperatures, we may neglect the difference between ρ_n/ρ_s and ρ_n/ρ, so that

$$\frac{\rho_n}{\rho_s}\approx\frac{\mathrm{N}-\mathrm{N}_0}{\mathrm{N}}=\frac{4\pi\mathrm{A}'}{\mathrm{N}}\Gamma(t+1)\zeta(t+1)(k\mathrm{T})^{t+1}, \quad . \quad . \quad . \quad . \quad (2)$$

by expanding the denominator of the integrand in powers of $\exp(-\mathrm{E}/k\mathrm{T})$ and integrating term by term. ζ is the Riemann zeta-function. The free energy per unit volume is given by

$$\mathrm{F}=4\pi\mathrm{A}'k\mathrm{T}\int_0^\infty d\mathrm{E}\ \mathrm{E}^t\log[1-\exp(-\mathrm{E}/k\mathrm{T})], \quad . \quad . \quad . \quad (3)$$

from which we obtain for the entropy the expression

$$\mathrm{S}=-\frac{\partial\mathrm{F}}{\partial\mathrm{T}}=4\pi\mathrm{A}'k(k\mathrm{T})^{t+1}(t+2)\Gamma(t+1)\zeta(t+2). \quad . \quad . \quad . \quad (4)$$

Substituting for S and $\partial\mathrm{S}/\partial\mathrm{T}$ in the expression for c_2 we get

$$c_2^2=\frac{\mathrm{N}k\mathrm{T}}{\rho}\,\frac{(t+2)\zeta(t+2)}{(t+1)\zeta(t+1)}. \quad . \quad . \quad . \quad . \quad . \quad . \quad . \quad (5)$$

It is interesting that this expression is independent of A′, and only varies quite slowly with t or n. Inserting for N/ρ the value $1{\cdot}6\times10^{23}$ appropriate to liquid helium, we deduce that at very low temperatures $c_2\approx45\mathrm{T}^{\frac{1}{2}}$ metres/sec. Thus, if the above method of calculating ρ_s/ρ_n is correct, we should expect the behaviour of c_2 at very low temperatures to be practically independent of the distribution of energy-levels. Now it is known, Pellam and Scott (1950), that the curve for c_2 begins to turn upwards at a temperature just above 1° K. and they report a value of 33·9 m./sec. at some unknown temperature below this. This is not a high enough value to exclude the possibility that the law just mentioned is obeyed at very low temperatures but very recent work in the Mond Laboratory by Atkins and Osborne (1950), in which velocities up to 150 m./sec. have been observed, seems to rule out this possibility quite definitely.

§5. CALCULATIONS OF c_2 ACCORDING TO LANDAU.

We now give the calculation for the same set of models according to Landau's method (1941). We shall apply it first of all to the general assembly obeying Bose–Einstein statistics, the Debye model and the perfect gas then appearing as particular cases. (There is, however, no difficulty in applying it to assemblies obeying Fermi–Dirac statistics for which the complete energy-spectrum is known, knowledge of the low energy end of the spectrum being no longer sufficient.) The method is as follows :— We suppose the whole assembly in statistical equilibrium with a body moving with a very small velocity, v, along the z-axis and then calculate the mean value of the momentum, the energy-levels of the assembly first being modified to the values that would be measured by an observer moving with the velocity v. Now there will be no change in the potential-energy if the whole assembly is referred to moving axes, while the change in kinetic energy associated with the rth state will be $vp_z^{(r)}$, where $p_z^{(r)}$ is the z component of momentum referred to fixed ones.

The justification of this process is as follows : Schrödinger's equation for non-interacting particles in a potential field V is

$$\frac{h^2}{8\pi^2 m}\nabla^2\psi-\frac{ih}{2\pi}\frac{\partial\psi}{\partial t}-V\psi=0.$$

Taking axes moving relative to the original ones with a velocity v in the z-direction, we have

$$z=z'+vt', \qquad t'=t,$$

and the equation becomes

$$\frac{h^2}{8\pi^2 m}\nabla^{2\prime}\psi-\frac{ih}{2\pi}\frac{\partial\psi}{\partial t'}+\frac{ih}{2\pi}v\frac{\partial\psi}{\partial z'}-V\psi=0,$$

which shows, from the definition of the momentum operator, that the energy is changed by vp_z by the change of axes.

A slight logical difficulty arises for the " particles in a box " model, because the Schrödinger equation cannot be solved in a compact form using the set of axes moving relative to the end wall of the box. It is necessary therefore, either to assume that the assembly is " infinite " in the z direction, or else that the z-ends of the " box " are joined up to make a torus, in which case the model becomes a limiting case of the " rotation " model considered below. In a true " box " model, the introduction of the term vp_z can have no effect on the distribution of momentum in the positive and negative z directions (in spite of the difference in energies) because the amplitudes of the forward and backward travelling waves are constrained by walls perpendicular to the z direction to be the same. With an " infinite " or toroidal " box " this difficulty does not arise. Landau is therefore calculating the modifications in the occupation numbers of the wave-functions referred to the fixed axes that has to occur in order that the assembly may be in equilibrium relative to an observer moving with the new axes. The method can quite easily be generalized to a model requiring the many-body wave-equation.

Thus, for the assembly in equilibrium with a moving body, we must replace E_r, the energy of the rth level, by $E_r-vp_z^{(r)}$. The mean value of the momentum in the z-direction is then

$$\int_0^{2\pi}\int_0^{\pi}\int_0^{\infty}\frac{p_z\,.\,p^2\,dp\sin\theta\,d\theta\,d\phi}{\lambda\exp\left(E-vp_z\right)/kT-1}, \qquad (6)$$

which, to the first order in v, may be written

$$-\int_0^{2\pi}\int_0^{\pi}\int_0^{\infty} p\cos\theta\,.\,pv\cos\theta\,.\,\frac{\partial}{\partial \mathrm{E}}\left(\frac{1}{\lambda\exp(\mathrm{E}/k\mathrm{T})-1}\right)p^2\,dp\sin\theta\,d\theta\,d\phi. \quad . \; . \; . \quad (7)$$

Since $\mathrm{E}=\mathrm{A}p^n$ we have $\partial/\partial\mathrm{E}\equiv(1/n\mathrm{A}p^{n-1})(\partial/\partial p)$ and we may now integrate by parts with respect to p, the integrated term vanishing at both limits (provided $n<5$). The integration over the angular coordinates in momentum space leads to the factor $4\pi/3$ so that the total momentum of the assembly is then

$$\frac{4\pi}{3}\,\frac{5-n}{n\mathrm{A}}\,v\int_0^{\infty}\frac{p^{4-n}\,dp}{\lambda\exp(\mathrm{E}(p)/k\mathrm{T})-1}\ \text{per unit volume,} \quad . \; . \quad (8)$$

and the effective mass, identified by Landau with the "mass of the normal fluid" is obtained simply by dividing this by v. For an assembly such as the Debye model, where the number of quanta present is not fixed, we have $\lambda=1$, while for a degenerate Bose–Einstein assembly λ is very nearly unity and we have

$$\mathrm{N}=\frac{1}{\lambda-1}+4\pi\int_0^{\infty}\frac{p^2\,dp}{\exp(\mathrm{E}(p)/k\mathrm{T})-1}, \quad . \; . \; . \; . \quad (9)$$

the energy of the lowest level being taken as zero. For the perfect gas $\mathrm{E}=p^2/2m$ so that $n=2$ and $\mathrm{A}=1/2m$, in which case expression (8) is exactly equal to the integral in equation (9) multiplied by mv, which means that the atoms in the very lowest state do not participate in the motion, this state contributing to equation (9) but not contributing to expression (8) because the momentum of the very lowest state, referred to the fixed axes, is zero for a large assembly. Thus, for the perfect gas, both methods of calculation give the same result for ρ_s/ρ and therefore for c_2 also whereas, if the energy is any other function of the momentum, as will occur if there are interactions between the atoms, the results of the two methods of calculation may be quite different. For example, if n equals unity, we conclude that c_2 tends to the constant value $\mathrm{A}/\sqrt{3}$ at low temperatures, just as was found by Landau for phonons for which $\mathrm{A}=c_1$, the velocity of ordinary sound, whereas equation (5), with $t=\frac{1}{2}$, gives the result to be expected using the London–Tisza type of approach, plus the assumption that the superfluid is identical with the lowest state of the assembly.

Equations (6)–(9) can easily be modified to suit the Fermi–Dirac assembly and, for the perfect gas, we conclude that the "effective" mass of the assembly is precisely the same as its actual mass, so that nothing of the nature of a "superfluid component" is to be expected according to Landau's method of calculation. The non-appearance of superfluidity in liquid He^3 cannot therefore be regarded as evidence against Landau's theory.

§6. ARE LANDAU'S TWO METHODS OF CALCULATING ρ_s/ρ_n EQUIVALENT?

We return to the perfect Bose–Einstein gas, but we suppose it to be contained in a cylinder of radius a and length d. The possible wave-functions and energy-levels are

$$\left.\begin{aligned}\psi_{l,n,\nu}&=\sin\frac{l\pi z}{d}\,\mathrm{J}_\nu\left(\frac{j_{n,\nu}r}{a}\right)\exp\,(\pm\nu i\theta),\\ \mathrm{E}_{l,n,\nu}&=\frac{h^2}{8\pi^2m}\left[\frac{l^2\pi^2}{d^2}+\frac{(j_{n,\nu})^2}{a^2}\right],\end{aligned}\right\}\quad . \quad . \quad . \quad (10)$$

where $j_{n,\nu}$ is the nth zero of $\mathrm{J}_\nu(x)$ which is given by the asymptotic expression $j_{n,\nu}\sim(n+\frac{1}{2}\nu-\frac{1}{4})\pi$ which is, in fact, fairly accurate even for small values of n and ν. By forming the partition function, replacing the sums by integrals in the usual way, and changing the variables of integration from n and ν to $n+\frac{1}{2}\nu$ and $n-\frac{1}{2}\nu$, we can easily show that, as we should expect, the partition function is in the limit, the same for a cylindrical enclosure as for a rectangular one and that the assembly shows the phenomenon of "condensation" into the lowest level in exactly the same way. It is possible to deal with a toroidal box by introducing Y_ν as well as J_ν. However, if we imagine the whole assembly in equilibrium with a body rotating with a small angular velocity and make a calculation analogous to that of equations (6) to (9) we reach a similar conclusion, with the difference that *all* the states with ν equal to zero are devoid of angular momentum, and can therefore contribute nothing to the mean angular momentum of the assembly. The "number of superfluid atoms" therefore now comprises not only the number in the very lowest state, but *all* those with $\nu=0$. The number N_1 of atoms in such states, apart from the very lowest, can be obtained by summing the ordinary expression for the occupation number over all possible values of l and n, which gives, if the sums are replaced by integrals:

$$\mathrm{N}_1=\int_0^\infty\int_0^\infty\frac{dl\,dn}{\lambda\exp\,[(h^2/8mk\mathrm{T})\,(l^2/d^2+n^2/a^2)]-1}\,. \quad . \quad . \quad (11)$$

This integral diverges if λ is precisely equal to unity, but, since $\mathrm{N}_0=1/(\lambda-1)$ expression (11) implies

$$\mathrm{N}_s=\mathrm{N}_0+\mathrm{N}_1=\mathrm{N}\left[1-\left(\frac{\mathrm{T}}{\mathrm{T}_0}\right)^{3/2}\right]+\frac{\mathrm{T}}{\mathrm{T}_0}\,\mathrm{O}(\mathrm{N}^{2/3}\log\mathrm{N}_0),\quad . \quad . \quad (12)$$

where T_0 is the transition temperature. Thus the difference between the two methods is actually negligible for the perfect gas model for a very large assembly unless the temperature is extremely low, but this calculation does at least show the possibility of the "linear" and "rotational" definitions of ρ_s/ρ_n giving differing results for some models,

§7. CONCLUSIONS.

(*a*) The assumption that Helium II is a condensed Bose–Einstein assembly and that ρ_s/ρ is proportional to the occupation of the lowest state is disproved by extending measurements of c_2 to lower temperatures.

(*b*) This experimental decision does not necessarily mean that liquid helium does not show Bose–Einstein condensation or something similar. It is possible to retain this assumption, provided that one admits that other states besides the very lowest one contribute to ρ_s in all cases except the perfect gas, which seems to be an "accidental" exception.

(*c*) The fact that He^3 does not show superfluidity does not, by itself, mean that Landau's ideas are wrong. As we have seen, Landau's (1941) method predicts no superfluidity for the perfect Fermi gas. No reasonable analogue of the Debye model is known that will represent the excitations of a degenerate Fermi assembly, so a calculation using such a model cannot be made.

ACKNOWLEDGMENTS.

I should like to thank Dr. K. R. Atkins and Mr. D. V. Osborne for showing me their results before publication, and for helpful discussions.

REFERENCES.

ANDRONIKASHVILI, E. L., 1948, *J. Exp. & Th. Phys. U.S.S.R.*, **18,** 429.
ATKINS, K. R., and OSBORNE, D. V., 1950, *Phil. Mag.*, **41,** 1078.
LANDAU, L., 1941, *Jour. Phys. U.S.S.R.*, **5,** 71.
PELLAM, J. R., and SCOTT, R. B., 1949, *Phys. Rev.*, **76,** 869.
TISZA, L., 1950, Report on Conference on Low Temperature Physics at Massachusetts Institute of Technology.

VIII *The Disintegration of Lead Nuclei by Cosmic Rays.*

By P. E. HODGSON,
Imperial College of Science and Technology, London*.

[Received October 25, 1950.]
[Plate V.]

SUMMARY.

Cosmic-ray stars in lead have been investigated by means of photographic plates in close contact with lead foil. The energy distributions of protons and alpha-particles from lead stars have been determined and are compared with the prediction of the evaporation theory. The mean ratio of doubly to singly charged particles is estimated, and an approximate value of the rate of star production in lead deduced.

§1. INTRODUCTION.

THE photographic plate method has already been used (Harding, Lattimore and Perkins 1949) to investigate nuclear disintegrations in the emulsion caused by high energy cosmic-ray particles. Unfortunately, however, the disintegrations cannot be ascribed to any particular element, apart from specific nuclear reactions in the light elements of the emulsion, which can be identified in exceptional cases. Also, although stars from which more than eight charged particles are emitted must be due to the disintegrations of one of the heavy elements of the emulsion, there still remains the ambiguity between silver and bromine.

In order to overcome this difficulty, Harding (1949) has used sandwich emulsions composed of alternate layers of emulsion and pure gelatine. Any star observed to start in the gelatine layer must be due to the disintegration of one of the constituents of gelatine, viz. carbon, oxygen or nitrogen. Attempts have also been made in this laboratory to study disintegrations of lead nuclei by incorporating layers of lead phosphate in the emulsion. However, the amount of lead which can be incorporated in this way without impairing the transparency of the emulsion is so small that to obtain a reasonable number of stars a prohibitively large plate area would have to be scanned.

In the experiment described in this paper we have exposed plates with the emulsion in contact with lead foil, and analysed the stars originating in it.

§ 2. EXPERIMENTAL PROCEDURE.

Lead foil was rolled on to the emulsion of Ilford C2 100 micron nuclear research plates. It adhered well but, in order to ensure that there was no gap between the foil and the emulsion, the plates were tightly clamped together.

---

* Communicated by Sir George Thomson, F.R.S.

After exposure to cosmic rays on the Jungfraujoch, the lead was peeled off the emulsion, which was then developed in the usual manner. The plates were scanned twice, at magnifications of 130 and 270, to reduce the possibility of missing stars originating in the lead.

C2 emulsion was used instead of the more sensitive G5, firstly because the large number of tracks crossing the latter emulsion makes searching difficult and also increases the number of apparent two-track stars in the lead due to the chance concurrence of unrelated tracks; secondly, C2 emulsion gives good discrimination between proton and alpha-particle tracks, permitting the (α/p) ratio to be found; thirdly, since only evaporated particles are recorded in C2 emulsion, it may be assumed that the particles observed were isotropically emitted from the lead nuclei, an assumption which greatly simplifies the calculation of their probabilities of observation.

Each lead star was examined and the numbers of protons and alpha-particles from it which ended in or passed through the emulsion were recorded. The distance of the centre of the star from the emulsion surface was found by a simple geometrical method. The projected range of each track and the difference in depth between the two ends of its emulsion path was measured and hence, assuming the thickness of the emulsion to be exactly 100μ, the range in emulsion of each particle was found. A geometrical calculation gave the range of the particle in the lead before it reached the emulsion. Any deviation of the emulsion thickness from the assumed value of 100μ produces a proportional error in all measurements perpendicular to the plane of the emulsion. Measurements on the undeveloped emulsion of similar plates led to the conclusion that such deviation can be of the order of 5 per cent.

Grain counts were made on all tracks of protons which passed through the emulsion except those making an angle of more than 56° with the plane of the emulsion. The latter were rejected, as grain counts on such steep tracks are unreliable. The energy–grain-density curve for the emulsion was constructed in the usual manner, using the tracks of protons and mesons which ended in the emulsion.

§ 3. Summary of Results and Method of Analysis.

The range and grain density measurements were used to determine the energy distributions of the protons and alpha-particles in the way described in §4. The results are shown in figs. 1 and 2. The mean energy of emission of the protons was 14·2 MeV., and that of the alpha-particles 27·7 MeV.

The apparent proton size distributions of the stars observed in the first and second fifty micron layers of lead from the emulsion surface are shown in Table I. The term "proton size distribution" means the distribution of star sizes obtained by counting only the protons associated with the stars. The constants of the best exponential curves to fit these distributions were found by the method of least squares. The justification for assuming that the size distribution is of exponential form is discussed in § 7. Then, using the size distribution conversion

Fig. 1.

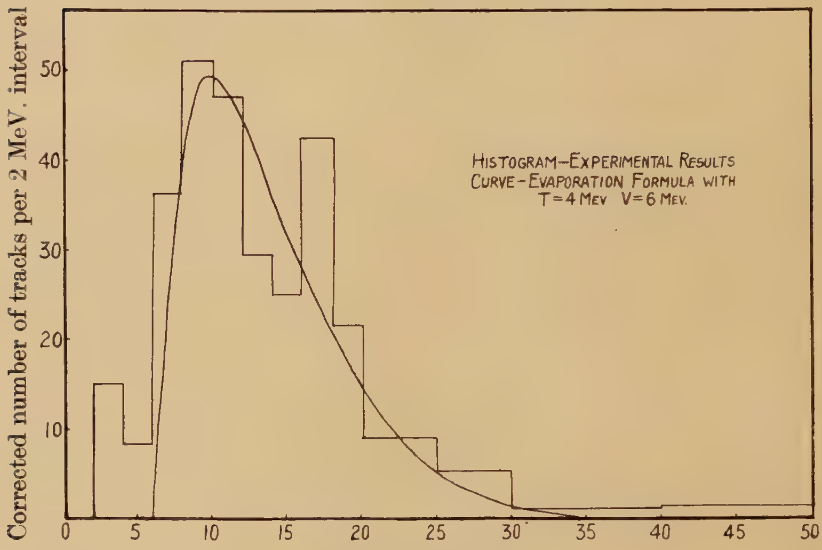

Corrected proton energy distribution for stars in lead based on 95 tracks.

Fig. 2.

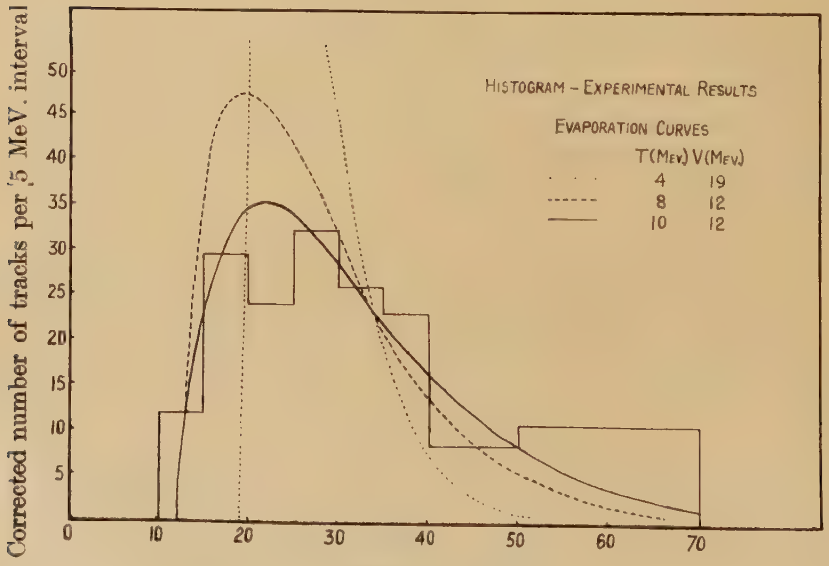

Corrected alpha-particle energy distribution for stars in lead based on 28 tracks.

functions derived in § 8, the proton size distribution of the stars in lead was deduced. Hence, using the value of the (α/p) ratio obtained in § 6, the total size distribution of the lead stars was found by an analogous use of the conversion functions. From the time of exposure and the area of plate scanned the rate of production of lead stars at the Jungfraujoch was deduced. These calculations are summarized in Table II.

A lead star, from which four protons and two alpha-partarcles reach the emulsion, is shown in Pl. V.

§ 4. DETERMINATION OF THE PROTON AND ALPHA-PARTICLE ENERGY DISTRIBUTIONS.

All the tracks due to particles from stars in the lead from which at least three particles reached the emulsion were examined. "Stars" having only two apparent tracks were excluded since many of these are due to the chance concurrence of unrelated single tracks (see § 10).

The energies of emission of particles which ended in the emulsion were evaluated directly from their ranges in emulsion and lead using the respective range-energy curves (H. Bradner *et al.* 1950, Montgomery 1949).

The energies at the mid-points of their emulsion paths of those particles passing through the emulsion were evaluated from the grain densities of their tracks. Then, as before, the energies of emission of the particles were calculated.

Each track was weighted by the reciprocal of the probability that a particle of that energy, emitted from a nucleus at that distance from the emulsion surface, should enter the emulsion or pass through it, whichever is applicable. Allowance was made for the tracks rejected on account of their steepness.

The proton and alpha-particle energy distribution histograms obtained are shown in figs. 1 and 2 together with evaporation curves calculated as follows :

Assume that

(*a*) The nucleus evaporates down the Heisenberg valley with $\partial N/\partial Z=2{\cdot}3$.

(*b*) The binding energies of the emitted particles are $Q_p=Q_n=7{\cdot}7$ MeV., $Q_\alpha=2{\cdot}6$ MeV.

(*c*) Only protons, alpha-particles and neutrons are emitted in the evaporation process.

In addition we have, from the experimental results :

(*d*) The energy distributions correspond to stars from which on the average about eight protons are emitted. This value was calculated from the true and observed proton size distributions and the distribution in depth of the stars in the lead.

(*e*) From the energy distributions the mean energies of emission are $\overline{E}_p=14{\cdot}2$ MeV., $\overline{E}_\alpha=27{\cdot}7$ MeV.

(*f*) The (α/p) ratio for lead stars is 0·34±0·07 (§ 6). Thus about three alpha particles are associated with a star from which eight protons are emitted. Also, to satisfy assumption (*a*), twenty-six neutrons must be emitted.

Let the mean nuclear temperature be T. Then
Energy removed by protons is $(14{\cdot}2+7{\cdot}7)\times 8$ MeV.
Energy removed by alpha particles is $(27{\cdot}7+2{\cdot}6)\times 3$ MeV.
Energy removed by neutrons is $(2\mathrm{T}+7{\cdot}7)\times 26$ MeV.,
i. e. mean excitation energy $\overline{\mathrm{U}}=52\mathrm{T}+466$ MeV.

It has been shown by Le Couteur (1950) that

$$3\mathrm{T}/2=\mathrm{T}_{\max}=\frac{2}{\Lambda}\sqrt{\overline{\mathrm{U}}}.$$

Also, for silver plus bromine, $\Lambda=\sqrt{\left(\frac{\mathrm{A}}{3{\cdot}1}\right)}$, where A=atomic weight.

$$\therefore\quad \overline{\mathrm{U}}=\frac{9\mathrm{T}^2\Lambda^2}{16}=37{\cdot}5\mathrm{T}^2,\quad \text{whence } \mathrm{T}\sim 4{\cdot}3 \text{ MeV.}$$

From the evaporation formula (Harding, Lattimore and Perkins 1949)

$$\mathrm{P(E)}\,d\mathrm{E}=\frac{\mathrm{E}-\mathrm{V}}{\mathrm{T}^2}\exp\left(-\frac{\mathrm{E}-\mathrm{V}}{\mathrm{T}}\right)d\mathrm{E},$$

where V is the height of the nuclear potential barrier, it can be shown that the mean energy of emission $\overline{\mathrm{E}}=2\mathrm{T}+\mathrm{V}$.

$$\therefore\quad \mathrm{V}_p=\overline{\mathrm{E}}_p-2\mathrm{T}=14{\cdot}2-8{\cdot}6\sim 6 \text{ MeV.}$$

and

$$\mathrm{V}_\alpha=\overline{\mathrm{E}}_\alpha-2\mathrm{T}=27{\cdot}7-8{\cdot}6\sim 19 \text{ MeV.}$$

where the suffixes p and α refer to the values of V, T and $\overline{\mathrm{E}}$ appropriate to the proton and alpha-particle energy distributions respectively.

The evaporation curve with T=4, V=6 fits the experimental proton results quite well, which shows that the energy–temperature relationship in lead is consistent with that in silver plus bromine, within the accuracy of the experimental results.

The value of the potential barrier height for protons is considerably less than the 9·6 MeV. obtained by interpolation from the results given by Bethe (1937), which, however, were determined from low energy scattering. This difference may be ascribed to (i) violent oscillations of the nucleus due to the high excitation causing local lowering of the potential barrier, (ii) quantum mechanical penetration of the barrier, and (iii) broadening of the energy distribution by experimental error. For emulsion stars in silver plus bromine of a similar size to the lead stars examined, Harding, Lattimore and Perkins obtained a value V∼4 MeV., which is less than the value for lead, as expected. The number of nucleonic collisions made by the primary in the target nucleus increases with A, but the resulting temperature for the same initial excitation decreases as A increases.

The temperature of 4 MeV. found for the lead disintegrations is less than the $5\frac{1}{2}$ MeV. found by Harding, Lattimore and Perkins for silver plus bromine, which indicates that the latter effect outweighs the former, although the experimental errors make comparison uncertain.

Considering the alpha-particle energy distribution, we should have

$$V_\alpha=2V_p. \qquad \therefore \quad V'_\alpha=12 \text{ MeV.}; \qquad \therefore \quad T'_\alpha=\tfrac{1}{2}(27{\cdot}7-12)\sim 8 \text{ MeV.}$$

The experimental results agree better with $V'_\alpha=12$, $T'_\alpha=8$ than with $V_\alpha=19$, $T_\alpha=4$. This indicates that the alpha-particles cannot all be considered as sharing in the normal evaporation, a conclusion also reached by Harding, Lattimore and Perkins from the examination of silver plus bromine stars. They suggested that the alpha-particles are evaporated off in an initial process of higher excitation and, therefore, higher nuclear temperature. Another explanation, which does not exclude this process, is that some of the alpha-particles are not evaporated at all, but come from the disintegration of highly excited nuclear splinters (Perkins 1950, Hodgson 1950).

In these calculations no account has been taken of the deuterons and tritons which, since they form about 15 per cent of the particles from silver plus bromine stars, are probably emitted also from lead stars. There is little advantage in increasing the accuracy of theory and experiment until the proportion of such particles has been evaluated. This can only be done by a series of grain counts on long tracks parallel to the surface of the emulsion. From the very nature of this experiment such tracks are not available.

§ 5. DETERMINATION OF P_p AND P_α.

Let P_p and P_α be respectively the probabilities that a proton or an alpha-particle from a star in the lead is observed in the emulsion. Both are functions of f, the distance from the star to the emulsion surface. Since C2 emulsion, in which only low energy particles are recorded, was used, it may be assumed that the particles were isotropically emitted from the lead nuclei.

Particles whose directions of emission make a small angle with the emulsion surface have less chance of being observed than those making a large angle, both because of their limited range and the increasing likelihood of their being missed due to the limited field of view of the microscope objective. Therefore

$$P=\int_0^{\pi/2}\frac{\sin\theta}{2}R(f,\theta)D(f,\theta)\,d\theta,$$

where θ is the angle the track makes with the perpendicular to the emulsion surface, and $R(f,\theta)$ is the probability that a track has range greater than $f\sec\theta$, *i. e.*

$$R(f,\theta)=\int_{E_1}^{\infty}\frac{E-V}{T^2}\exp\left(-\frac{E-V}{T}\right)dE,$$

where T and V are the constants of the energy distribution and E_1 is the energy of a particle of range f sec θ in lead (Montgomery 1949). $D(f, \theta)$ is the probability that a track of inclination θ passing right through the emulsion from a star f microns in the lead is found. Since it depends on the distance from where the particle enters the emulsion to the foot of the perpendicular from the star to the emulsion, it may be written

$$D(f, \theta) \sim D(f \tan \theta).$$

$D(f \tan \theta)$ is unity for values of $f \tan \theta$ from 0 to about 100 microns, after which it drops quite steeply to zero. It depends, of course, on the care with which the plates are scanned, and on the field of view of the objective used.

Fig. 3.

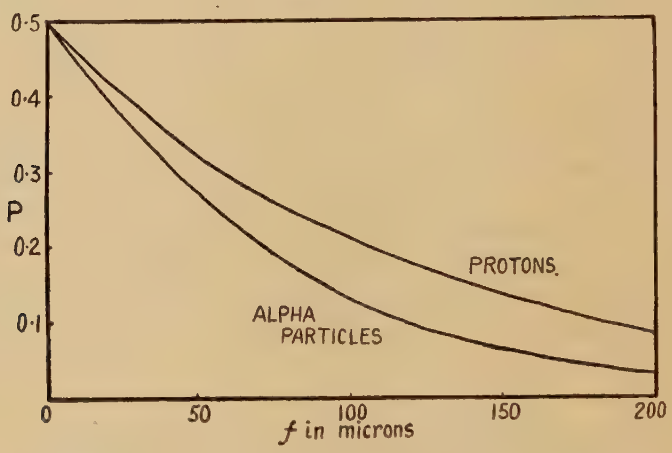

Variation of P with f for protons and alpha-particles.

The distribution in θ of the proton tracks from stars from which at least three particles entered the emulsion was measured for several ranges of f and compared with the curve of $\frac{1}{2} \sin \theta \, R(f, \theta)$. This curve represents the distribution expected if $D(f, \theta) \equiv 1$, that is, no tracks missed, and it was calculated from the appropriate energy distribution (see § 4). From the amounts by which the experimental results fell short of those expected, $D(f \tan \theta)$ was calculated for several values of $f \tan \theta$. The mean value of $D(f \tan \theta)$ was used to find P_p and P_α as functions of f by graphical evaluation of the above integral. The results are shown in fig. 3.

These curves show that it is best to ignore all stars for which $f > 100\,\mu$, as the probability of particles from them being detected is small.

§ 6. THE α/p RATIO FOR LEAD STARS.

The numbers of alpha-particles and protons from stars in various ranges of f were counted and divided by the corresponding P. This gave a mean value for the α/p ratio, averaged over all star sizes, of $0{\cdot}34 \pm 0{\cdot}07$.

Here, as elsewhere, the α/p ratio means, more strictly, the ratio of the number of doubly charged to the number of singly charged particles. Fig. 4 shows the variation of mean α/p ratio with nuclear charge, based on the results of several authors.

Fig. 4.

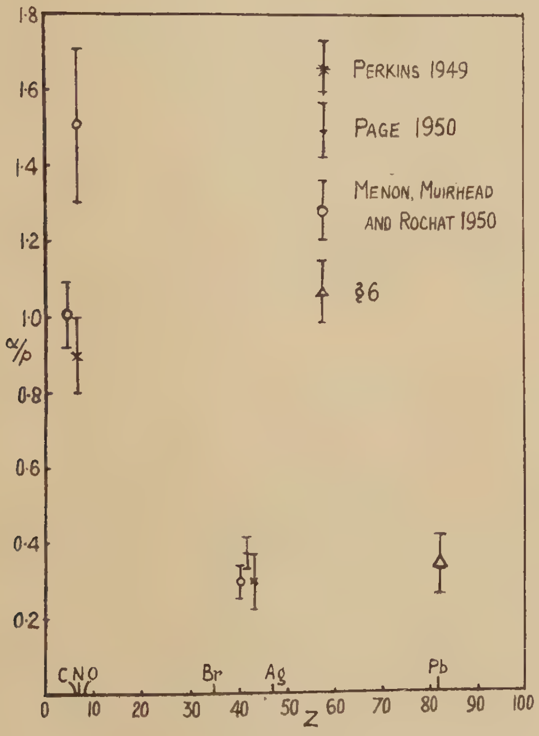

Variation of mean α/p ratio with nuclear charge.

§ 7. THE SIZE DISTRIBUTION ASSUMPTION.

Several authors (George and Jason (1949), Page (1950) and unpublished work at Imperial College) have shown that the size distribution of stars formed by cosmic rays in C2 emulsion at 3500 m. may be represented by the formula

$$N_n = N_0 \exp(-\xi n),$$

where N_n is the number of stars of n tracks, N_0 is a constant and

$$\xi \sim 0{\cdot}5 \quad \text{for} \quad 3 \leqslant n \leqslant 8$$

$$\text{and} \quad \xi \sim 0{\cdot}33 \quad \text{for} \quad n > 8.$$

These figures for the differential size distribution have been calculated from those given by George and Jason for the integral size distribution.

Emulsion stars can be formed either in the light elements carbon, oxygen and nitrogen, or in the heavy elements silver and bromine. The largest star that can be produced in the light elements is one of eight tracks in oxygen, but, since the stars in light elements have about the same numbers of alpha-particles as protons, very few light element stars have more than five tracks.

These observations strongly suggest that the emulsion size distribution is composed of the superposition of two exponential curves, one of the form exp $(-0{\cdot}33n)$ for the heavy elements, and another, of greater slope, for the light. The slope of the light element curve may be calculated from the figures given above, and is found to be $\sim 0{\cdot}6$.

It therefore seems reasonable to assume that the size distribution for lead stars has exponential form also.

The assumption is only approximate, since it gives a finite number of stars with $n > \mathrm{Z}$, whereas the true number is zero.

§ 8. Size Distribution Conversion.

Suppose the stars produced in the lead have a proton size distribution given by

$$\mathrm{N}_n^p = \mathrm{N}_0 \exp(-\xi_p n) \qquad (n \geqslant 2),$$

where n = number of protons evaporated from the nucleus,
N_n^p = number of stars with n evaporated protons,
N_0 and ξ_p are constants.

N_0 depends on the intensity of the star-producing radiation, the number of lead nuclei and the time of exposure, and ξ_p on the material in which the stars are produced and on the energy distribution of the star-producing radiation.

Then an n-track star in a layer distant between f and $f+df$ from the emulsion surface will have a probability of being observed as an m-track star in the emulsion given by

$$\frac{n!}{(n-m)!\,m!}\,\mathrm{P}_p^m(1-\mathrm{P}_p)^{n-m},$$

where P_p is a function of f.

The total number of m-track stars from the layer df observed in the emulsion will therefore be

$$\mathrm{M}_m\,df = \sum_{n=m}^{n=\mathrm{N}} \frac{n!}{(n-m)!\,m!}\,\mathrm{P}_p^m(1-\mathrm{P}_p)^{n-m}\mathrm{N}_0 \exp(-\xi_p n)\,df.$$

N is the number of tracks in the largest possible star in lead. Since the number of stars with $n > \mathrm{N}$ predicted on an exponential law is extremely small for lead (less than 1×10^{-4} per cent), N may, without appreciable error, be replaced by infinity in the above sum.

$$\therefore\quad \mathrm{M}_m=\sum_{n=m}^{n=\infty}\frac{n!}{(n-m)!\,m!}\,\mathrm{P}_p^m(1-\mathrm{P}_p)^{n-m}\mathrm{N}_0\exp(-\xi_p n).$$

$$=\mathrm{N}_0\mathrm{P}_p^m\exp(-\xi_p m)\{1-(1-\mathrm{P}_p)\exp(-\xi_p)\}^{-(m+1)}$$

$$=\frac{\mathrm{N}_0}{1-(1-\mathrm{P}_p)\exp(-\xi_p)}\left\{\frac{\mathrm{P}_p\exp(-\xi_p)}{1-(1-\mathrm{P}_p)\exp(-\xi_p)}\right\}^m$$

$$=\mathrm{M}_f\exp(-\xi_f m),$$

where

$$\mathrm{M}_f=\frac{\mathrm{N}_0}{1-(1-\mathrm{P}_p)\exp(-\xi_p)}\qquad\text{and}\qquad\exp(\xi_f)=\frac{\exp(\xi_p)-(1-\mathrm{P}_p)}{\mathrm{P}_p}.$$

This is the observed proton size distribution of the stars produced in the layer *df*. Thus, provided P_p is known, the actual proton size distribution of the stars in lead at any particular depth f can be calculated from the observed proton size distribution.

§ 9. THE TOTAL SIZE DISTRIBUTION.

The method of determining the proton size distribution has been outlined in § 8, and that for the (α/p) ratio in § 6. It has also been shown (unpublished work at Imperial College) that the distribution of alpha-particles and protons among the stars is nearly random in the sense that the emission of one particle gives no information on the probability of emission of another similar particle. Recent work (Perkins 1950, Hodgson 1950) has shown that close pairs or triplets of particles from the disintegration of unstable nuclear fragments are sometimes emitted from stars, but the frequency of such events is so small that their effect on the randomness of emission can be neglected.

The total size distribution of the lead stars was deduced from the proton size distribution in exactly the same way as the latter was found from the observed proton size distribution. The formulae of § 8 were used with ξ_p replaced by ξ, ξ_f by ξ_p, N_0 by N, and M_f by N_0. P was replaced by the probability that a given track from a star is a proton,—that is, $p/(\alpha+p)=[(\alpha/p)+1]^{-1}$.

The total size distribution of the stars in lead is then given by

$$\mathrm{N}_n=\mathrm{N}_\mathrm{T}\exp(-\xi n),$$

where n=number of charged particles in a star,

N_n=number of stars with n charged particles,

N_T, ξ constants as before.

§10. EXPERIMENTAL RESULTS FOR THE RATE OF STAR PRODUCTION.

The proton size distributions of the stars observed in the lead are shown in Table I. The numbers of apparent two-track stars have been corrected for those due to the chance coincidence of unrelated single tracks. These are quite a serious source of error, being as numerous as the real two-track stars on the plates used, and hence the final number of two-track stars is subject to considerable uncertainty. The number of spurious three- or more-track stars is negligible.

TABLE I.

Numbers of Lead Stars with Different Numbers of Protons, with Two-track Stars corrected for Chance Coincidences of Single Tracks.

Range of f	Number of protons								
	2	3	4	5	6	7	8	9	10
$0<f<50\ \mu$	11·7	7	3	3	1	—	—	1	1
$50<f<100\ \mu$	12·1	7	2	2	—	—	1	—	—

The best values of ξ_f and M_f to fit these distributions, together with the proton and total size distributions calculated from the observed proton size distribution, are shown in Table II. The close agreement between the final values of ξ is probably fortuitous in view of the poor statistics. However, the slope of the lead size distribution is certainly less than that for silver plus bromine, which is expected from the considerations of § 7.

TABLE II.

Results of Calculation of Total Size Distribution. To convert to stars per nucleus per day at the Jungfraujoch, multiply the numbers of stars obtained by substituting the above values in the exponential formula by 5×10^{-24}.

Range of f	Apparent proton size distribution			Real proton size distribution			Total size distribution	
	ξ_f	M_f	P_p	ξ_p	N_0	$[(\alpha/p)+1]^{-1}$	ξ	N_T
$0<f<50\ \mu$	0·45	22·8	0·42	0·21	12·1	0·75	0·17	9·5
$50<f<100\ \mu$	0·71	52·5	0·26	0·24	21·4	0·75	0·18	16·8

The variation of slope of size distribution with nuclear charge is shown in fig. 5 together with the results of other authors. Those of Barbour and Greene were obtained with G5 plates, and so are rather lower than the other values of ξ, which refer to stars in C2 plates. The result of Harding, obtained by the gelatine sandwich method, is based on a rather small number of stars, and therefore has less accuracy than the value obtained in § 7.

The final values of N_T, which should be equal, are only considered reliable to within about a factor of two.

Fig. 5.

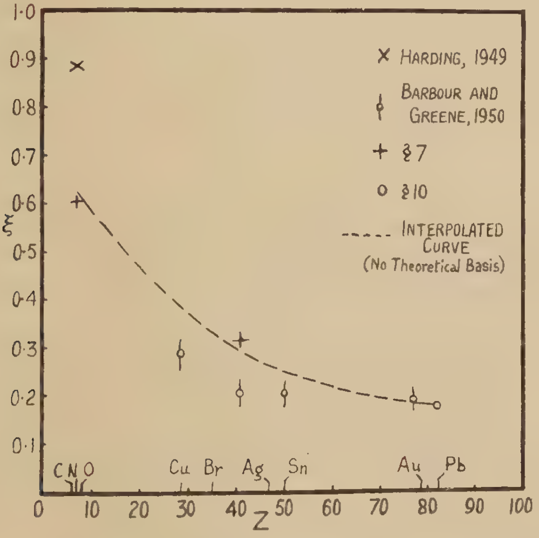

Variation of slope of size distribution with nuclear charge.

§ 11. Conclusions.

The method outlined here for investigating cosmic-ray stars is only suitable for materials of high nuclear charge. This is due to the relatively small probability ($\sim 0\cdot 3$ on the average for stars with $0 < f < 100\,\mu$) that a track from a star outside the emulsion will be observed, and to the variation of size distribution slope with nuclear charge. This results in stars in light elements appearing in most cases as two-track stars, if at all. It is very difficult to correct accurately for spurious two-track stars: indeed, it is probably best to neglect them altogether. Therefore only a very small fraction of the stars from a light element will be analysed, and thus a prohibitively large plate area would have to be scanned to find a sufficient number.

For light elements the sandwich method of Harding is therefore superior. But for heavy elements, which cannot be incorporated in a sandwich in satisfactory quantities, the method described here is preferable.

Recently, Barbour and Greene (1950) have exposed metal foils with emulsion on either side. This doubles the value of P, and so the above objections do not apply to this method providing the foil is thin and is in good contact with both emulsions. These conditions are, however, very difficult to fulfil in practice.

All methods will tend to give a low value for the relative cross-section, because stars outside the emulsion are very much more difficult to find than those in it.

ACKNOWLEDGMENTS.

I should like to express my gratitude to Professor Sir George Thomson, Mr. N. C. Barford and Mr. J. B. Harding for many valuable discussions, and to Dr. K. J. Le Couteur for suggesting the calculations of § 4. I am also indebted to Mr. S. Lattimore who initiated the experiment, carried out the preliminary exposures, and has been a constant source of assistance and advice.

REFERENCES.

BARBOUR, I., and GREENE, L., 1950, *Phys. Rev.*, **79,** 406.
BETHE, H. A., 1937, *Rev. Mod. Phys.*, **9,** 172.
BRADNER, H., SMITH, F. M., BARKAS, W. H., and BISHOP, A. S., 1950, *Phys. Rev.*, **77,** 462.
GEORGE, E. P., and JASON, A. C., 1949, *Proc. Phys. Soc.* A, **62,** 243.
HARDING, J. B., LATTIMORE, S., and PERKINS, D. H., 1949, *Proc. Roy. Soc.* A, **196,** 325.
HARDING, J. B., 1949, *Nature, Lond.*, **163,** 440 (and private communication).
HODGSON, P. E., 1950, *Nature, Lond.*, **165,** 355.
LE COUTEUR, K. J., 1950, *Proc. Phys. Soc.*, **63,** 259 (and private communication).
MENON, M. G. K., MUIRHEAD, H., and ROCHAT, O., 1950, *Phil. Mag.*, **41,** 583.
MONTGOMERY, D. J. X., 1949, *Cosmic Ray Physics*, p. 350 (Princeton University Press).
PAGE, N., 1950, *Proc. Phys. Soc.* A, **63,** 250.
PERKINS, D. H., 1949, *Phil. Mag.*, **40,** 601 ; 1950, *Proc. Roy. Soc.* A, **203,** 339.

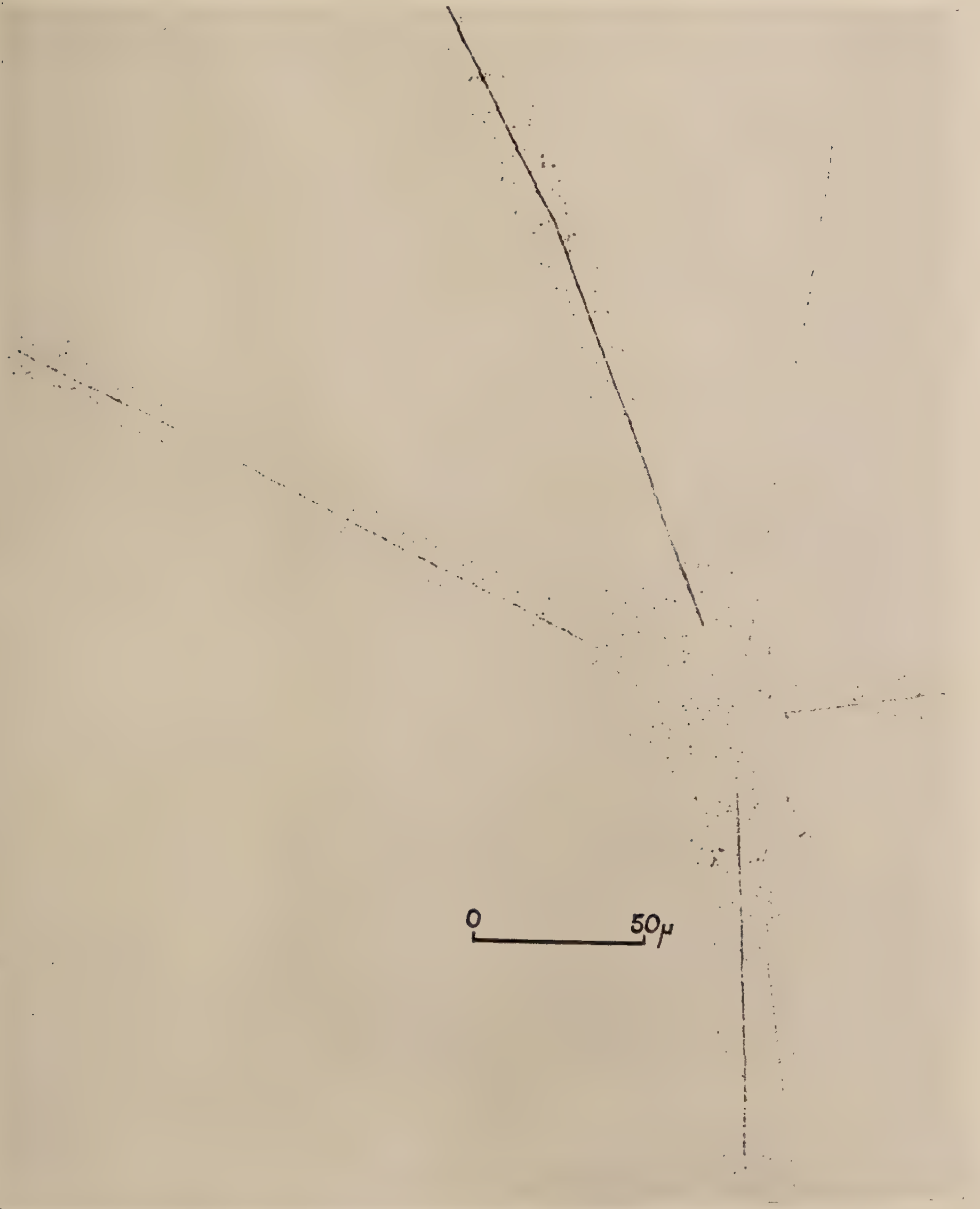

Disintegration of a lead nucleus from which four protons and two alpha particles reach the emulsion.

IX. *Landau Diamagnetism and Meissner Effect.*

By A. Papapetrou,
Physics Department, University of Manchester*.

[Received October 26, 1950.]

Summary.

A magnetic field of the form

$$H_z=2\pi H_0 \, . \cos\left(2\pi\frac{y}{\lambda}\right), \qquad H_x=H_y=0,$$

is considered, and its influence on free electrons is discussed to the first approximation. A field of the form

$$H_z=2\pi H_0 \, . \cos\left(2\pi\frac{x}{\lambda}\right) . \cos\left(2\pi\frac{y}{\lambda}\right)$$

has been considered too. It is shown that, if in a superconductor the distribution of the electrons in momentum space differs a little from the spherical one, an internal field of the second type will be formed inside the superconductor; the Meissner effect then follows for not too strong external fields.

§1. Introduction.

Landau's first investigation of the influence of a magnetic field on the orbital motion of free electrons has been followed by a number of similar calculations, for free electrons as well as for real metal-electrons. All these calculations refer to a homogeneous magnetic field, this being justified by the very small magnetic susceptibility of the metals under ordinary conditions.

An entirely different situation presents itself in the case of a superconductor, in which an external magnetic field penetrates only to a very small depth (order of magnitude 10^{-5} cm.). Instead of considering a homogeneous field now it is more reasonable to split the magnetic field into its Fourier components. In the simplest case of a superconductor in the form of an infinite plane slab (of constant thickness) we get the one-dimensional Fourier components

$$H_z=2\pi H_0 \cos\left(2\pi\frac{y}{\lambda}\right), \qquad H_x=H_y=0. \quad . \quad . \quad . \quad . \quad (1)$$

(Oy-axis normal to the slab, Oz-axis in the direction of the field.) The most important components will have wavelengths of the order of magnitude

---

* Communicated by the Author.

of the penetration depth, *i. e.* $\lambda \approx 10^{-5}$ cm. For a superconductor of prismatic form the Fourier components will be two-dimensional. The most important components will be

$$H_z = 2\pi H_0 \cos\left(2\pi \frac{x}{\lambda}\right) \cos\left(2\pi \frac{y}{\lambda}\right), \quad . \quad . \quad . \quad . \quad . \quad (2)$$

again with $\lambda \approx 10^{-5}$ cm.

In the present paper we shall investigate the behaviour of the metal-electrons in a magnetic field firstly of the form (1), and then of the form (2), in both cases to the first approximation only. As we shall see later, the results of this investigation show us a possible explanation of the Meissner effect.

Strictly speaking we ought to base our calculations on the properties of the real metal-electrons, *i. e.* to consider not only the magnetic field (1) or (2), but also the periodic electrostatic field of the lattice. However, such a calculation would be extremely complicated, if possible at all. Hence, we shall restrict ourselves to the case of free electrons. The results will, in any case, have only qualitative significance.

In the first section we shall consider the one-dimensional magnetic field (1); in the second section the two-dimensional field (2). In the third section we shall discuss the results of those calculations in connection with the Meissner effect.

§ 2. THE ONE-DIMENSIONAL FIELD.

We assume that the electron-gas occupies the whole space and we impose on the wave-functions the usual periodicity condition with a period-length a. The unperturbed wave-functions are then

$$\psi_{\xi,\eta,\zeta} = a^{-3/2} \cdot \exp\left\{\frac{2\pi i}{a}(\xi x + \eta y + \zeta z)\right\}, \quad . \quad . \quad . \quad . \quad (3)$$

ξ, η, ζ being integer numbers (positive or negative). The unperturbed energy is

$$E_0 = \epsilon_1(\xi^2 + \eta^2 + \zeta^2), \quad . \quad . \quad . \quad . \quad . \quad . \quad . \quad . \quad (4)$$

with

$$\epsilon_1 = \frac{h^2}{2ma^2}. \quad . \quad . \quad . \quad . \quad . \quad . \quad . \quad . \quad . \quad (4a)$$

The vector-potential of the field (1) is

$$A_x = -H_0 \lambda \sin\left(2\pi \frac{y}{\lambda}\right), \qquad A_y = A_z = 0. \quad . \quad . \quad . \quad . \quad (5)$$

In the general formula for the perturbing potential

$$V = \frac{ieh}{2\pi mc}(\mathbf{A}\ \mathrm{grad}) + \frac{e^2}{2mc^2}\mathbf{A}^2$$

we shall omit the second term, since we restrict oursleves to the first approximation. We find then immediately

$$V\psi_{\xi,\eta,\zeta}=\frac{ehH_0\xi}{2imcn_0}\left(\psi_{\xi,\eta+n_0,\zeta}-\psi_{\xi,\eta-n_0,\zeta}\right), \quad \ldots \quad (6)$$

where

$$n_0=\frac{a}{\lambda}=\text{positive integer.} \quad \ldots \quad (7)$$

The perturbation method gives then for the perturbed wave-function

$$\Psi_{\xi,\eta,\zeta}=\psi_{\xi,\eta,\zeta}+\frac{ieH_0\xi\lambda^2}{hc}\left(\frac{1}{2\eta+n_0}\psi_{\xi,\eta+n_0,\zeta}+\frac{1}{2\eta-n_0}\psi_{\xi,\eta-n_0,\zeta}\right). \quad \ldots \quad (8)$$

This formula shows that we shall have single states only if we assume

$$n_0=\text{odd integer,} \quad \ldots \quad (7a)$$

since in this case there will be no vanishing denominators in (8). The final results of the calculations are the same for n_0=even or odd. We can, therefore, introduce the assumption (7a)—which simplifies the summation over the occupied electron states—without imposing any unnecessary restriction. The magnetic energy will then be zero for all states,

$$\delta E=0, \quad \ldots \quad (9)$$

i. e. in this approximation the energy of the electron state reduces to (4).

The state described by the wave function Ψ is associated with a current density **s** given by the general formula

$$\mathbf{s}=\frac{he}{i\,.\,4\pi mc}\left(\Psi^*\operatorname{grad}\Psi-\Psi\operatorname{grad}\Psi^*\right)-\frac{e^2}{mc^2}\Psi\Psi^*\mathbf{A}.$$

Introducing in this formula the expression (8) we find

$$s_x=\frac{e^2H_0}{mc^2a^2n_0}\,.\,\sin\left(2\pi\frac{y}{\lambda}\right).\left[1+\frac{2\xi^2}{n_0}\left(\frac{1}{2\eta-n_0}-\frac{1}{2\eta+n_0}\right)\right]+\frac{he\xi}{mca^4}. \quad (10)$$

The last term, which does not contain H_0, can be disregarded because it gives a vanishing contribution when we sum over all occupied states. The components s_y, s_z contain only the term corresponding to the last one in (10), and consequently we may put

$$s_y=s_z=0.$$

Taking into account (5) we may write (10) in the form

$$s_x=-\frac{e^2A_x}{mc^2a^3}\left[1+\frac{2\xi^2}{n_0}\left(\frac{1}{2\eta-n_0}-\frac{1}{2\eta+n_0}\right)\right]. \quad \ldots \quad (10a)$$

Before going further it is worth seeing up to what values of H_0 our formulæ will be valid. The condition for the validity of the perturbation method is that the coefficients of $\psi_{\xi,\eta\pm n_0,\zeta}$ in (8) be small compared with 1. For the large majority of occupied states we have $|\xi|\approx\xi_{\max}$ and $|2\eta\pm n_0|\approx\eta_{\max}=\xi_{\max}$. Therefore, the condition for the validity of our formulæ will be

$$\frac{eH_0\lambda^2}{hc}<1\,;$$

Now we see that the quantity $1/\eta(\omega_0'(\eta))$ changes slowly even in the neighbourhood of $\eta=0$, and consequently we can evaluate the sum appearing in (15) by integration :

$$\sum_\eta \frac{1}{\eta}\,\omega_0'(\eta)=-4\epsilon_1\int_{-\infty}^{+\infty}\frac{dy}{1+\exp(\epsilon_1\eta^2-\epsilon_0/k\mathrm{T})}.$$

We are interested in the case

$$\epsilon_0 \gg k\mathrm{T},$$

in which this integral can be evaluated by a well-known method*. The result is

$$\sum_\eta \frac{1}{\eta}\,\omega_0'(\eta)=-8\epsilon_1^{1/2}\epsilon_0^{1/2}\left[1-\frac{\pi^2}{24}\left(\frac{k\mathrm{T}}{\epsilon_0}\right)^2\right].$$

Introducing this in (15) we get

$$S_x=-\frac{2\pi}{3}\,\frac{e^2n_0^2\mathrm{A}_x}{mc^2a^3}\sqrt{\left(\frac{\epsilon_0}{\epsilon_1}\right)}\cdot\left[1-\frac{\pi^2}{24}\left(\frac{k\mathrm{T}}{\epsilon_0}\right)^2\right]. \quad . \quad . \quad (15a)$$

The dependence of S_x on the temperature is not shown directly in (15 *a*) because ϵ_0 itself is dependent on T. The dependence of ϵ_0 on T can be determined by calculating the number N of electrons in terms of ϵ_0 and T. The result is

$$\mathrm{N}=\frac{8\pi}{3}\left(\frac{\epsilon_0}{\epsilon_1}\right)^{3/2}\cdot\left[1+\frac{\pi^2}{8}\left(\frac{k\mathrm{T}}{\epsilon_0}\right)^2\right]=\frac{8\pi}{3}\left(\frac{\epsilon_{00}}{\epsilon_1}\right)^{3/2},$$

if we denote by ϵ_{00} the value of ϵ_0 for $\mathrm{T}=0$. Introducing ϵ_{00} in (15*a*) and taking into account (4 *a*) we finally find

$$\mathrm{S}_x=-\frac{2\pi}{3}\,\frac{e^2\mathrm{A}_x}{mc^2\lambda^2h}\sqrt{(2m\epsilon_{00})}\cdot\left[1-\frac{\pi^2}{12}\left(\frac{k\mathrm{T}}{\epsilon_{00}}\right)^2\right]. \quad . \quad . \quad (16)$$

This result can be brought to a more familiar form. Let us calculate a distribution of magnetic moment **m** equivalent to the distribution of current **S** by means of the general formula

$$\mathbf{S}=\mathrm{curl}\,\boldsymbol{m}.$$

If then we introduce the magnetic susceptibility χ,

$$\boldsymbol{m}=\chi\mathbf{H},$$

we find (provided that χ is independent of x, y, z)

$$\mathbf{S}=\chi\,.\,\mathrm{curl}\,\mathbf{H}. \quad . \quad . \quad . \quad . \quad . \quad . \quad . \quad . \quad (17)$$

Hence in our case

$$\chi=\mathrm{S}_x\Big/\frac{\partial\mathrm{H}_z}{\partial y}.$$

Considering (16) we find

$$\chi=-\frac{e^2\sqrt{(2m\epsilon_{00})}}{6\pi mc^2h}\cdot\left[1-\frac{\pi^2}{12}\left(\frac{k\mathrm{T}}{\epsilon_{00}}\right)^2\right], \quad . \quad . \quad . \quad . \quad . \quad (18)$$

---

* See *e. g.* Fröhlich, Elektronentheorie der Metalle (Springer 1936), p. 357.

which is identical with the Landau susceptibility of free electrons in a homogeneous field. This is not surprising at all, since *e. g.* for $\lambda \approx 1$ cm. we should have demanded that our calculations lead to the Landau susceptibility (18); our conclusion is now that this is generally true, if only $n_0 \ll \eta_{\max}$*.

Coming back to equation (10 a) we stress an important feature of it. The current s_x produced by the magnetic field (1) acting on any given electron state is *not of the order of* S_x/N, *but very much larger.* The smallness of S_x (or of χ) is the consequence of a very complete cancellation of much larger terms, this cancellation being due to the spherically symmetric distribution of the electrons in momentum space†. If we disregard the states with $\xi^2 \lesssim n_0^2$—which are relatively few because of the assumption $n_0 \ll \eta_{\max} = \xi_{\max}$—, the second term in the bracket of (10 a) will be predominant. We see then that we shall have a strong *paramagnetic*‡ current if $|\eta| < n_0/2$, or a strong *diamagnetic* current if $|\eta| > n_0/2$. We shall make use of this fact in the last section of the present paper.

Instead of the metal extending infinitely in all three dimensions we may equally well consider a slab of finite thickness in the Oy-direction, *e. g.* the one filling the space $0 < y < a$. The calculations are very similar to those given above. But there is one characteristic difference in so far that we cannot now start with the field H_z given by (1). The reason is that, as can be seen immediately, the quantity $V\psi$ cannot in this case be developed in a series of the unperturbed wave functions ψ. The difficulty disappears if we consider the field

$$H_z = 2\pi H_0 \sin\left(2\pi \frac{y}{\lambda}\right),$$

i. e. a field *vanishing on the surface of the metal.* The perturbation method gives then for s_x a formula very similar to (10 a); for S_x and χ we get again equations (16) and (18).

§3. THE TWO-DIMENSIONAL FIELD.

The calculations are similar to those for the one-dimensional field. Therefore, it will be sufficient if we just indicate the main points and give the final results.

Since we wish to arrive again at a relation of the form $\mathbf{s} \propto \mathbf{A}$, we must impose on $\mathbf{A}$ the condition

$$\operatorname{div} \mathbf{A} = 0.$$

---

* In the case $n_0 \approx \eta_{\max}$ or $n_0 \gg \eta_{\max}$ the evaluation of the sum in (11) would have lead to a final result different from (16); but these cases are of no physical importance, and, therefore, we do not discuss them here.

† The same is true also in the case of a weak homogeneous field; compare Papapetrou (1937).

‡ It is well known that the first term in the bracket of (10 a) by itself would lead to a diamagnetic current as strong as that which is necessary for the explanation of the Meissner effect.

We find, then, that the vector-potential of the field (2) is

$$\left.\begin{aligned} A_x &= -\tfrac{1}{2}H_0\lambda \cos\left(2\pi\frac{x}{\lambda}\right)\sin\left(2\pi\frac{y}{\lambda}\right), \\ A_y &= \tfrac{1}{2}H_0\lambda \sin\left(2\pi\frac{x}{\lambda}\right)\cos\left(2\pi\frac{y}{\lambda}\right), \\ A_z &= 0. \end{aligned}\right\} \quad . \quad . \quad . \quad . \quad (19)$$

We shall consider the case of an infinitely large piece of metal, in which the unperturbed wave functions will be given by (3). The perturbation method leads, then, to the following expression for the perturbed wave functions :

$$\begin{aligned} \Psi_{\xi,\eta,\zeta} &= \psi_{\xi,\eta,\zeta} \\ &+ \frac{ieH_0\lambda^2}{8hc}\left\{(\xi-\eta)\left(\frac{1}{\xi+\eta+n_0}\psi_{\xi+n_0,\eta+n_0,\zeta} + \frac{1}{\xi+\eta-n_0}\psi_{\xi-n_0,\eta-n_0,\zeta}\right)\right. \\ &\left. -(\xi+\eta)\left(\frac{1}{\xi-\eta+n_0}\psi_{\xi+n_0,\eta-n_0,\zeta} + \frac{1}{\xi-\eta-n_0}\psi_{\xi-n_0,\eta+n_0,\zeta}\right)\right\} \quad (20) \end{aligned}$$

where again $n_0 = a/\lambda$. This formula shows that we shall have degenerate states when $\xi \pm \eta = \pm n_0$. These degenerate states, for which a separate calculation would be necessary, cannot be avoided by an assumption like (7*a*). But again we could avoid them if we replaced the field (2) by a field of the form

$$H_z = 2\pi H_0 \cos\left(2\pi\xi_0\frac{x}{a}\right) . \cos\left(2\pi\eta_0\frac{y}{a}\right)$$

with *e. g.* $\xi_0 - \eta_0 = 1$; if $\xi_0, \eta_0 \gg 1$, this field is physically equivalent to the field (2). The degenerate states occurring in the case $\xi_0 = \eta_0 = n_0$ have only the effect of making the calculation of the total current **S** (by summation of **s** over the occupied states) essentially more complicated. But the final results are exactly the same in both cases, *i. e.* with and without degenerate states. Hence, it will be sufficient if we consider here the non-degenerate states described by (20).

The current **s** associated with the state described by (20) is found to be

$$\mathbf{s} = -\frac{e^2\mathbf{A}}{mc^2a^3}\left[1 + \frac{1}{2}\left\{\frac{(\xi-\eta)^2}{(\xi+\eta)^2-n_0^2} + \frac{(\xi+\eta)^2}{(\xi-\eta)^2-n_0^2}\right\}\right] . \quad . \quad . \quad (21)$$

The calculation of the total current **S** from **s** can be made in much the same way as in the one-dimensional case. The final result is

$$\mathbf{S} = -\frac{4\pi}{3}\,\frac{e^2\mathbf{A}}{mc^2\lambda^2h}\sqrt{(2m\epsilon_{00})} . \left[1 - \frac{\pi^2}{12}\left(\frac{kT}{\epsilon_{00}}\right)^2\right], \quad . \quad . \quad . \quad (22)$$

differing from the corresponding one-dimensional formula (16) by a factor 2. If we calculate the equivalent susceptibility from (17), we find again the Landau value (18).

As in the one-dimensional case, here also the small value of **S** or χ is due to a cancellation of much larger contributions of the individual states, again because of the spherical distribution of the electrons in momentum space. If we disregard the (relatively few) states for which $\xi^2, \eta^2 \lessapprox n_0^2$, we see from (21) that the states for which either $(\xi-\eta)^2<n_0^2$ or $(\xi+\eta)^2<n_0^2$ are strongly paramagnetic; those are the states which in momentum space occupy positions inside the two layers of thickness $n_0\sqrt{2}$ along the planes $\xi\pm\eta=0$. The states situated outside those two layers are strongly diamagnetic.

Instead of the metal extending infinitely in all three dimensions we could consider a prismatic piece of the metal, *e. g.* one filling the space $0<x, y<a$. When we try to solve the perturbation problem, we see again, as in the one-dimensional case, that this cannot be done with the field (2); instead we must take the field

$$H_z=2\pi H_0 \sin\left(2\pi\frac{x}{\lambda}\right)\sin\left(2\pi\frac{y}{\lambda}\right),$$

which vanishes on the surface of the metal. The calculation leads, then, to a formula for **s** which is essentially the same as equation (21). We notice for the subsequent discussion that the paramagnetic states have momentum vectors whose projections on the ξ, η-plane are directed at 45° to the normal on the surface of the metal.

§ 4. DISCUSSION. THE MEISSNER EFFECT.

Equation (11) can be written in the form

$$\mathbf{S}=-\frac{e^2\mathbf{A}}{mc^2a^3}N_{\text{eff}}, \quad \ldots\ldots\ldots \quad (23)$$

with

$$N_{\text{eff}}=N+\sum_{\xi\eta\zeta} f\frac{2\xi^2}{n_0}\left(\frac{1}{2\eta-n_0}-\frac{1}{2\eta+n_0}\right). \quad \ldots\ldots \quad (24)$$

A similar relation holds in the two-dimensional case. It has been stressed by London a long time ago that the Meissner effect demands for N_{eff} a value of $N_{\text{eff}}\approx N$.

The results of the previous calculations suggest a very simple way for increasing N_{eff} to a value of $N_{\text{eff}}\approx N$. This will be the case if the effect giving rise to superconductivity produces a certain deformation of the otherwise spherically symmetric distribution of the electrons in momentum space, without influencing appreciably the wave functions and the currents **s** of the individual states; *i. e.* if we assume that in the superconductor the distribution of the occupied states in momentum space is not exactly spherical, but that there are certain *prominences* on top of the Fermi sphere. The alternative independent explanation would be by assuming that in the superconductor the distribution of the electrons remains essentially spherical, but the wave functions and the currents **s** of the electron states are changed as much as is needed in order to account for the necessary increase of N_{eff}. Though both these factors most probably contribute to the actual increase of N_{eff}, we shall restrict ourselves to the discussion of the first one, for the simple reason that even a qualitative discussion of the second factor would be extremely difficult. After all, it is almost certain that the first will be present in any case ; and its effects will, most probably, be there even in the presence of the second factor.

By closer examination one sees that it is not possible to explain the Meissner effect by simply assuming that the prominences will be oriented in such a way as to contain strongly diamagnetic states. The reason is obvious. There are other orientations in which the prominences would contain paramagnetic states. And since diamagnetism corresponds to an increase of energy, while paramagnetism leads to a decrease of energy, the prominences will actually take the orientations corresponding to the strongest possible paramagnetism.

If the prominences are not too small, this tendency towards paramagnetism may lead to the formation of a self-consistent *internal magnetic field*. By this we mean a field **H** either of the form (1) or (2), which gives rise to a current **S** so large that, in its turn, this current produces just the field **H**. It is possible to determine the order of magnitude of the size of the prominences required for this purpose. From the general relation

$$\Delta \mathbf{A} = -4\pi \mathbf{S}$$

we find

$$N_{\text{eff}} \approx -\frac{mc^2 V}{e^2 \lambda^2} \qquad (V = a^3).$$

On the other hand, it follows from (10 *a*) or (21), if we denote by N′ the number of electrons contained in the prominences*,

$$N_{\text{eff}} \approx -N' \frac{\xi^2{}_{\max}}{n_0^2} = -N' \frac{\xi^2{}_{\max}\lambda^2}{a^2}.$$

Combining the last two relations, and taking in account that $\xi^3{}_{\max} \approx N$, we find

$$\frac{1}{\lambda^4} \approx n' n^{2/3} \frac{e^2}{mc^2}, \quad . \quad . \quad . \quad . \quad . \quad . \quad . \quad . \quad . \quad (25)$$

with $n = N/V$, $n' = N'/V$. Introducing the values $\lambda \approx 10^{-5}$ cm. and $n \approx 10^{22}$ cm^{-3} we get from (25) $n' \approx 10^{-4} n$.

It seems to-day certain that the effect leading to superconductivity is the interaction of the metal-electrons with the thermal vibrations of the lattice, as suggested recently by Fröhlich (1950). It is significant that in Fröhlich's theory prominences of the size required above are energetically possible. We, therefore, introduce the following *postulate*: *The superconducting state is associated with an internal magnetic field of the form* (2)*. In view of the very peculiar magnetic properties of the superconducting state the assumption that this state has an intrinsic magnetic structure is quite plausible. The only general restriction which we might, at present, impose on this structure is that it must be of a *microscopic* nature, since in the absence of an external field the superconductor shows no macroscopic field at all. This condition is fulfilled by the field (2).

---

* If there were one prominence only, we should have to consider the last term in the expression of **s** given by (10) : a state with one prominence only is associated with a permanent current independent of the magnetic field. We avoid such a state—which, according to the general theorem of Bloch, cannot be the state of lowest energy—by assuming that prominences occur in pairs directed in opposite directions.

The explanation of the Meissner effect is now straightforward. According to the remark at the end of § 3 the prominent directions will be at right angles to the Oz-axis and at 45° to the normal on the surface of the metal. As regards the external magnetic field, which declines exponentially inside the superconductor, it is to be expected that the prominences will act on it in the same way as on the one-dimensional field (1) (with the axis Oy along the normal to the surface). Since $n_0 \ll \eta_{\max}$, the states contained in the prominences will have $|\eta| > n_0/2$ and, therefore, we shall have diamagnetism for the external field. Of course, this will be true only for not too strong external fields $\mathbf{H}'$: Because of the diamagnetism of the superconductor as regards external fields, the field $\mathbf{H}'$ will increase the energies of the electron states inside the prominences. Hence, it will tend to decrease the size of the prominences; and when $\mathbf{H}'$ reaches a certain critical value, the prominences will disappear, *i. e.* the superconducting state will be destroyed.

The present considerations leave the value H_0 of the internal field entirely undetermined; we might only guess that this value should be of the same order of magnitude as the critical magnetic field of the superconductor. For a theoretical determination of H_0 it will be necessary to pursue the calculations to a higher approximation.

REFERENCES

FRÖHLICH, H., 1950, *Phys. Rev.*, **79**, 845.
PAPAPETROU, A., 1937, *Z. Phys.*, **107**, 387.

---

* A field of the form (1) could exist only in an infinite layer or, alternatively, in a thin closed cylindrical ring.

X. CORRESPONDENCE.

Calculation of the Density of States Curve for the 3d Electrons in Nickel.

By G. C. Fletcher† and E. P. Wohlfarth,
Department of Mathematics, Imperial College, London‡.

[Received November 23, 1950.]

It is the purpose of this letter to present some preliminary results of calculations of the density of states, N(E), for the 3*d* electrons in a face-centred cubic lattice, using the approximation of tight binding. The calculations are applied in the main to nickel. The final results have an important bearing on the physical properties of transition metals, such as magnetic, electrical and thermal properties. Comparison may be made with the results of analogous calculations by Krutter (1935) and Slater (1936), who employed the cellular approximation.

The details of the tight binding approximation are well known (see, for example, Mott and Jones 1936). The atomic wave functions which have been used, and which correspond to the fivefold degenerate 3*d* level of the isolated atom, are

$$\phi_1=a_1xyf(r)/r^2,\quad \phi_2=a_2yzf(r)/r^2,\quad \phi_3=a_3zxf(r)/r^2,$$
$$\phi_4=a_4(x^2-y^2)f(r)/r^2,\quad \phi_5=a_5(3z^2-r^2)f(r)/r^2, \quad . \quad (1)$$

where $f(r)$ is the normalized radial function of the isolated atom and the a_1 are normalizing constants for the angular functions. Using (1) Bloch type functions may be constructed and the energy calculated from the determinantal equation

$$|\mathrm{H}_{mn}-\mathrm{E}\delta_{mn}|=0,\quad m=1\ldots5,\quad n=1\ldots5. \quad . \quad . \quad . \quad (2)$$

The elements H_{mn} may be expressed in the general form

$$\mathrm{H}_{mn}=\sum_{l=1}^{3}\mathrm{A}_{mn}^{(l)}\eta_{mn}^{(l)}(\mathbf{k}). \quad . \quad . \quad . \quad . \quad . \quad . \quad . \quad . \quad (3)$$

Here the $\eta_{mn}^{(l)}$ are functions of the three Cartesian components of the reduced wave vector **k**, expressible in terms of circular functions of $\frac{1}{2}ak_x$, $\frac{1}{2}ak_y$, $\frac{1}{2}ak_z$, where a is the lattice constant. The coefficients $\mathrm{A}_{mn}^{(l)}$ have the general form

$$\mathrm{A}_{mn}^{(l)}=\int\phi_i^*(\mathbf{r}-\mathbf{R})\Delta\mathrm{V}\phi_j(\mathbf{r}-\mathbf{R}')d\tau, \quad . \quad . \quad . \quad . \quad . \quad . \quad (4)$$

---

† Now at Department of Mathematics, University College, Exeter.
‡ Communicated by Professor H. Jones.

where **R**, **R′** refer to the position of a central atom and one of its nearest neighbours, and where ΔV is the difference in the potential due to an atom when isolated and when in interaction with its nearest neighbours in the metal. Owing to the symmetry properties of the angular functions in (1) some of the coefficients vanish and the others are interdependent, such that only six independent coefficients had to be calculated. For this purpose the most suitable available values of $f(r)$ in (1) and of $V(r)$, the potential due to an isolated atom, were taken to be those of Hartree and Hartree (1936) for Cu^+ with exchange. These could be approximated to closely by simple algebraical expressions, involving exponentials. The atomic polyhedron was taken to be spherical and the assumption made that $\Delta V=0$ inside the central polyhedron and that outside it $\Delta V=V(|\mathbf{r}-\mathbf{R}'|)$. The integrations in (4) were carried out using prolate spheroidal coordinates. The resulting algebraical expressions for the coefficients were evaluated using the appropriate value of the interatomic distance. The values of the six independent coefficients range from 0·033 eV. to 0·260 eV., and these values, as that for the total width of the 3*d* band, are of such an order of magnitude as to justify the use of the tight binding approximation in this case.

With the H_{mn} known at all points in the Brillouin zone the energy may be calculated by solving (2). The functions $\eta^{(l)}_{mn}$ are, however, quite complicated, and hence it was decided, *in the first place*, to neglect arbitrarily certain of the non-diagonal elements such that the quintic equation (2) breaks into a cubic (arising from the atomic functions ϕ_1, ϕ_2 and ϕ_3) and a quadratic (arising from ϕ_4 and ϕ_5). This approximation also underlies the calculations of Jones and Mott (1937) on the body-centred cubic lattice and is implicit in much of the work of Brooks (1940) on ferromagnetic anisotropy. Calculations are now proceeding which aim at solving the complete quintic in the energy range of interest for nickel, near the top of the band. Certain results may, however, be obtained at once, and, in addition, such comparison as may be made gives very close agreement with experiment using the curve which has been calculated so far. It is believed that although inclusion of the remaining H_{mn} may distort the energy surfaces derived from the two independent equations, the effect on the final N(E) curve is less serious. The highest energies are found, in any case, to correspond to regions of the zone where the neglected H_{mn} are small. Finally the energy values which have already been computed may, in many cases, be used as first approximations to the roots of the complete quintic.

The two resulting determinantal equations were solved in the range k_x, k_y, $k_z>0$ at all points of a lattice formed by taking intervals of $\pi/6a$, Cardan's method being used to solve some 500 cubics. (In the cellular approximation it was possible to calculate the energies at only very much fewer points in the zone). Constant energy contours were constructed in the planes $k_z=\nu\pi/6a(\nu=0\ldots12)$ for each of the five solutions. Finally N(E) curves were calculated by graphical integration.

A check on this stage of the calculation is provided by the fact that the area under each of the five curves corresponds to one electronic state per atom. The resulting provisional N(E) curve, the sum of the five constituent curves, is shown in the figure.

The following deductions of particular interest may be made :

(1) The total width of the $3d$ band is 2·70 eV. This result is independent of the neglect of the non-diagonal elements mentioned. The value is about half that given by Slater (1936), with whose N(E) curve the present curve may be compared.

(2) The value of the degeneracy temperature for nickel calculated for 0·3 vacant states per atom, corresponding to the right-hand vertical line in the figure, is $2{\cdot}04 \times 10^3$ deg. K., in very close agreement with the value deduced by Wohlfarth (1949) from the magnetic and thermal properties.

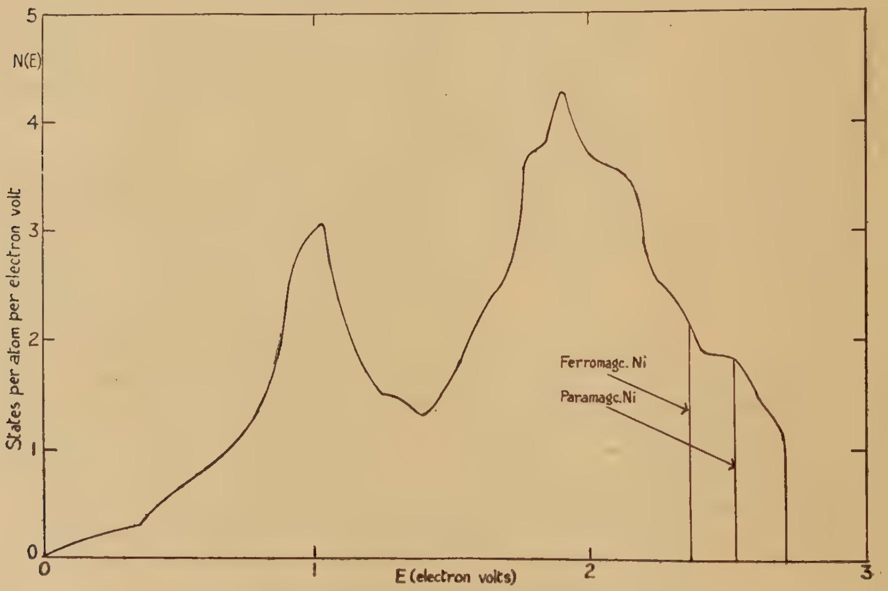

Provisional density of states curve for nickel.

E, electronic energy in eV., measured from zero at the bottom of the band. N(E), density of states, such that the total area under the curve corresponds to five states per atom of either spin. Fermi limits for paramagnetic, ferromagnetic nickel as shown.

(3) The linear low temperature electronic heat coefficient, γ, for ferromagnetic nickel (left-hand vertical line) is deduced to be $1{\cdot}15 \times 10^{-3}$ cal mol.$^{-1}$ deg^{-2}. The observed value is $1{\cdot}74 \times 10^{-3}$, but as this includes a contribution due to the conduction electrons, the significant value for comparison is somewhat lower, possibly $1{\cdot}5 \times 10^{-3}$.

(4) A completely general result concerning the degeneracy character at the centre of the zone, $\mathbf{k}=0$, states that here the five energy levels split into a threefold and a twofold degenerate level, separated, in general,

by a finite gap. This result is completely verified in the present case, the gap being found to be 0·88 eV., again independently of the neglect of the non-diagonal elements mentioned. In calculations using the cellular method, on the other hand, the degeneracy at **k**=0 is found to be almost invariably fivefold—a result of the approximations used in the method.

It is hoped to publish fuller details when the effect of the approximation indicated above has been more completely investigated. The necessary calculations are, however, so troublesome that it was felt that a preliminary account of work already completed may be of interest.

We are indebted to Professor H. Jones for his most helpful advice, and one of us (G. C. F.) to London University for a postgraduate studentship.

REFERENCES.

BROOKS, H., 1940, *Phys. Rev.*, **58**, 909.

HARTREE, D. R., and HARTREE, W., 1936, *Proc. Roy. Soc.* A, **157**, 490.

JONES, H., and MOTT, N. F., 1937, *Proc. Roy. Soc.* A, **162**, 49.

KRUTTER, H. M., 1935, *Phys. Rev.*, **48**, 664.

MOTT, N. F., and JONES, H., 1936, *Theory of the Properties of Metals and Alloys* (Oxford : University Press).

SLATER, J. C., 1936, *Phys. Rev.*, **49**, 537.

WOHLFARTH, E. P., 1949, *Proc. Roy. Soc.* A, **195**, 434.

Stars produced in Nuclear Emulsions by 150 MeV. Neutrons.

By E. W. TITTERTON [*],
Atomic Energy Research Establishment, Harwell [†].

[Received November 6, 1950.]

GARDNER AND PETERSON (1949) and Gardner (1949) have used the Berkeley cyclotron to carry out an investigation of stars induced in nuclear emulsions under deuteron and α-particle bombardment. Several authors, notably Harding *et al.* (1948) and Page (1950) have investigated cosmic ray induced stars and recently there have been several papers describing stars induced by π^- meson capture both for cosmic-ray mesons (Menon *et al.* 1950) and artificially created mesons (Chester and Goldfarb, Adelman and Jones 1950).

In the present experiments a fast neutron beam, obtained from the Harwell Cyclotron by bombarding a beryllium target with 170 MeV. protons, has been used to irradiate C_2, G_5 and NT_4 plates and the neutron induced stars have been studied. The neutron spectrum (Cassels *et al.* 1950) is indicated in fig. 1 and gives a maximum yield at 150 MeV. The neutron flux was determined by integration and includes neutrons from 60 MeV. to the maximum of the spectrum. At the plate location the flux was 2×10^5 n/cm.^{2}/sec.

---

[*] Communicated by the Author.

[†] Now on the staff of the Australian National University, Canberra.

Fig. 1.

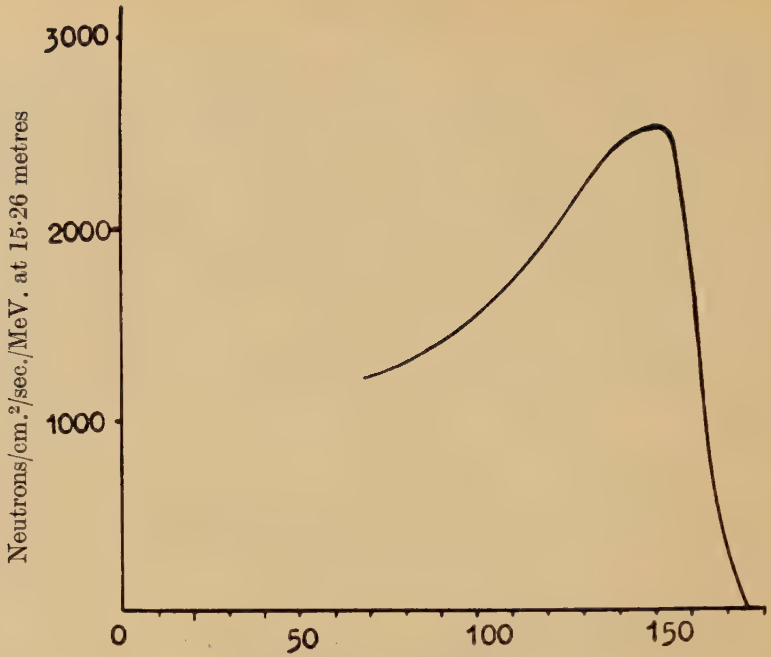

Neutron energy MeV.

Fast neutron spectrum from Beryllium target bombarded by 170 MeV protons.

Fig. 2.

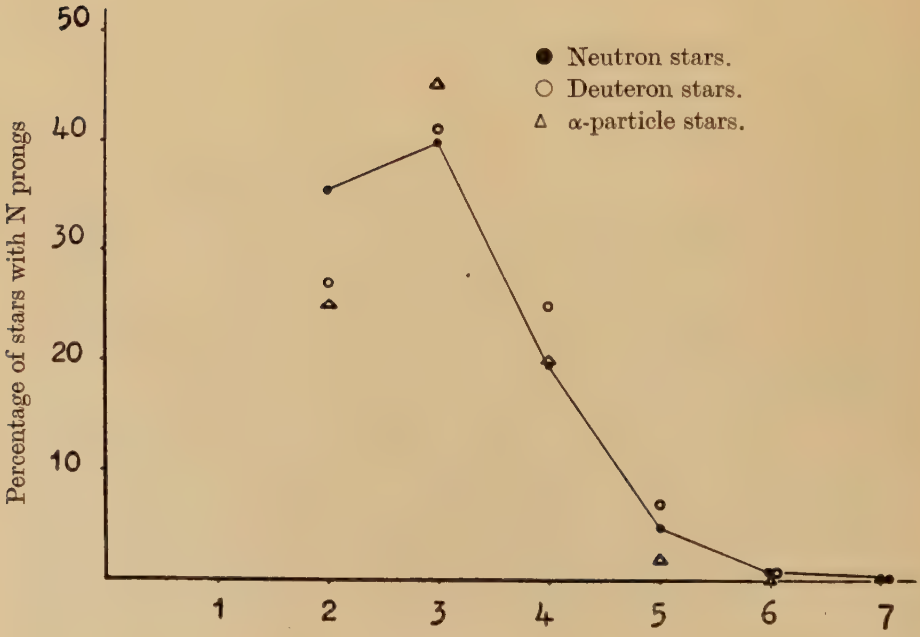

Number of prongs.

Percentage of stars having N prongs plotted against prong number.
Full circles : Present neutron induced stars.
Open circles : Deuteron stars (Berkeley).
Triangles : α-particle stars (Berkeley).

Five thousand stars have been examined to date and preliminary results were reported at the Harwell Conference (Titterton 1950). The stars can be classified into three main groups :—

1. Those having a single energetic proton in addition to other low energy prongs. The proton is apparently knocked-on by the incoming neutron and the remaining excited nucleus breaks up to give further fragments. The spectrum of the knocked-on protons has been examined and extends to 55 MeV.
2. Stars in which the prongs are collimated in the forward direction but contain low energy tracks. These stars are presumably caused by disintegration of the light elements O, C, N present in the emulsion.

Fig. 3.

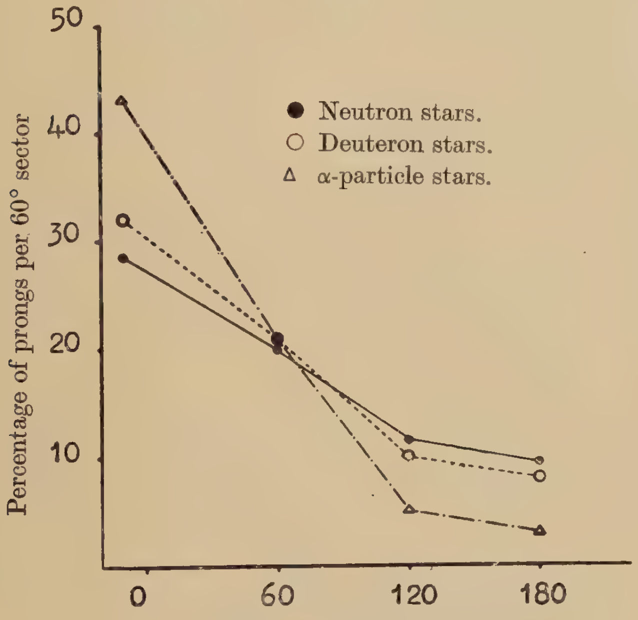

Angle (degrees) with beam direction.

Angular distribution of star prongs measured in the plane of the emulsion.
Full circles : Neutron induced stars.
Open circles : Deuteron induced stars.
Triangles : α-particle induced stars.

3. Stars in which the prongs are distributed more or less isotropically about the incoming neutron direction. These probably result from the Ag and Br atoms in the emulsion and are true evaporation stars. Evaporation stars are well known in plates exposed to the cosmic radiation and have been treated theoretically by Le Couteur (1950).

The prong spectrum of the stars is plotted in fig. 2 where it is compared with spectra obtained in Berkeley for deuteron and α-particle induced stars. The distributions are similar except that more two-prong stars are found in the present experiments. This difference is probably due to the fact that the emulsions employed were more sensitive than those used in the Berkeley experiments where protons of energy greater than 17 MeV. were not recorded. The angular distribution of the star prongs about the beam direction in the focal plane of the objective is shown in fig. 3 where the fraction of prongs falling in 60° sectors is given as a function of the angular position of the sector. Comparison with Berkeley results shows good agreement with the deuteron distribution which might be expected, since in this case, many of the stars are probably formed by the capture of a proton or neutron in a stripping process. The greater predominance of tracks in the forward direction in the α-particle bombardment is compatible with the greater momentum transfer in this case.

As the relative contributions to the star population by the heavy and light constituents of the emulsion are unknown the cross-section for star production is averaged over all the elements in the emulsion, excluding hydrogen which cannot give rise to a multiparticle star. The value obtained is 54 mB which is considerably smaller than the 210 mB found for 170 MeV. α-particles by Gardner (1949).

If it is assumed, as seems reasonable, that in this energy range the cross-sections are in the ratio of the geometric cross-sections then the cross-section for star production in the light elements (C, N and O) is 25 mB and in the heavy elements (Ag and Br) is 95 mB. Because of uncertainties in the measurement of the neutron flux these values are not accurate to better than ±30 per cent.

The plates were searched by Miss E. M. Chellingworth, Miss M. Hart, Miss K. B. Treacy and Mrs. B. Naish. The help of Mr. M. M. Cheshire, of the Cyclotron Group, in operating the machine is gratefully acknowledged.

REFERENCES.

ADELMAN and JONES, 1950, *Science*, **111**, 226.
GARDNER, 1949, *Phys. Rev.*, **75**, 379.
GARDNER and PETERSON, 1949, *Phys. Rev.*, **75**, 364.
CASSELS, RANDLE, PICKAVANCE and TAYLOR, 1950, *Harwell Conference Report*, A.E.R.E., G/M 68, p. 24.
MENON, MUIRHEAD and ROCHAT, 1950, *Phil. Mag.*, **41**, 583.
PAGE, 1950, *Proc. Phys. Soc.* A, **63**, 250.
HARDING, LATTIMORE and PERKINS, 1949, *Proc. Roy. Soc.* A, **196**, 325.
LE COUTEUR, 1950, *Proc. Phys.* A, **63**, 259.
CHESTER and GOLDFARB, 1950, *Phys. Rev.*, **78**, 683.
TITTERTON, 1950, *Harwell Conference Report*, A.E.R.E. G/M 68, p. 25.

Hammer Tracks in Neutron and Proton Induced Stars.

By E. W. TITTERTON†,
Atomic Energy Research Establishment, Harwell‡.

[Received November 6, 1950.]

IN the course of the experiments described in the preceding letter, 21 of the 5000 neutron stars were observed to be characterized by " hammer " tracks. Of these stars 18 were found in C_2 and 3 in G_5 emulsions. Such events are common in emulsions exposed to the cosmic radiation (Franzinetti and Payne 1948) but were not reported by Gardner and Peterson (1949) or by Gardner (1949) in the work with deuterons and α-particles. The events are usually attributed to ^{8}Li nuclei which, after coming to rest in the emulsion, undergo decay according to the scheme $^8\mathrm{Li} \xrightarrow{\beta-} {}^8\mathrm{Be}^*$, $^8\mathrm{Be}^* \rightarrow 2\,^4\mathrm{He}$. An alternative possibility has been suggested by Alvarez (1950) following his discovery of the nucleus ^{8}B which undergoes a similar decay scheme $^8\mathrm{B} \xrightarrow{\beta+} {}^8\mathrm{Be}^*$, $^8\mathrm{Be}^* \rightarrow 2\,^4\mathrm{He}$.

The hammer tracks observed in the present experiment, whether they are due to ^{8}Li or ^{8}B, almost certainly result from the break-up of light elements since the emission of such fragments from Ag or Br nuclei at these excitation energies would be an improbable process due to the impenetrability of the Coulomb barrier. The prong spectrum and angular distribution for the 21 stars are compared with the equivalent distributions obtained in the case of neutron induced stars without hammer tracks in fig. 1 (*a*) and fig. 1 (*b*). The comparison is compatible with the view that the events are due to the disintegration of the light elements in the emulsion.

Accepting this view application of the principles of charge and, to a lesser degree, momentum conservation, then allows conclusions to be drawn about the reactions responsible for these stars. Thus of the three-particle stars the majority (7) appear to result from the reaction

$$C^{12}+n=Li^8+He^4+H^1-22{\cdot}7\ \mathrm{MeV}. \quad . \quad . \quad . \quad . \quad . \qquad (1)$$

and three from the reaction

$$O^{16}+n=Li^8+Be^7+H^1+n-49\ \mathrm{MeV}. \quad . \quad . \quad . \quad . \qquad (2)$$

the proton being knocked-on with high velocity as indicated in the micrograph of fig. 2.

Of the seven four-particle stars only one can be due to carbon as all others have, in addition to the hammer track, at least one other prong of charge two. Four appear to be described by the reaction

$$N^{14}+n=Li^8+He^4+2H^1+n-35\ \mathrm{MeV}. \quad . \quad . \quad . \quad . \qquad (3)$$

---

† Communicated by the Author.

‡ Now on the staff of the Australian National University, Canberra.

Fig. 1(*a*).

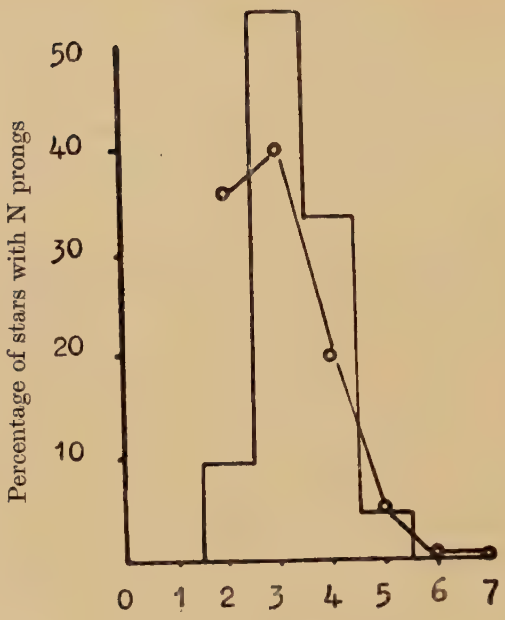

No. of prongs.

Per cent of stars with N prongs plotted agaist the prong number N.

Histogram : Stars with hammer tracks.
Circles : All other stars.

Fig. 1(*b*)

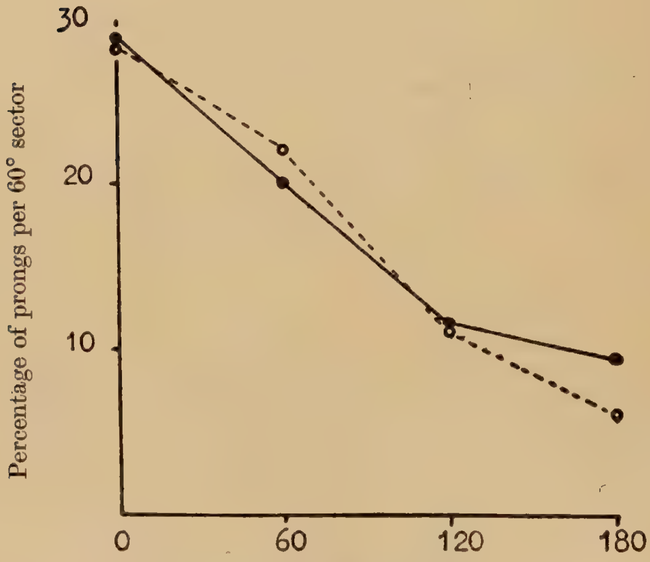

Angle from beam direction.

Per cent of prongs per 60° sector as a function of angle between centre of sector and the beam direction.

Open circles : Stars with hammer tracks.
Closed circles : Stars without hammer tracks,

and two by the reaction

$$O^{16}+n=Li^8+He^4+He^4+H^1-30 \text{ MeV}. \quad . \quad . \quad . \quad . \quad (4)$$

The five-prong star can only be due to oxygen and may be described by

$$O^{16}+n=Li^8+He^4+3H^1+2n-58 \text{ MeV}. \quad . \quad . \quad . \quad . \quad (5)$$

Of the 21 events only the two-particle stars could reasonably involve the nucleus B^8_5. One of these comprises the hammer track plus a fast proton and on charge conservation grounds is therefore

$$C^{12}+n^1=B^8+H^1+4n^1-54 \text{ MeV}. \quad . \quad . \quad . \quad . \quad . \quad (6)$$

the other shows a gross momentum unbalance about the incoming neutron direction and has a second track of $Z \geqslant 2$. It could be either Li^8 or B^8.

Fig. 2.

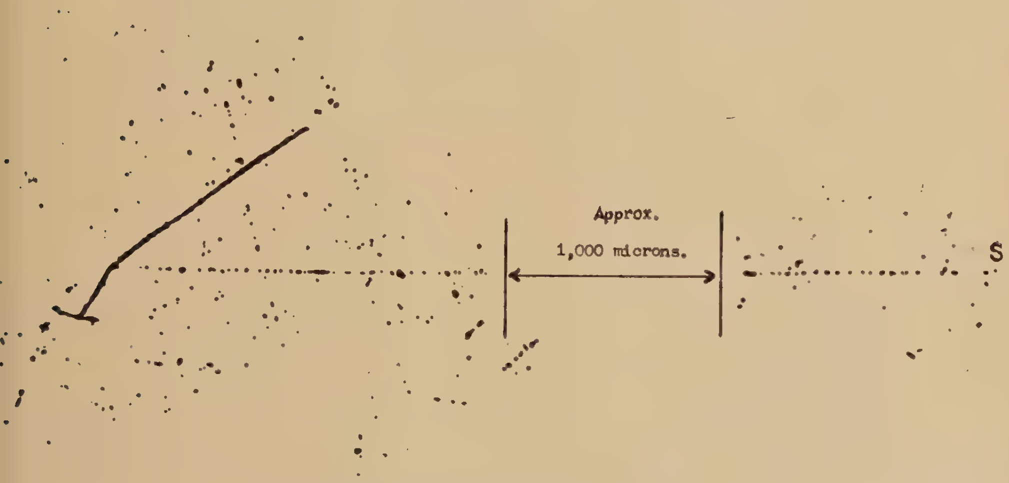

Micrograph of star assigned to reaction (2).

These results suggest that Li^8 is a much more likely residual nucleus than B^8 and, accepting the above assignments, the cross-section for Li^8 production, averaged over C, N and O atoms in emulsion is found to be $0{\cdot}6 \pm 0{\cdot}2$ mB. The energy spectrum of the Li^8 nuclei is indicated in fig. 3 (*a*) and the energy release in the break-up of the resulting Be^8 nuclei is given in fig. 3 (*b*). The latter histogram is in agreement, within the statistics, with that found for Be^8 resulting from the reaction $Be^9\gamma pLi^8$ (Titterton 1950).

Experiments are now in progress to study stars produced by 170 MeV. protons and the preliminary results show a similar percentage of stars with hammer tracks. This agrees with Wright (1950) who finds that ^8Li is formed when a variety of elements are bombarded with 340 MeV. protons and also with 190 MeV. deuterons. Furthermore, in a study of 3000 π^- meson induced stars Adelman and Jones found 11 cases of hammer track emission. This frequency compares well with that observed in the present experiments with neutrons and protons as might be expected since the nuclear excitation in this case would be about the same value (142 MeV.). Combination of these results suggests that ^{8}Li should be found as a residual nucleus in the break-up of highly excited light nuclei and it should therefore have been found in the high energy α-particle bombardments.

Fig. 3(*a*)

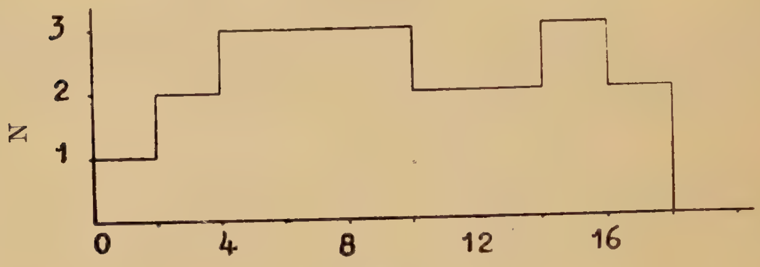

E(MeV.)

Energy spectrum of ^{8}Li nuclei emitted from the stars.

Fig. 3(*b*)

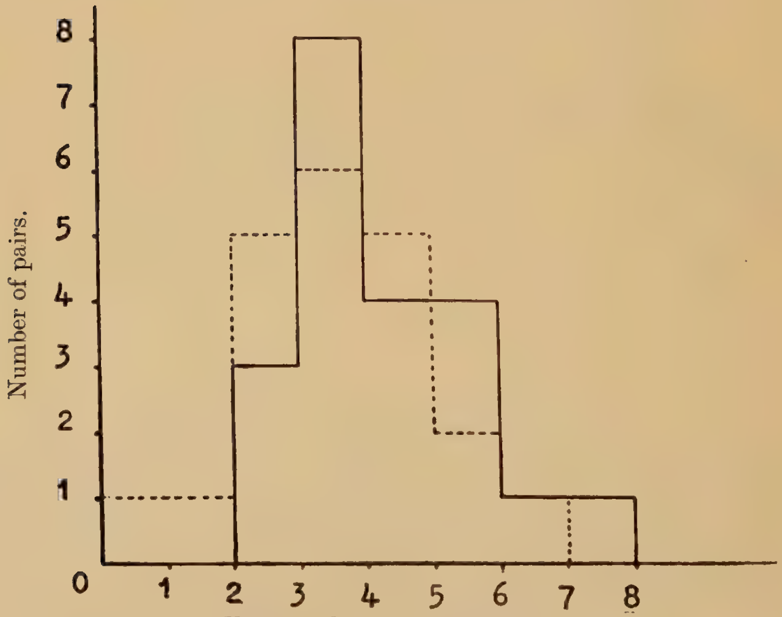

Energy of α-particle pair MeV.

Energy release in the break-up of the ^{8}Be nucleus forming the head of the hammer.

Full lines, present 21 events.

Dotted lines, events resulting from the reaction $Be^8\ \gamma p\ Li^8$.

The mechanism proposed by Wright (1950) to explain Li^8 production from light elements requires the incoming particle to be captured and the compound nucleus to boil off the necessary number of neutrons and protons leaving a residue consisting of ^8Li. This is not in general agreement with the present observations. As shown above an excited nucleus is formed by inelastic scattering or by capture of the neutron and then breaks up into charged particles of which a large proportion are α-particles. In general very few neutrons are emitted.

Thanks are due to Miss M. Hopkins for microscope work and Mr. T. A. Brinkley for the photomicrograph.

REFERENCES.

ADELMAN and JONES, 1950, *Phys. Rev.*, **111**, 226 ; *Science*, **111**, 226.
ALVAREZ, 1950, *Harwell Conference Report*, A.E.R.E. G/M 68, p. 43.
FRANZINETTI and PAYNE, 1948, *Nature, Lond.*, **161**, 735.
GARDNER, 1949, *Phys. Rev.*, **75**, 379.
GARDNER and PETERSON, 1949, *Phys. Rev.*, **75**, 364.
TITTERTON, 1950, *Nature, Lond.*, **165**, 721.
WRIGHT, 1950, *Phys. Rev.*, **79**, 838.

XI. *Notices of New Books and Periodicals received.*

Progress in Biophysics. Edited by J. A. V. Butler and J. J. Randall, F.R.S. (Butterworths.) Price 50*s.*

The boundaries of biophysics have never been easy to define, but this well-produced volume helps both to indicate the fringe of recent advances and to consolidate the ground already won. As the editors point out, biochemistry and physiology have their own domains and mere application of a physical or chemical technique to a biological problem does not necessarily constitute a passport to this mandated territory. Perhaps the main justification for a subdivision of science such as biophysics is that it provides opportunities for cross-fertilization which may generate offspring more bold and vigorous than the parents.

Throughout the volume, with separate chapters by a number of experts, there is noticeable a healthy tendency to stress what may be called the dynamic aspects of the various subjects.

There is a good author index but the subject index is rather brief for a volume covering so wide a field. For most readers too, it would be more convenient if the separate bibliographies were arranged in alphabetical order. It would also be helpful if in future editions all the contributors could be induced to provide summaries of their material and personal views.

Dr. Butler and Professor Randall have performed a valuable service in producing a work in which there is so much information, some wisdom and no little wit.
W. G-W.

Cosmical Electrodynamics. By H. Alfvén. (Oxford.) Price 25*s.*

The subject of which this book treats is a new one. It deals with the electromagnetic behaviour of an ionized compressible gas in hydrodynamic motion, and with the applications of this study to problems in astrophysics.

At present we are very far from having a complete solution of the electrodynamic-hydrodynamic problem in its most general form. Unfortunately a proper investigation of the astrophysical effects requires nothing short of such a complete solution. So we are forced to makeshift methods. These have mostly followed one or other of two lines. There is the cautious school of thought that accepts only those electromagnetic effects that seem unavoidable. The second school of thought, on the other hand, accepts every electromagnetic effect whose existence cannot be disproved. For example, this school will regard an electric field as being present in a particular problem so long as its existence cannot be disproved, whereas the first school will not accept the existence of the electric field unless its absence can be disproved. Dr. Alfvén belongs to the second school of thought, and to the reader of his book this carries an important advantage. For Dr. Alfvén's applications of electromagnetism to astrophysics are so extensive that many of the ideas set forth in his book are reasonably certain to have permanent value. Which these are, however, the reader must discover by his own efforts.

One of the most important current issues concerns the relation between the electric current density in an extremely diffuse ionized gas, the electromagnetic field, and the motion of the gas. This affects not only the structure of the solar atmosphere, but also whether or not there can be a galactic magnetic field of appreciable magnitude. Alfvén quotes a formula due to Cowling without apparently noticing that Cowling's result depends on the assumption that the gas is not being appreciably accelerated. This places an important restriction on the use of Cowling's formula which may be stated briefly as follows:—To an observer moving with a particular element of gas the electric and magnetic fields at the position of the element are substantially parallel. Without this result it seems impossible to attempt, as Alfvén does, the investigation of very diffuse gases.

Another question that is now open to doubt is whether under normal conditions the general solar magnetic field can extend much above the photosphere. Certainly the observed variations of angular velocity from one part of the Sun's atmosphere to another are inconsistent with the simple dipole field assumed by Alfvén. This has serious repercussions on the sections dealing with the structure of the chromosphere and corona.

In reading this book one can hardly fail to notice the author's tendency to claim a displacement of a problem as its solution. For instance, it would not be reckoned a complete answer to a question such as : " Why did you arrive at work so early this morning ? " to say : " Because I left home an hour before my usual time." Yet this is what Alfvén does on numerous occasions ; for example, in the problem of the reversal of the magnetic polarities of sunspots, in that of the darkening of sunspots, and in postulating the electric field necessary to accelerate the auroral particles.

But in spite of all criticism, and the author can hardly expect some of his ideas to escape criticism, this book cannot fail to be most useful to all who are interested in the problems of solar physics and of cosmic rays. It should be on the book-shelves of every astrophysicist. F. Hoyle.

A Hundred Years of Physics. By William Wilson. [Pp. 519.] (Duckworth and Co., London, 1950.) Price 21*s*.

Those who hope to find in this volume a history of the revolutionary changes in physical ideas which have taken place during the period covered (1850–1950) may be somewhat disappointed. The book is rather a kind of supplementary text, suitable for revision purposes, in which rather more than the usual emphasis is laid on the chronology of the various topics considered. An honours graduate in Physics—actual or potential—could read it with pleasure and profit ; but the author's claim in his preface that the reader needs very little previous knowledge of physics and very slight mathematical equipment must be taken *cum grano salis*. For the rest, the book is well written, well produced, with many references to the original publications and a satisfactory index. N.T.

Contributions to Mathematical Statistics. By R. A. Fisher. Wiley (Chapman and Hall.) Price 60*s*. net.

This volume is a collection of reprints of 43 papers by an eminent statistician selected by him as the more important of his published papers. They cover a wide variety of subjects and are accompanied in many cases by author's notes added for the purpose of the volume. Though photographically reproduced from the original journals, the volume is attractively prepared on good paper. Many will find in it a useful work of reference and study.

Methods of Mathematical Physics. By H. and B. S. Jeffreys. Second Edition. [Pp. 708.] (Cambridge University Press.) Price £4 4*s*. 0*d*. net.

The value of this important work is shown by the appearance of a second edition only four years after the original. The first edition was reviewed in this journal (Vol. 38, p. 226, 1947). It has now been considerably revised, in some cases by the addition of new material or the expansion of old, as in the account of matrices and the treatment of relaxation methods. In other cases the subject-matter has been mainly re-written, as in the chapter on multiple integrals. Where possible the proofs have been either replaced by shorter ones or generalized.

An extraordinarily wide range of topics is covered, as indeed must be the case in achieving the authors' aim to give an account of those parts of pure mathematics that are most frequently needed in physics.

[*The Editors do not hold themselves responsible for the views expressed by their correspondents.*]

NOTICE TO CONTRIBUTORS

UNIT OF HEAT

The Council of the Royal Society, having considered a memorandum entitled "The Unit of Heat", recommends that quantities of heat and all other dependent concepts such as specific heat, latent heat, entropy etc., should in future be expressed both in joules and in calories.

The Editors express the hope that, in submitting papers for publication in the *Philosophical Magazine*, contributors will also adopt this precedure.

ERRATA.

An Interferometric Study of some Optical Properties of Evaporated Silver Films, by R. C. Faust, *Phil. Mag.*, 1950, **41**, 1238.

P.1241, line 5, *read* "glass substrate" *for* "glass substitute".

P.1243, line 30, *read* "rate of evaporation" *for* "rate of absorption".

P.1254, Insert the reference

Brossel, J., 1947, *Proc. Phys. Soc. Lond.*, **59**, 224.